Universidade de Aveiro
Departamento de Electrónica, Telecomunicações e Informática,
2011

Mariana
da Silva Cascalheira

Antena para orientação indoor
Antenna for indoor guidance

"Engineering is not merely knowing and being knowledgeable, like a walking encyclopedia; engineering is not merely analysis; engineering is not merely the possession of the capacity to get elegant solutions to non-existent engineering problems; engineering is practising the art of the organized forcing of technological change... Engineers operate at the interface between science and society..."

— Gordon S. Brown

Mariana
da Silva Cascalheira

Antena para orientação indoor
Antenna for indoor guidance

Dissertação apresentada à Universidade de Aveiro para cumprimento dos requesitos necessários à obtenção do grau de Mestre em Engenharia Electrónica e de Telecomunicações, realizada sob a orientação científica do Professor Doutor Nuno Borges de Carvalho, Professor do Departamento de Electrónica, Telecomunicações e Informática da Universidade de Aveiro e o Professor Doutor Pedro Renato Tavares de Pinho, Professor do Departamento de Engenharia Electrónica, Telecomunicações e Computadores do Instituto Superior de Engenharia de Lisboa.

o júri / the jury

presidente / president

Prof. Doutor João Nuno Pimentel da Silva Matos
Professor associado da Universidade de Aveiro (por delegação da Reitora da Universidade de Aveiro)

vogais / examiners committee

Prof. Doutor Nuno Borges de Carvalho
Professor associado com agregação da Universidade de Aveiro (orientador)

Prof. Doutor Pedro Renato Tavares de Pinho
Professor adjunto do Instituto Superior de Engenharia de Lisboa (co-orientador)

Prof. Doutor Rafael Ferreira da Silva Caldeirinha
Professor coordenador da Escola Superior de Tecnologia e Gestão do Instituto Politécnico de Leiria

agradecimentos / acknowledgements

Após cinco anos de diversos altos e baixos não poderia deixar passar a oportunidade de fazer uma pequena homenagem a todos os que me ajudaram a chegar ao fim deste percurso. Em primeiro lugar gostaria de agradecer à minha mãe pela paciência, por estar sempre disposta a ouvir-me e apoiar-me em qualquer altura. Quero também agradecer a Deus por toda a força interior que me proporcionou e que me fez nunca baixar os braços nos momentos em que quase quis desistir. Um obrigado especial à minha avó Clarinda e ao meu pai por todo o apoio e compreensão. Não menos importante um grande obrigado ao Dr. José Pires por todo o apoio e amizade que tem demonstrado desde que me lembro. Neste momento é também necessário fazer um agradecimento especial a todos os meus amigos que fizeram com que estes cinco anos passassem rapidamente, e que me fazem desejar que o tempo volte para trás. Obrigada por todos os conhecimentos, aventuras e experiências partilhadas!

Gostaria de agradecer a todos os professores que se cruzaram no meu percurso académico por transmitirem os conhecimentos que irei utilizar na próxima etapa. Um especial obrigado ao Prof. Nuno Borges de Carvalho e ao Prof. Pedro Pinho pela disponibilidade, boa disposição, motivação, entusiasmo, compreensão, e acima de tudo pela ajuda, sem os quais não teria sido possível terminar este trabalho.

Por fim e não menos importante, queria agradecer aos meus discos por serem capazes de me preencher em qualquer momento e também aos livros que tanta vez me esclareceram as minhas dúvidas e me transportaram para um outro mundo.

Palavras-chave Orientação indoor, agregado de antenas impressas, balun, dipolos.

Resumo

Com os avanços tecnológicos que se têm registado nos últimos anos torna-se, cada vez mais, necessário desenvolver soluções que permitam facilitar o dia-a-dia das pessoas que sofrem de alguma impossibilidade física. É de facto crucial começar a aplicar a tecnologia no desenvolvimento de sistemas que permita a essas pessoas tornarem-se independentes e capazes de responder a todas as tarefas diárias. Assim, inspirado pelo Instrument Landing System (ILS), que é um sistema que permite aos pilotos aterrarem os aviões em segurança quando as condições metereológicas e visuais não são as mais favoráveis, pretende-se desenvolver um mecanismo que permita aos invisuais identificarem a aproximação de uma porta, e consequemente ajudá-los a entrar ou sair da divisão.

De um modo geral, este trabalho foca-se no desenvolvimento de uma antena que permita fazer a identificação da porta. Pretende-se que a antena apresente um diagrama de radiação com a forma de uma *bolacha*, pois a detecção do máximo irá levar à entrada ou saída correcta da porta. Para atingir este objectivo, a antena a ser desenvolvida é um agregado linear e uniforme de dipolos, cujo o diagrama de radiação cumpre as especificações pretendidas. Outro aspecto importante acerca do agregado de dipolos diz respeito à sua construção, pretende-se que a antena a desenvolver seja impressa. Esta opção prende-se com a sua relação simplicidade e baixo custo com eficiência e desempenho.

Keywords Indoor guidance, balun, printed antenna array, dipole.

Abstract

With all the technological developments that have happened during the past few years, it has become necessary to come up with systems that are capable of improving everyday tasks of people who have physical disabilities. Actually, it is important to improve the living conditions of these people by providing them mechanisms that would make them stop relying on the others. Bearing this in mind, the idea for this dissertation was inspired by the ILS, which is a landing system that allows pilots to land with safety in poor visibility and weather conditions. It is aimed to design an antenna for a system that helps the visually impaired or the blind to guide themselves indoor. In fact, it is intended to develop a system that helps them to identify a door, and at the same time guide them to enter or exit the room correctly.

In general, this work is focussed in the design of a suitable antenna for door identification. The main specification that the antenna has to meet is having an extremely narrow radiation pattern. The reason behind this specification is due to the way that the receiver would know when to tell the user that a door entrance is approaching, in other words, the identification of a door is made through maximum search of the radiation pattern. When this maximum value is found, the person knows that he or she is correctly positioned to enter or exit the room. The antenna would be a linear array of uniform amplitudes and spacing of dipoles with a radiation pattern similar to a *cookie*.

Another aspect concerning the antenna is what materials it would be made of. Considering the relation between simplicity and low-cost with efficiency and performance, a printed antenna would be the ideal solution for the project's system.

Contents

List of Figures

List of Tables

Acronyms

ILS Instrument Landing System

DDM Difference in Depth Modulation

HFSS High Frequency Structure Simulator

PCB Printed Circuit Board

ADS Advanced Design System

VNA Vector Network Analyser

GPS Global Positioning System

GIS Geographic Information System

RFID Radio Frequency Identification

FLC Fluorescent Light Communications

WLAN Wireless Local Area Network

AF Array Factor

RF Radio Frequency

SMA SubMiniature version A

Chapter 1

Introduction

1.1 Background

The purpose of this work emerged from the necessity of blind people to guide themselves inside buildings. As a matter of fact, with developments in technology happening so hastily in past few years, it is a major concern to come up with solutions that would improve the living conditions of those who have physical disabilities. It is important for the blind and the visually impaired to reach their independence, in other words, to stop relying on other people to help them perform everyday activities. Fortunately, there are the seeing eye dog and the canes that help them to walk through the streets. However, there is few done to assist them to move inside the buildings with security and without relying on other people.

In what concerns the situation in Portugal, there is effectively much to be improved and to be done. For instance, one of the greatest problems is the height of traffic signs, which might turn into serious damage if the person hits it. This situation barely occurs to the people who are responsible for signalling the roads. Another problem is related with the zebra crossing, since there are few equipped with a system that emits an audible signal that allows the person to know when to cross. It is utterly important and urgent to discover and implement mechanisms that facilitate the everyday activities of the blind and the visually impaired.

A possible solution to this problem was inspired by ILS, which is a landing system used in severe weather conditions that do not allow the pilot to see clearly the runaway. This system consists of two directional beams produced by arrays of dipoles which cover the total width of the runway. These arrays are located beyond the departure end of the runway. One of this beams is modulated at 90 Hz and is slightly shifted from the centre line, and the other is modulated at 150 Hz and slightly shifted from the centre line too. In addition, one of them would be pointing to left and the other to the right, allowing the measurement of Difference in Depth Modulation (DDM), which would be zero in the very centre of the runway (see figure 1.1).

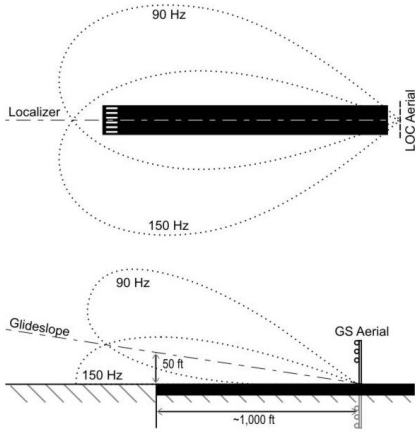

Figure 1.1: Directional beams produced by the antenna arrays of ILS [1].

There is also a group of three antenna arrays placed within a certain distance from the runway, that are responsible for warning the pilot in advance that he is approaching the airport. When the plane is near one of those antenna arrays a light appears in the control panel indicating which marker it has reached. These arrays are named outer, middle and inner marks and their colours on the control panel are blue, yellow and white, respectively. These arrays are separated by a determined distance between them and positioned in line with the centre of the runway. To provide vertical guidance there is an antenna placed in one of the sides of the runway as well. Basically, the aim of the pilot is to place the plane in the position of 0° in order to land with proper security.

Inspired by this landing system, the scope of this work is to develop an antenna array that produces a very tight radiation pattern similar to the one provided in figure 1.2. This antenna is to be placed exactly in the middle of the door casing allowing blind people to know precisely where to enter (see figure 1.2).

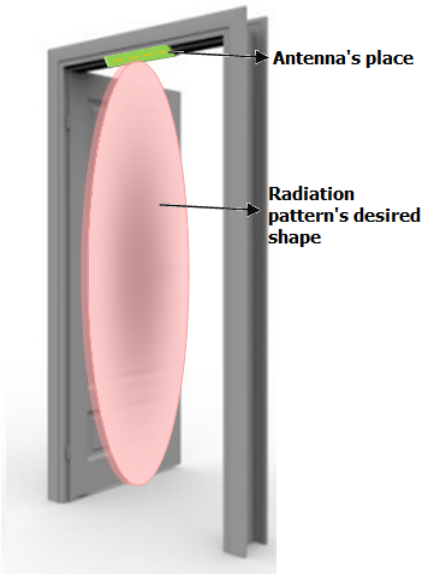

Figure 1.2: General concept of the system that is intended to be developed [2].

Based on the sketch of the system from figure 1.2 that is intended to develop, it is necessary to have an antenna whose radiation pattern is similar to a *cookie* and very narrow. The reason behind these specifications lies in the way the system is supposed to work: the person would be oriented through the search of the maximum value of power emitted by the door's antenna. As the person approaches the door, the receiver is supposed to detect the signal from the emitter antenna, advising the person that he or she is close to the door. Then, the receiver is supposed to emit some kind of audible signal that allows the person to know how to move. When the maximum is found, the audible signal produced by the receiver would be different from the previous one, meaning that one should go straight ahead to enter the room. If the radiation pattern is too large, the person would only know that an entrance is nearby, but would not be able to know with certainty where to turn.

As one could observer in figure 1.2, this antenna is to be placed in the casing, therefore it has to be small and light. Another problem that might arise is related to the esthetic point of view, because the antenna should not be too large to avoid marring the indoor design, and should be placed in a discrete manner i.e, without being noticed by other people. Usually, this problem is solved by using a printed antenna, which fits the characteristics mentioned before. Besides, printed antennas are very cheap, easy to build and have a relatively good performance. With all the environmental concerns, it is also necessary to develop a system that is energetically efficient i.e., it should be low-power as possible.

In conclusion, this work is specially focussed in the development of the antenna that would meet the system specifications.

1.2 Objectives

This dissertation aims to develop an antenna which allows door identification for the blind or the visually impaired. The development process starts with simulations and study of the single dipole and then of arrays of two and four elements. In general, it is intended to narrow gradually the radiation pattern until the maximum values of power emitted by the antenna become concentrated in the middle of the door entrance. After performing all the simulations, both antennas will be measured in the VNA and also in the anechoic chamber. Finally, it is supposed to portray a real situation of door identification by placing the antennas in the door casing.

1.3 State of the art

Before trying to discover a solution to this problem, a search on what is available in the market or in the academic research concerning the guidance of the blind or the visually impaired inside buildings had to be done. There are indeed a few prototypes and commercial systems aimed to help these people in their everyday motion.

In the outdoor environment, for instance, the Global Positioning System (GPS) is commonly used, allowing people to have access to detailed maps in which descriptions of the obstacles, points of interest (restaurants, hotels, pharmacies, etc) and possible dangerous situations are available. Recently with the emergence of smartphones, there are few applications available for the mobile phones, specially the ones from Nokia that use the *Symbian OS*. For example, *Loadstone GPS* and *Wayfinder Access* are two possible applications for outdoor guidance [3, 4]. What is more, an application for PDA named *Trekker* [5] is also available and a device called *BrailleNote GPS*[6, 7, 8, 9]. In short, the outdoor applications for guidance rely on four technologies: GPS, Geographic Information System (GIS)[10], electronic compass and also wireless digital video transmission or remote vision. All of these applications interact with the blind or the visually impaired through a speech mechanism.

The indoor guidance is less developed, but several solutions were already studied and analysed. As a matter of fact, it appears that indoor systems for guidance rely either on Radio Frequency Identification (RFID) or in 3D-modeling and image processing, and sometimes even both. When considering the RFID technology for instance, the system from [11] uses matrixs of RFID tags which guide the person through the shortest path using an algorithm. The main drawback of [11] is its weight and size. Another system described in [12, 13] combines RFID, Bluetooth and Fluorescent Light Communications (FLC) to help the blind or the visually impaired reaching a specified location inside a building. The RFID tags are used to identify the important objects, elevators, stairs, etc; the fluorescent lights are responsible for determining the position of the person with the help of the RFID tags; and the bluetooth is used to get a map of the lights in the building. According to its authors, the determination of the person's position needs to be improved. In addition to these two systems, there is another RFID based system that places tags on the ground providing the path the blind or the visually impaired have to follow. These tags have a very short range of detection, therefore the person needs to be correctly positioned in order to detect the tag[14]. Using the 3D- modelling and image processing, there is a system from [15] in which the cane is responsible for identifying objects through the use of a camera. What is more, the system in [16] combines a sensor module containing a direction sensor and a stereo camera with a small portable computer for handling the 3D environment in order to provide proper guidance. In short, the location of the person is determined through the measurement of the signals strength from the access points (Wireless Local Area Network (WLAN)), and with the sensor module the objects could be identified and directions provided.

The most similar system to what is intended to develop with this project is the one referenced in [17], which provides door detection. Contrary to what is proposed, the door detection uses image processing through detection of corners and edges, because they are more reliable than detecting the casing or the jamb. Further explanations on this project are to be found in [17].

1.4 Dissertation's structure

In short, this dissertation is arranged according to the following structure:

Chapter 1 explains the necessity of the system that is intended to be designed and provides an overview of what is already available. This chapter is also responsible for explaining the choice of the type of antenna and for providing a brief study on what has been done in academic research concerning the antenna that is to be developed;

Chapter 2 concerns the design and simulation of two topologies of printed dipoles: with the arms on the same side of the substrate layer and with the arms on opposite sides of the substrate layer. The simulations are focussed on the measurement of the return loss and radiation pattern of the printed dipoles;

Chapter 3 aims to design and simulate a set of a printed dipoles with different geometries for the balun in order to provide balanced feeding;

Chapter 4 intends to use the printed dipoles with balanced feeding to design and simulate arrays of two and four elements. It also provides the experimental measurement of the radiation pattern and return loss of one array of two elements and other of four elements that had the best performance according to the High Frequency Structure Simulator (HFSS) results. In addition, this chapter includes a set-up that shows if the system is working properly, when portraying a real situation.

Chapter 5 is an overview of the developed project and it has some suggestions for further work on this system.

1.5 The system's antenna

1.5.1 The half-wavelength dipole

As already stated, it is the aim of this project to develop an antenna with a radiation pattern similar to figure 1.2 i.e., resembling a *cookie*. The type of antenna that seem to produce such a result is the linear wire or printed dipole, which have a radiation pattern shape like a *doughnut*, if its length is inferior or equal to λ. According to [18, p 162] the most commonly used dipoles are the ones with a total length of $\frac{\lambda}{2}$ due to its input impedance of 73Ω, which is very close to the 75Ω characteristic impedance of some transmission lines. Even when the transmission line has a characteristic impedance of 50Ω, the matching is easily done by using a quarter-wavelength transformer. Considering a free-space propagation ($\eta = 120\pi$), the radiation resistance is given by:

$$R_r = \frac{2P_{rad}}{|I_0|^2} = \frac{\eta}{4\pi} C_{in}(2\pi) = 30(2.435) = 73\Omega \tag{1.1}$$

Although the equation provided in 1.1 concerns the radiation resistance, in a half-wavelength dipole the radiation resistance is the input impedance, because the maximum of current occurs at the input terminals. It is important to notice that the radiation resistance is by definition the resistance referred to the maximum current. This known value of impedance for a dipole of length $\frac{\lambda}{2}$ does not only have real part, but also an imaginary part of $42.5j$. However, to reduce the reactance to near zero there are two options: to do the matching or to shorten the dipole's length. It is stated in [18, p 164] that in this type of dipoles the length is usually reduced instead of performing the matching. Another consideration to bear in mind is that the thicker the wire, the larger the segment that has to be removed.

Due to the ease of matching and its radiation pattern shape, the half-wavelength dipole is the appropriate antenna for this project.

1.5.2 The array of half-wavelength dipoles

After the choice of antenna type for this work, it is aimed to find an arrangement of dipoles that narrows the radiation pattern of the half-wavelength dipole. The main reason for considering an array of half-wavelength dipoles is essentially the ease of matching as previously stated. Actually, a

single-element would produce a tighter radiation pattern with the increase of the length of the dipole for values greater than λ, but there are inconvenient and significant secondary lobes. In figure 1.3, it is possible to observe the radiation pattern narrowing with the increase in the dipole's length. In addition, there is a radiation pattern in the same picture produced by a dipole with a length of 1.25λ, in which is possible to see the existence of secondary lobes that start to appear when the length is greater than λ [18, p 154,155].

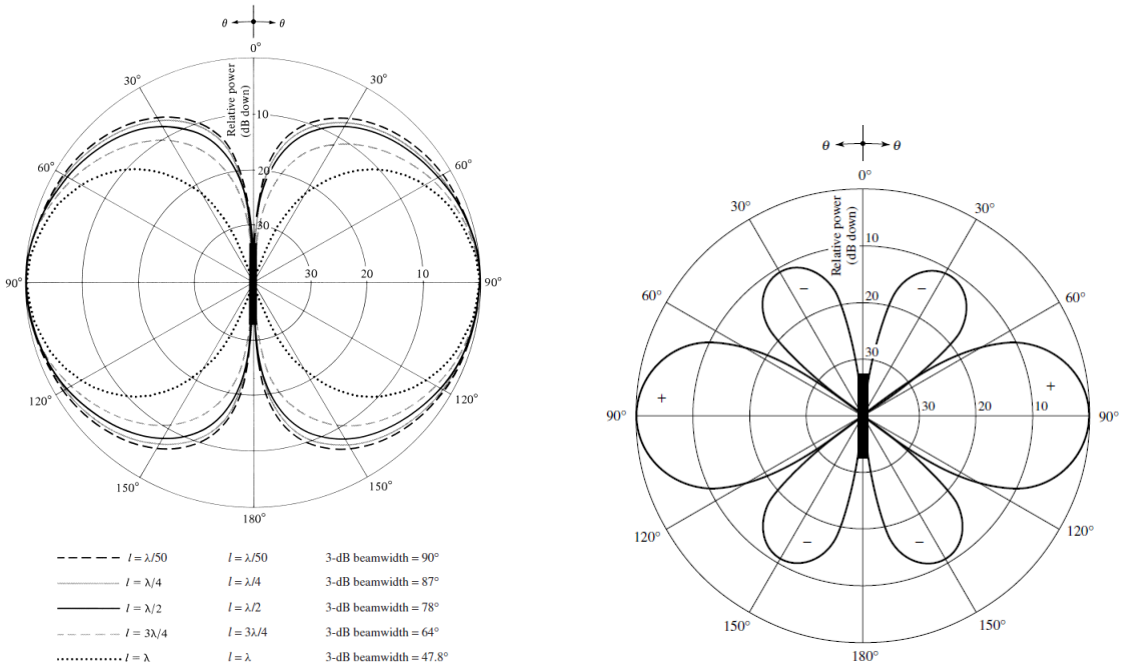

(a) Radiation pattern produced by dipoles with lengths inferior to λ.

(b) Radiation pattern produced by a dipole with a length of 1.25λ

Figure 1.3: 2D view of radiation patterns produced by dipoles in the XY and XZ planes [18].

The solution for tightening the radiation pattern is then to design an array of dipoles in which the fields produced by the elements interact with each other in order to originate the desired final result. There are five possibilities to achieve this: the arrangement of the elements, the space between elements, the radiation pattern from the single-element, the excitation amplitude of the single element, and finally the excitation phase of the individual elements.

N-element linear array of uniform amplitude and spacing

According to what is stated in [18], the linear array of uniform amplitude and spacing seemed to be a suitable antenna array for the project's needs, which would be proved in this section.

To begin with, a uniform array is an array of identical elements with equal magnitude and with a progressive phase difference. To give a better understanding of its functioning, it is important to determine the electric field of the single element and the Array Factor (AF). Based on figure 1.4, considering each element a single point source and assuming no coupling between them, the total electric field is given by equation 1.2, where β is the difference in phase excitation.

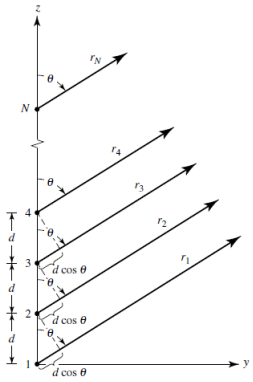

Figure 1.4: Far-field geometry of a N-element array.

$$\begin{aligned}\mathbf{E}_{total} &= E_1 + E_2 + ... + E_N \\ &= j\eta\frac{kI_0l}{4\pi}\left\{\frac{e^{-j[kr_1-\beta]}}{r_1}\cos\theta_1 + \frac{e^{-j[kr_2-\beta]}}{r_2}\cos\theta_2 + \ldots + \frac{e^{-j[kr_N-\beta]}}{r_N}\cos\theta_N\right\} \end{aligned} \tag{1.2}$$

Assuming far-field observations (see figure 1.4),

$$\theta_1 \simeq \theta_2 \simeq \ldots \simeq \theta_N \simeq \theta \tag{1.3}$$

$$r_2 \simeq r_1 - d\cos\theta$$

$$r_3 \simeq r_1 - 2d\cos\theta$$

...

$$r_N \simeq r_1 - (N-1)d\cos\theta \rightarrow \ phase\ variations \tag{1.4}$$

$$r_2 \simeq r_3 \simeq \ldots \simeq r_1 \rightarrow \ amplitude\ variations \tag{1.5}$$

Replacing equations 1.3, 1.4 and 1.5 in equation 1.2, the total electric field is given by the following expression:

$$\mathbf{E}_{total} = j\eta\frac{kI_0le^{-jkr_1}}{4\pi r_1}\cos\theta\left\{1 + e^{j[kd\cos\theta+\beta]} + \ldots + e^{j(N-1)[kd\cos\theta+\beta]}\right\} \tag{1.6}$$

Another way of looking at equations 1.2 and 1.6 is:

$$\mathbf{E}_{total} = [\mathbf{E}_{single\ element\ at\ a\ reference\ point}] \times [array factor] \tag{1.7}$$

In equation 1.7, the array factor is a parameter that concerns the geometry of the array and the excitation phase i.e., it is a function of the spacing (d), number of elements, geometrical arrangement of elements, relative magnitudes and relative phases. When varying these range of parameters, it is possible to control the behaviour of the array factor. In agreement with [18, p 258], if the single element is not an isotropic source, the array factor could be calculated using equation 1.8. In addition, all of the elements that compose the array must be equal in order to use equation 1.8.

$$\begin{aligned} AF &= 1 + e^{j[kd\cos\theta+\beta]} + \ldots + e^{j(N-1)[kd\cos\theta+\beta]} \\ &= \Sigma_{n=1}^{N} e^{j(n-1)\psi},\ where\ \psi = kd\cos\theta + \beta \end{aligned} \tag{1.8}$$

The radiation pattern produced by an array could be seen as a pattern multiplication of the radiation pattern originated by the single element and the radiation pattern from the array factor. To provide a better understanding an example is granted in figure 1.5.

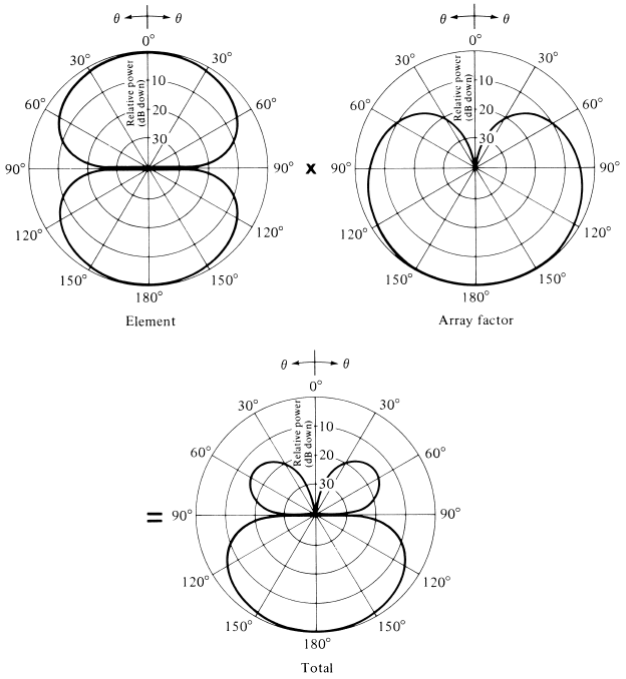

Figure 1.5: Radiation pattern illustrating the pattern multiplication considering a 2-element array of infinitesimal horizontal dipoles with $\beta = 0$ and $d = \frac{\lambda}{4}$.

Broadside Array

In this case, it is desirable to have a maximum gain value normal to the axis in which the array is placed. From the observation of figure 1.2, one could see that the fact that the antenna is to be placed on the door's casing led to this conclusion. To accomplish this task, it is necessary do design a broadside array which has a radiation pattern like the one from figure 1.6 according to [18, p 262]. In order to radiate efficiently, one has to be careful determining the characteristics of the single element.

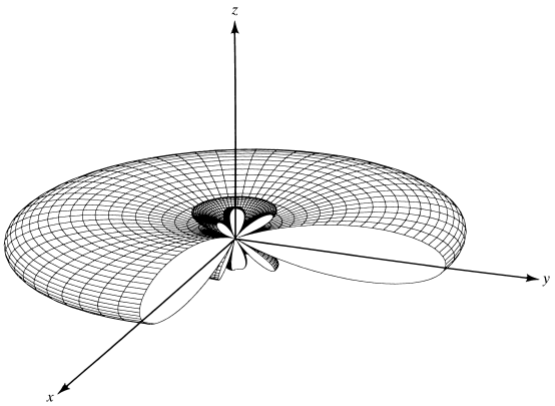

Figure 1.6: Radiation pattern from a broadside array with a spacing of 0.25λ and equal phase excitation.

To produce a radiation pattern similar to the one provided in figures 1.2 and 1.6 , the single element and the array factor should have its maximum when $\theta^\circ = 90$, which in the case of the array factor (see equation 1.8) is justified by equation 1.9:

$$\psi = kd\cos\theta + \beta = 0 \leftrightarrow \psi = kd\cos\theta + \beta|_{\theta=90^\circ} = 0 \leftrightarrow \beta = 0 \tag{1.9}$$

- d - spacing between elements

- β - phase excitation

Still considering equation 1.9, one could conclude that to achieve a broadside radiation pattern, all elements must be excited with the same phase and same amplitude ($\beta = 0$). In what concerns the distance between elements, it could be of any value except for the multiples of λ to avoid the appearance of grating lobes (multiple maxima) whenever $\beta = 0$ [18, p 262]. In conclusion, to ensure the inexistence of grating lobes, it requires a spacing between elements inferior to the wavelength.

The approach to the antenna design would be the addition of elements to the array until a good result in terms of radiation pattern is accomplished. In general, it is intended to study the behaviour of the single element and then build an array of 2 and 4 elements, which might be enough for the system that is going to be developed.

1.5.3 Brief reference to the academic research on these type of antennas

Despite what was already mentioned in section 1.3 in terms of available systems to guide the blind or the visually impaired, there was nothing found on the subject of the antennas used in those systems. Actually, none of the systems found is supposed to work like the one that is proposed in this project. Thus, it is acceptable that none of the antennas used in those systems possess the characteristics that are described in 1.1.

Before the design and simulation of the proposed antenna from section 1.5.2, it was necessary to do some research on the developments of this type of antennas. As a matter of fact, an antenna with the characteristics mentioned previously might have already been developed.

On the subject of printed dipoles, there was one particular structure that might become a good choice for using in the printed antenna array, which is described in detail in [19]. However, it was not understandable how it was possible to join several elements of that in the same substrate. It is important to emphasize that their authors claim that the structure is balanced and its radiation pattern is similar to the one produced by an ordinary dipole without balanced feeding, which would be an advantage for this project. Another article was found [20] where several of this elements were arranged into an array antenna, but each element was connected to a SMA connector i.e., there were as many SMA connectors as printed dipoles. This antenna was also discarded because the radiation pattern produced did not meet the project needs[20].

What is more, several antennas arrays consisting of printed dipoles were found, but there were always problems concerning the radiation pattern[21, 22, 23]. Usually, they would have the radiation pattern a little warped and not very uniform as it is intended to have. In addition to the shape, some of them they were not radiating backwards[24].

Despite all the ones referred before, there was one paper on printed arrays of dipoles that had the most interesting results. The authors of these paper present a design of the single element, two-element array and finally, four element array[25, 26]. In fact, the arrangement of the proposed array of four elements do not produce that radiation pattern that these project demands, because they are arranged in a different way in the substrate. However, this could be fixed by re-arranging the array. The problem with this antenna is the feeding, which the authors do not explain with clarity. They use quarter-wavelength transformers that they claim that are built according to microstrip technology, but there is no ground plane. This was the main reason for discarding this antenna, because its design was not very understandable.

For this sort of applications, there seems to be a lack of antennas that possess a radiation pattern with the characteristics described. There are many solutions for indoor location, but not indoor guidance. All in all, from what is published so far, the radiation patterns produced by those arrays, either are affected by the ground plane or the dipole's arrangement do not allow the *thin doughnut* shape. To provide a proper behaviour, the dipole structure has to be balanced, therefore a balun is required. The drawback of this type of antennas (printed antennas) is the balun existence, which is usually build in microstrip technology, and that does not allow the antenna to radiate backwards due to the ground plane area.

1.5.4 An overview on indoor propagation of RF signals

The aim of this section is to evidence some problems regarding the Radio Frequency (RF) signals propagation inside buildings. What is more, it is intended to discover what might deteriorate the performance of the printed antenna array, and consequently the overall system.

The environment that surrounds us is responsible for the *multipath* phenomena, which happens whenever there are more than one path for the signal propagation. There are three phenomena that condition the RF signal propagation, no matter if it is indoor or outdoor: reflection, refraction, diffraction and scattering. These are responsible for the signal losses, distortion and fades. On the subject of reflection, this occurs when the RF signal impinges upon an object with significant dimensions when compared to the wavelength. For instances, the earth surface and buildings originate the reflection phenomena. Although the reflected signals usually arrive later at the receiver, they might cause some problems by partially cancelling the original signal (see figure 1.7).

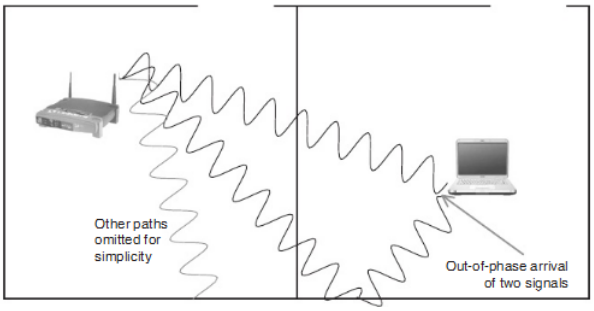

Figure 1.7: Multipath phenomena.

The phenomena of diffraction is produced when the signal is blocked by a large object with accented edges during its path leading to a significant attenuation. This attenuation might weaken so much the signal that it would not originate a reliable connection between transceivers. In what concerns the refraction, this phenomena happens when an electromagnetic wave suffers a change in its direction due to a change in its speed. This change in speed is a result of passing from one medium to another, with different refraction indices, and it happens at any angle despite 0° and 90°. All in all, it is important to provide an unobstructed path between the antennas. When working at higher frequencies, both reflection and diffraction phenomena strongly depend on the geometry of the object and also, the amplitude, phase and polarization of the incident wave. Finally, the scattering phenomena is related to the capacity of a signal in going through an object, a surface or the air. In fact, the scattering phenomena happens when the object that the signal hits has dimensions inferior to the wavelength. However, this effect could be minimized when there are a large number of objects per unit of volume. All of these happen either in indoor or outdoor environments, but one could say that these effects become worst inside buildings.

To grant an idea of how the different materials influence the signal propagation, in table 1.1 it is possible to observe the signal losses according to the type of material. The values described concern a working frequency of 2.4 GHz.

Table 1.1: Losses suffered by 2.4 GHz signal propagating indoors [27].

Attenuation range	Materials	Loss (dB)
Low	Non tinted glass, wooden door, cinder block wall, plaster	2-4
Medium	Brick wall, marble, wire mesh or metal tinted glass	5-8
High	Concrete wall, paper, ceramic bullet-proof glass	10-15
Very high	Metal, silvering (mirrors)	>15

In conclusion, the working frequency for this project would be the 2.4 GHz, which is the WLAN working frequency, thus suitable for indoor RF signal propagation. The system that is intended to be developed would not interfere with the WLAN signals because it does not contain any information

in it. In addition, it is important to consider that all of the objects surrounding the antenna would lead to undesired effects in the its behaviour, specially in its radiation pattern. When testing the antenna on the door's casing, it is necessary to verify which type of materials are surrounding the door's entrance in order to understand and solve possible problems that might arise.

Chapter 2

Printed dipoles without balanced feeding

2.1 Brief introduction

A printed dipole consists of two arms made of a conducting material and stamped in a dielectric substrate. Similar to the linear wire dipole, these two arms are separated by a specific spacing and the their length vary according to the frequency that it is intended to work. Other important considerations are the thickness of the dielectric and the width of the arms. In figure 2.1 it is possible to observe a generic structure of a printed dipole.

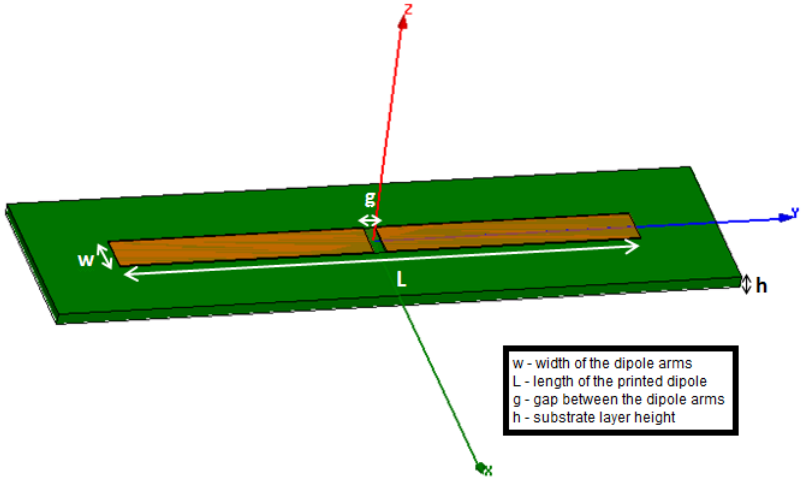

Figure 2.1: General design of a printed dipole.

To design a linear wire dipole it is necessary to choose the resonance frequency and then, calculate the wavelength using the formula $\lambda = \frac{c}{f}$, because the electromagnetic waves propagate mainly in free space. Once the wavelength is calculated, it is possible to obtain the dimensions of the arms or the total length (L) of the printed dipole. Usually, the variable L is a fraction or a multiple of the wavelength and its value is related with the desired shape for the radiation pattern and, consequently, with gain or directivity. However, when the aim is to design a printed dipole, there are no formulas to be used to estimate L or other parameter. A good start point is to follow the steps that were described before for the linear wire dipole, and then enhance the results using the simulator. The radiation pattern shown in figure 2.2 belongs to a unknown wavelength linear wire dipole which is equal to the one originated by a printed dipole, as proved in the following sections.

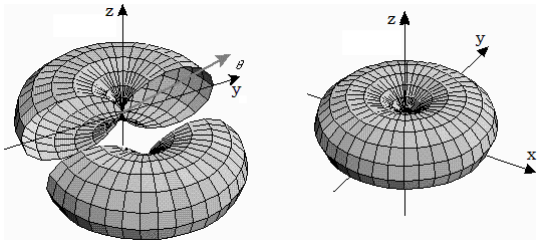

Figure 2.2: 3D radiation pattern of a linear wire dipole [28].

Every simulation provided in this work was accomplished with an electromagnetic field simulator named HFSS from Ansys. The main goals of this study are to identify the modifications in the radiation pattern and in the return loss plot when the printed dipole dimensions vary. In order to do the matching of an antenna to a specific frequency, it is necessary that its return loss trace has a value of at least -10 dB around the desired frequency. This is also what defines the bandwidth of the antenna, i.e., the range of frequency values that has a return loss value equal or inferior to -10 dB. The printed dipole presented is designed for the 2.4 GHz, which grants us a wave length of $\lambda = \frac{3\times10^8}{2.4\times10^9} = 0.125m = 125mm$. What is more, the characteristics of the materials used are provided in table 2.1.

Table 2.1: Characteristics from the materials used in the printed dipole design according to the simulator.

Material	Characteristics
Copper	$\varepsilon_r = 1, \mu_r = 1, \sigma = 5.8 \times 10^8 siemens/m$
FR-4	$\varepsilon_r = 4.4, \mu_r = 1, tg\delta = 0.02$

2.2 Printed dipole - topology 1

The first proposed topology is a printed dipole whose arms are stamped in the same side of the substrate layer (see figure 2.1). To begin with, the feeding port of the dipole was exactly placed between both arms, in other words, the connection to the coaxial cable is not considered. After the first set of simulations, the connection to the coaxial cable will be considered to verify its influence on the previous results.

2.2.1 Topology 1 - Without the SMA connector

L sweep - total length of the printed dipole

Since it is not possible to calculate the dimensions of a printed dipole, the simulator HFSS was used to find the most appropriate value for L. As suggested before, the start point for the total length of the dipole was $\frac{\lambda}{2} = 62.5mm$, which is the half-wavelength for the 2.4 GHz. It is important to refer that L includes the length of both arms and the width of the gap between them. To perform this simulation the constant values shown in table 2.2 were used for the dimensions of the dipole.

Table 2.2: Printed dipole dimensions for the L sweep.

Parameter	Value (mm)
w	2.9
g	0.8
h	0.8
Conductor thickness	0.1

The result produced when the entire length of the printed dipole was 62.5 mm is observable in

figure 2.3. Instead of the 2.4 GHz, which has a return loss value of approximately -3.2 dB, the dipole is matched to 1.91 GHz with $S_{(1,1)} = -24.5319$ dB. It was also decided to provide the impedance plot for this value of the dipole's length (see figure 2.4). In this plot one can see that the antenna has an impedance value for the 1.91 GHz very acceptable in terms of reactance (if one wanted, its value could be ignored) - $Z_L = 55.7896 - 2.4331j\ \Omega$ - which proves the fact that the half-wavelength dipoles are widely use due to the ease of matching as stated in section 1.5.1.

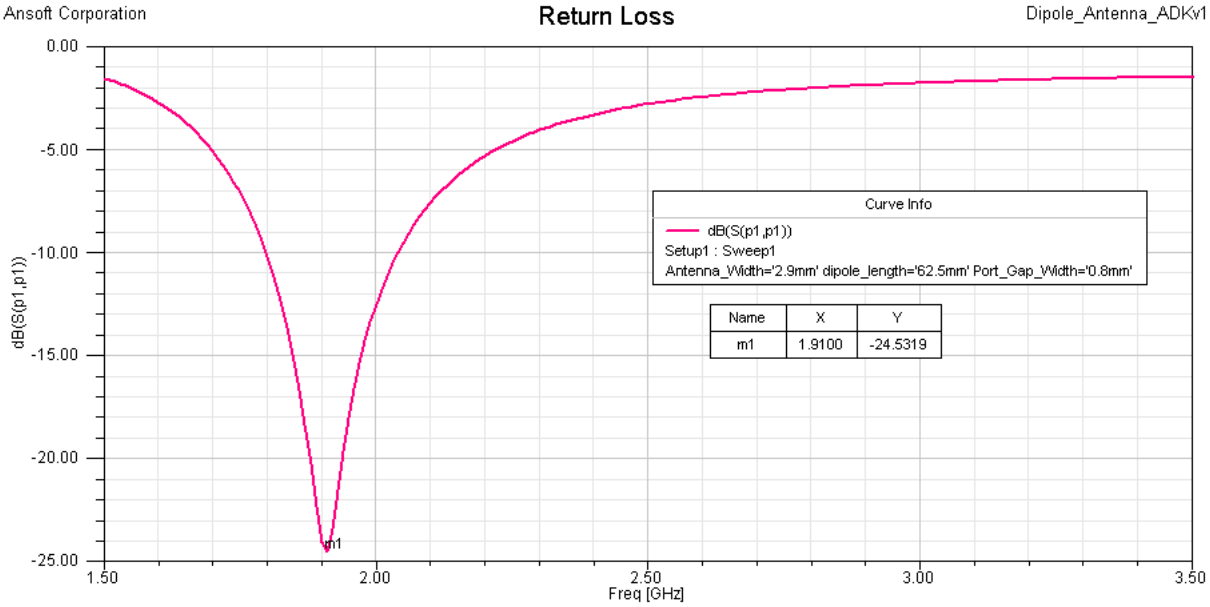

Figure 2.3: Return loss plot considering L=62.5 mm.

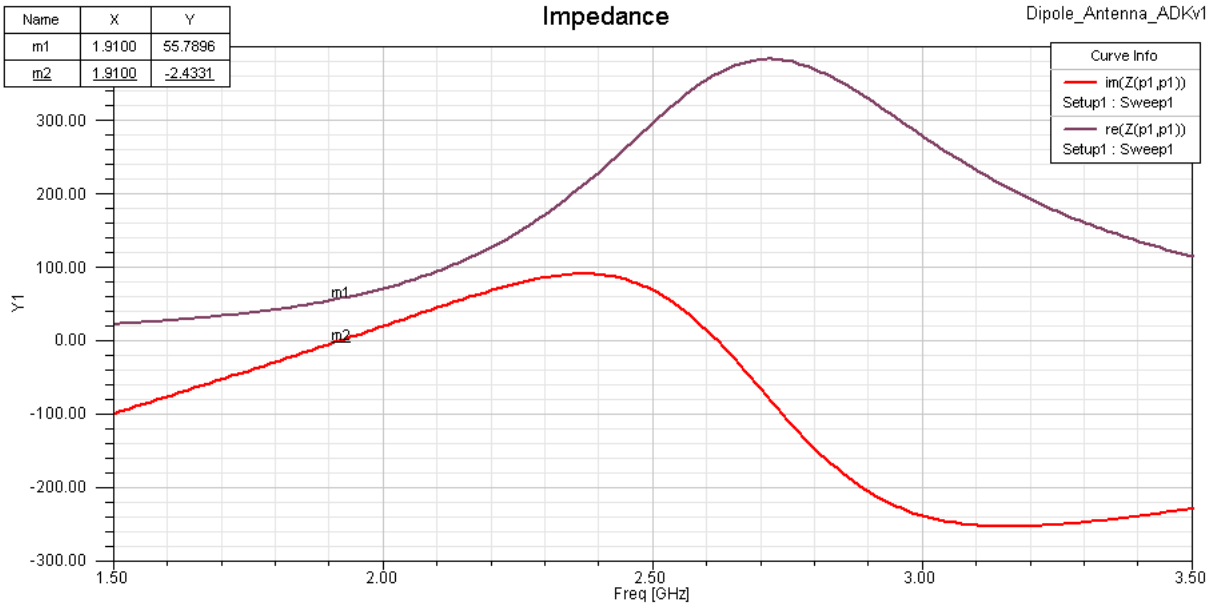

Figure 2.4: Impedance plot considering L=62.5 mm.

To find a more suitable length for the dipole arms, a sweep between 30 mm and 62.5 mm was performed in order to understand how the increase in the L parameter had influence in the behaviour of the return loss trace.

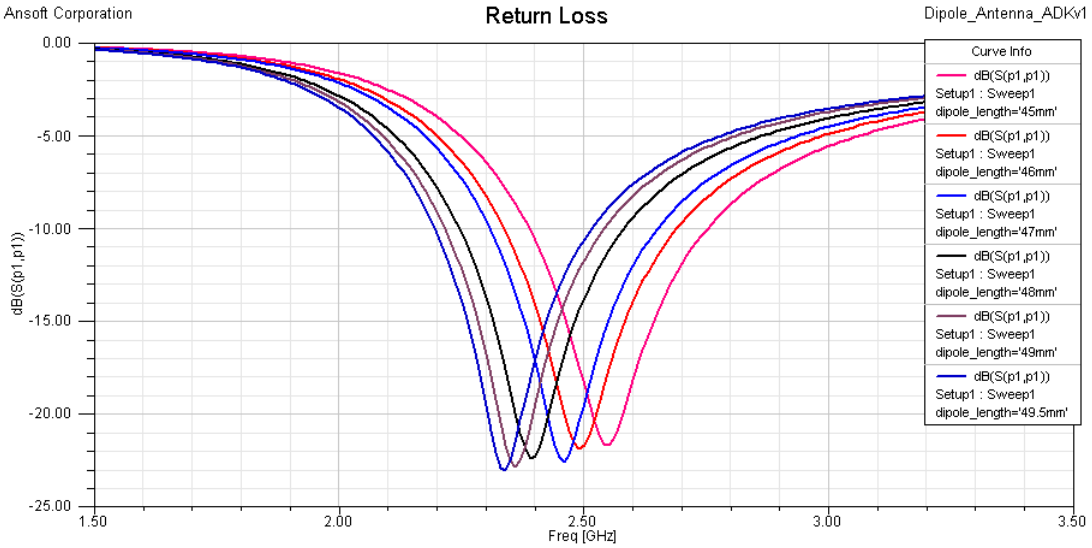

Figure 2.5: Return loss plot obtained from L sweep.

From the given picture (figure 2.5), it is proved that with the lengthening of L, which is represented by *dipole_ length* in the plot, the $S_{(1,1)}$ coefficient shifted to the left. In what concerns the numeric value of return loss, one can conclude that there were no significant changes within the traces. Also, one can state that the most suitable value for the total length of the printed dipole would be L=48 mm, considering a working frequency of 2.4 GHz. In this series of simulations, the radiation pattern produced was observed as well, but there were no major differences within the range of L values. It is important to mention that when L equals 100 mm for example, the radiation pattern narrows. In figure 2.6, it is shown the radiation pattern for L=48 mm, which represents the most suitable length for the dipole arms plus the width of the gap for the desired resonance frequency.

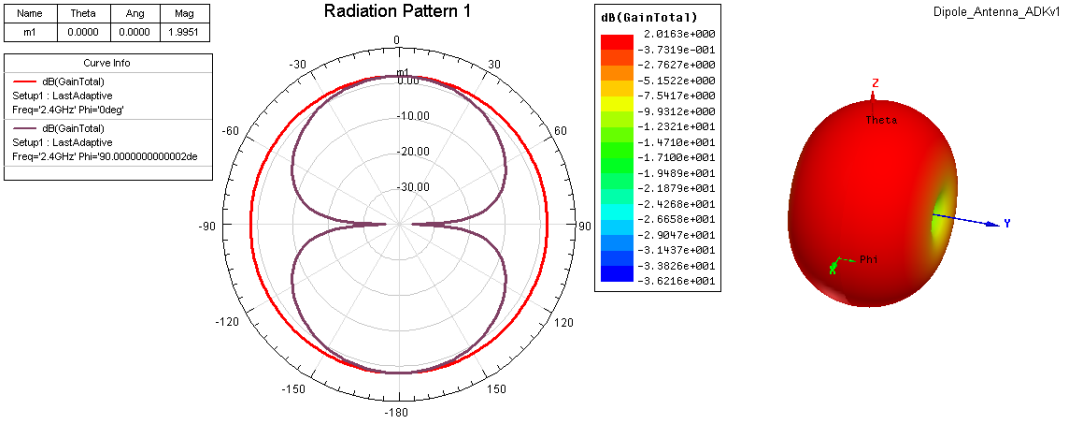

Figure 2.6: Radiation pattern plot when L=48 mm.

w sweep - width of the dipole arm

The next swept parameter was the width of the dipole arms while maintaining the rest of the dimensions constant (see table 2.3).

Table 2.3: Printed dipole dimensions for the w sweep.

Parameter	Value (mm)
L	48
g	0.8
h	0.8
Conductor thickness	0.1

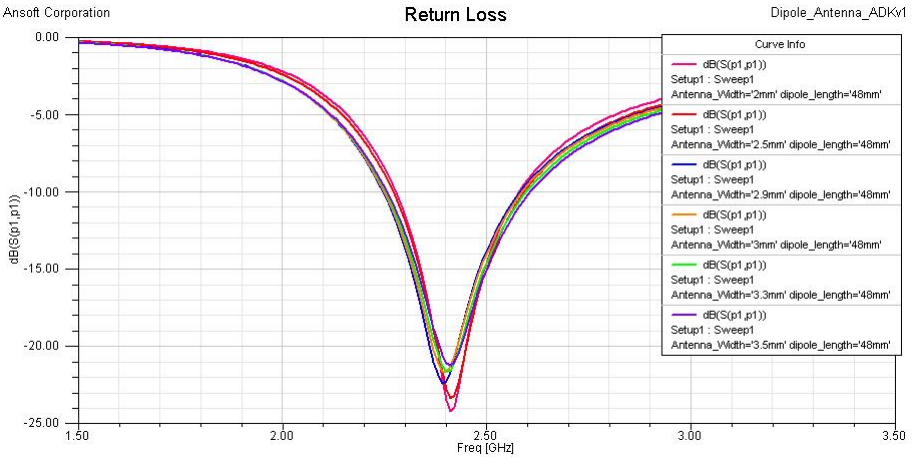

Figure 2.7: Return loss plot obtained from w sweep.

As one can see, the variance of w did not produce a shift in frequency as did the variance of L. In fact, its influence lies in the matching of the antenna but, even though, there were no significant differences within the traces. Any of the values tested would meet the project needs i.e., no matter what w was chosen from the range of values used, the return loss traces are adequate for the 2.4 GHz ($S_{(1,1)}$ is always below -10 dB). As for the radiation patterns produced by the w sweep, they resemble the one obtained when L=48 mm, which is the most adequate value considering the desired working frequency.

g sweep - width of the gap between the dipole arms

From the previous simulations, it was noticed that some values for the dipole parameters met the specifications, therefore those values were used as constants to perform the sweep of the width of the gap between the dipole arms (see table 2.4).

Table 2.4: Printed dipole dimensions for g sweep.

Parameter	Value (mm)
L	48
w	2.9
h	0.8
Conductor thickness	0.1

In figure 2.8 one can see the results achieved for a port gap width between 0.1 mm and 1.3 mm, which is enough to realize the influence of width in the return loss trace. It is also important to mention that g is called *Port_Gap_Width* in the plot from figure 2.8.

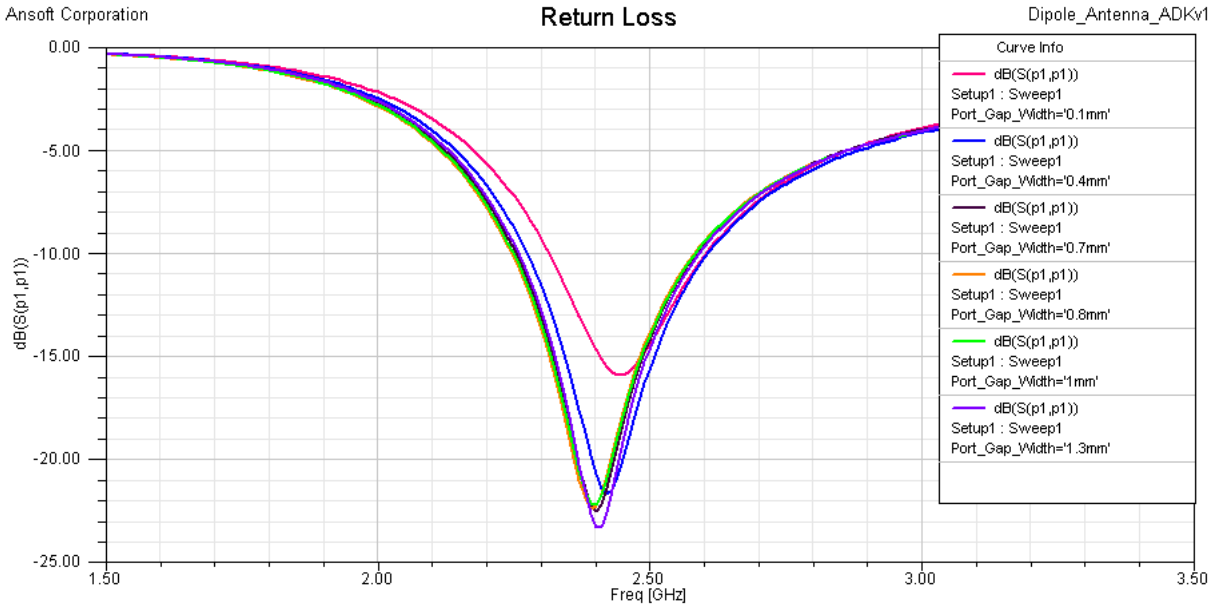

Figure 2.8: Return loss plot obtained from g sweep.

According to the return loss plot from figure 2.8, it is clear that the wider the gap between the dipole arms becomes, the better the antenna is matched to the 2.4 GHz. On the other hand, the decrease of g originated a little shift in frequency and a increase in the return loss values. In conclusion, it was proved that the value of g is determined by the specifications set for the antenna one aims to design. The radiation pattern remained very similar to the one presented in figure 2.6).

h sweep - thickness of the dielectric

To perform this simulation the values provided in table 2.5 were used. In this sweep only two values were tested for the dielectric substrate, 0.8 mm and 1.6 mm, because these are the common thicknesses for FR-4 substrate.

Table 2.5: Printed dipole dimensions for the h sweep.

Parameter	Value (mm)
L	48
w	2.9
g	0.8
Conductor thickness	0.1

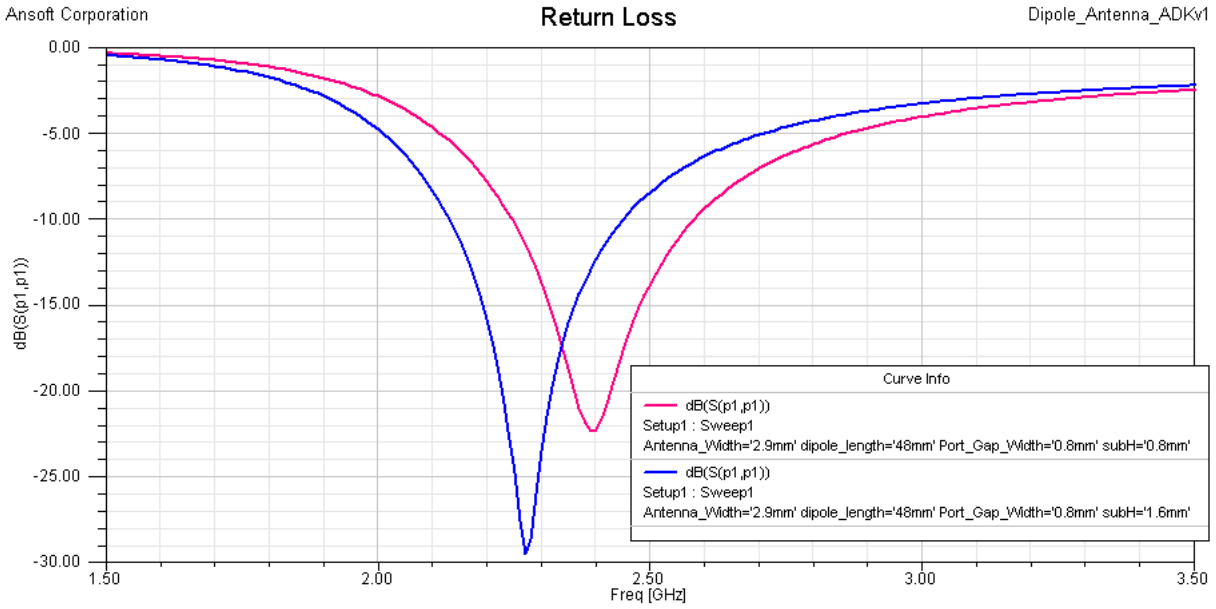

Figure 2.9: Return loss obtained with the sweep of the height of the dielectric.

From the observation of the plot from figure 2.9, it is proved that changing the dielectric height from 0.8 mm to 1.6 mm produced a shift in the frequency domain, but led to a worse matching considering a frequency of 2.4 GHz. Moreover, it might be necessary to adjust the dipole length again in order to have the antenna properly matched. It was observed that the radiation pattern is not much influenced by the dielectric thickness. In fact, the shape and maximum gain was the same when considering the two thicknesses and it maintained the shape already shown in figure 2.6.

2.2.2 Topology 1 - Addition of two conductors to feed the dipole

In this part of the work it had been decided to add two conductors to feed the dipole as exemplified in figure 2.10. The main reason for this change in the dipole's structure was the impossibility of doing the type of feed presented in section 2.2.1 if one wants to connect a coaxial cable to the dipole. In further sections, these two copper strips will be used to join a SMA connector.

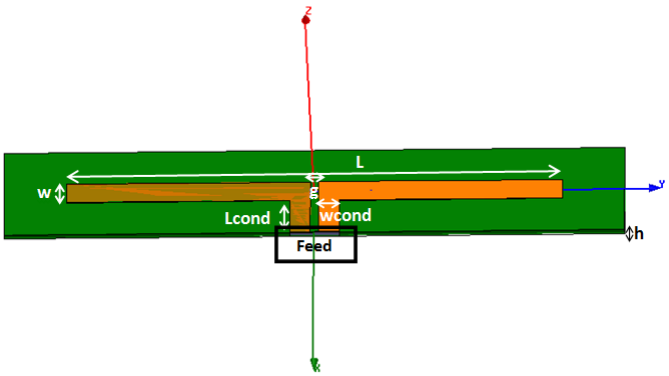

Figure 2.10: 3D-model used in simulations.

This time the results accomplished when L, w, g and h were swept would not be shown, because the dipole had the same behaviour of the previous structure (see figure 2.2). A set of suitable values obtained through the sweep of the parameters belonging to the printed antenna is provided in table 2.6. The results produced by the use of these dimensions could be seen in figure 2.11.

Table 2.6: Suitable dimensions for the printed dipole.

Parameter	Value (mm)
L	48
w	2.9
g	0.8
h	0.8
Conductor thickness	0.1
wcond	2.9
Lcond	5.075

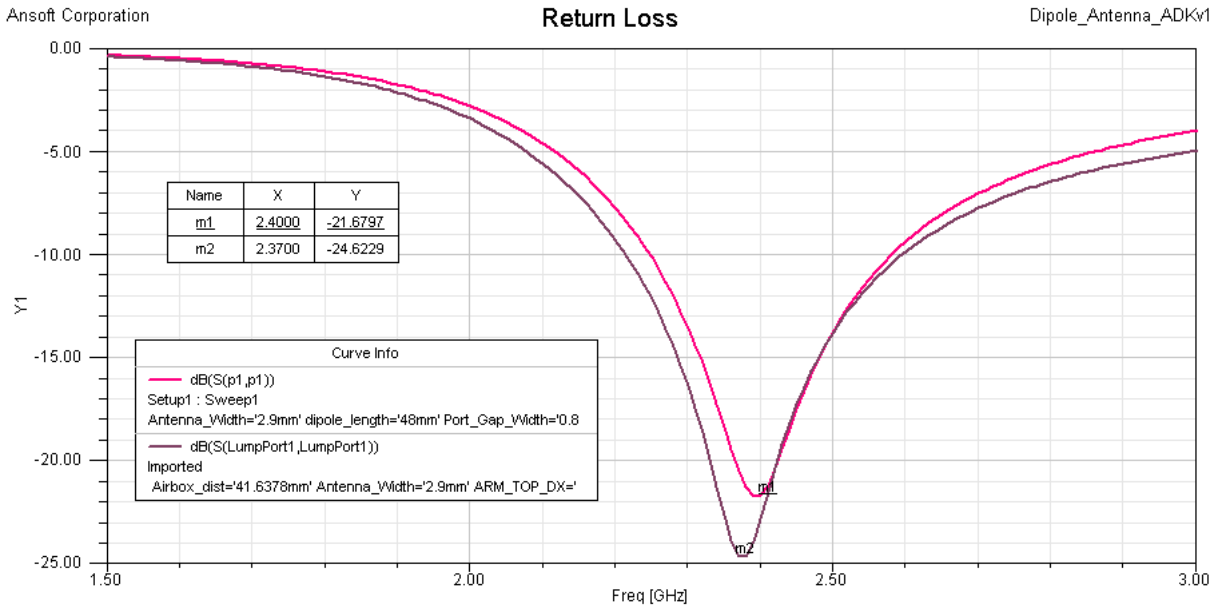

Figure 2.11: Return loss plot regarding values from table 2.6 and the return loss trace before and after the addition of a pair of conductors.

According to the plot from figure 2.11, it is proved that the addition of the feed conductors caused a slight shift in the return loss trace if *wcond*=2.9 mm, i.e., when the width of the conductors equals the width of the dipole arms. Moreover, this modification also decreases the return loss value and it seems to increase the bandwidth of the antenna. In what concerns the behaviour of the radiation pattern, there were no significant differences in shape or even gain when the two feed conductors were added. Actually, its shape continued resembling a *doughnut* and the maximum gain rounded the 2 dBi.

wcond sweep - width of the feed conductors

Since it had been decided to perform simulations considering the addition of two conductors, it was necessary to sweep the width of the conductors to observe their influence on the dipole's behaviour. Table 2.7 provides the values used to perform this simulation.

Table 2.7: Printed dipole dimensions for *wcond* sweep.

Parameter	Value (mm)
L	48
w	2.9
g	0.8
h	0.8
Conductor thickness	0.1
Lcond	5.075

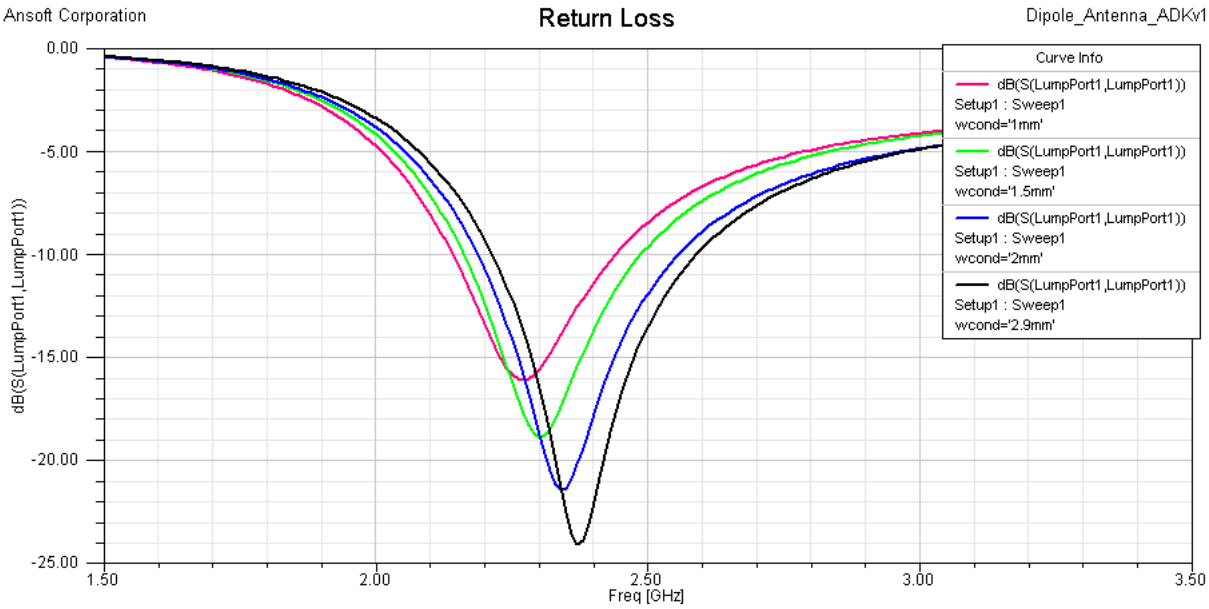

Figure 2.12: Return loss plot obtained from *wcond* sweep.

Based on figure 2.12 the *wcond* variance produces significant changes in the return loss trace. According to the simulations performed, it was observed that the best results are obtained when the width of the dipole arms are the same as the width of the conductors responsible for the connection to the SMA. Another problem is that if we widen too much the arms, they become closer to the SMA pins leading to inappropriate results. In what concerns the radiation pattern, it is possible to say that the width of the conductors does not influence much the shape and gain of the antenna.

Lcond sweep - length of the feed conductors

This is the last sweep that was done considering this topology. The return loss traces in the plot from figure 2.13 were obtained using the dimensions from table 2.8.

Table 2.8: Printed dipole dimensions for the *Lcond* sweep.

Parameter	Value (mm)
L	48
w	2.9
g	0.8
h	0.8
Conductor thickness	0.1
wcond	2.9

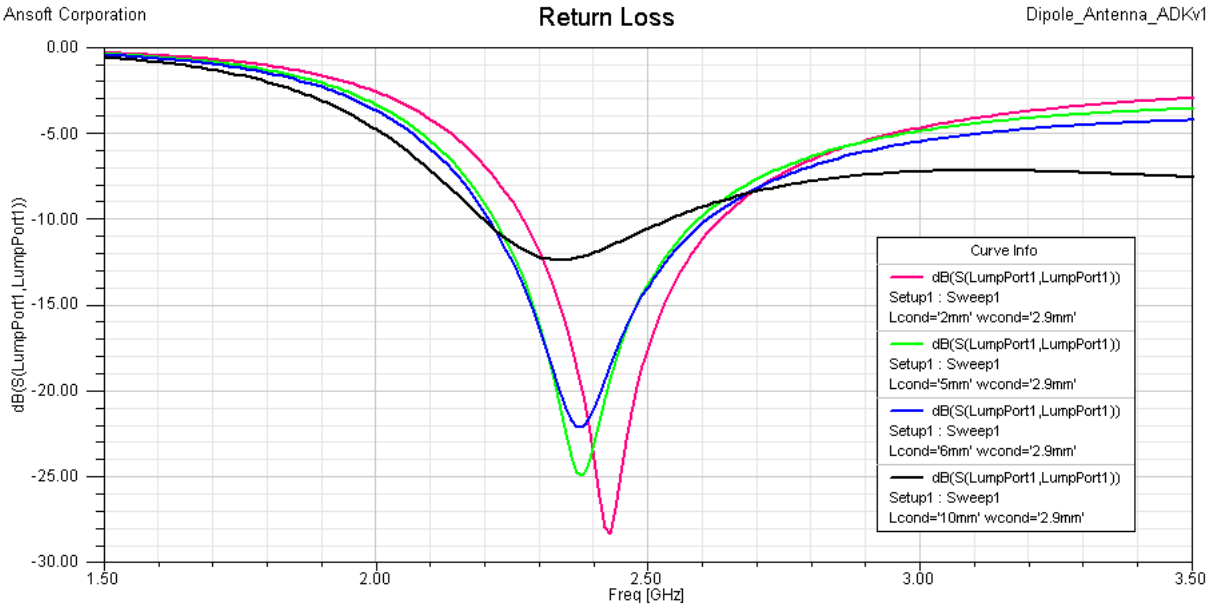

Figure 2.13: Return loss plot for the *Lcond* sweep.

Although the plot from figure 2.13 only shows the results for four different values of *Lcond*, they are enough to see that there is a significant influence on the antenna behaviour when the *Lcond* is lengthened. Looking at the plot it is possible to state that the most appropriate value for *Lcond* is either 2 mm or 5 mm. In short, one shall not choose a value for *Lcond* too large in order to avoid mismatching.

When looking at the radiation pattern, one could conclude that the addition of the conductors did not have a significant influence either in shape or gain. Its maximum gain still rounded the 2 dBi and its shape is similar to the one from figure 2.6.

2.2.3 Topology 1 - Addition of the SMA connector

The last part of the first series of simulation was studying the effect of the SMA connector in the printed antenna (see figure 2.14). The model used is provided below, and it important to notice that the variables *w, L, g, wcond* and *Lcond* refer to the same parameters shown in the figure 2.10, therefore they are not represented in this model. In addition, the SMA model was designed from scratch because it is not provided by the simulator.

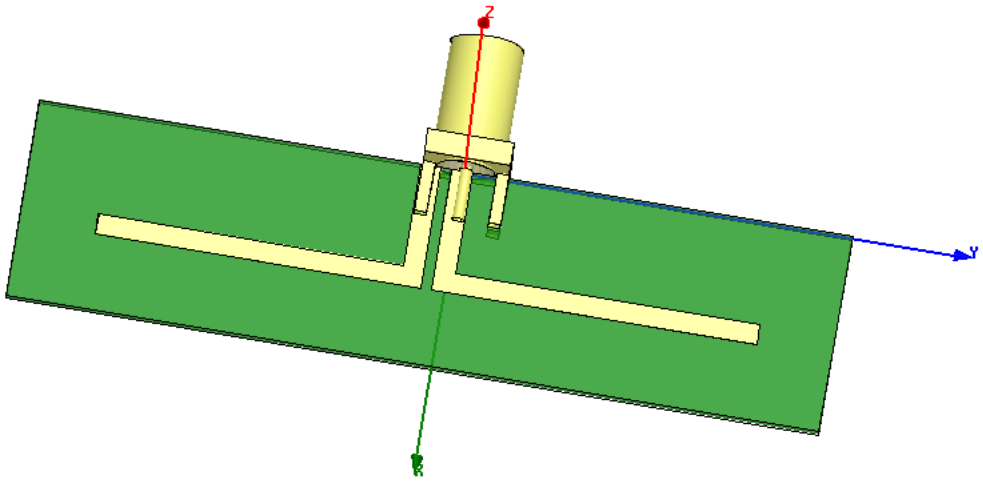

Figure 2.14: 3D-model used in simulations.

To begin with it was decided to merge the two cases already studied in previous sections and this new one with the SMA connector in one plot, so it would be possible to distinguish the differences (see figure 2.15). Table 2.9 shows the dimensions considered to plot these traces.

Table 2.9: Printed dipole dimensions.

Parameter	Value (mm)
L	48
w	2.9
g	0.8
h	0.8
Conductor thickness	0.1
wcond	2.9
Lcond	5.075

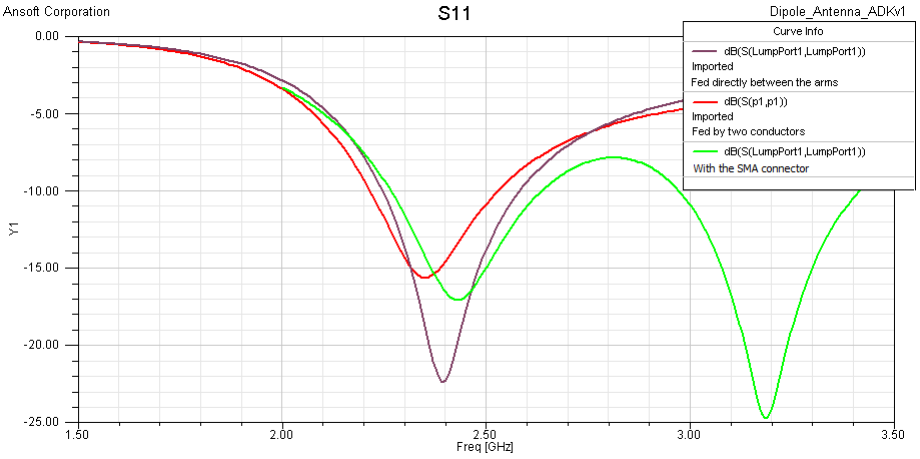

Figure 2.15: Return loss regarding the three changes in the printed dipole structure.

When the dipole is fed directly between its arms the return loss value is smaller than when two conductors were added, which leads to the conclusion that the two conductors introduce a slight mismatching. Moreover, they also originate a slight shift in frequency as well. The problem arises when the SMA connector was added, which caused a curious effect in the return loss behaviour. Apparently, the printed dipole is matched between approx. 2.28 GHz and 2.64 GHz, and then between approx. 2.98 GHz and 3.5 GHz. Based on the results of previous simulations, a sweep of the length of the conductors responsible for feeding the dipole and a sweep of the width were performed to see either if the printed dipole continued with the same behaviour or if it would be possible to eliminate the second resonance.

Adjusting the dipole parameters to meet the desired resonance frequency

To adjust the dipole's parameters in order to meet the desired results, the behaviours already observed were taken into consideration and also the help of the simulator. As figure 2.14 shows, the arm that is connected to the ground pin is very close to the one that is connected to the centre pin, so an adjustment of the parameters was done with the help of the simulator to place them as far as possible from each other.

Hinge on the work done, the task for this section was trying to reach values for the dipole dimensions that would provide adequate results for the 2.4 GHz. These values are expressed in table 2.10.

Table 2.10: Printed dipole dimensions that eliminate the second resonance of the antenna.

Parameter	Value (mm)
L	46
w	1.5
g	0.8
h	0.8
Conductor thickness	0.1
wcond	1.5
Lcond	6

Since the sweep of L, w and g did not eliminate the effect presented in figure 2.15 and did not lead to the expected results, the printed dipole was simulated by assuming a range of values for the length and width of the feed conductors. In this case the distance and width of the conductors were specially contemplated due to the SMA pins.

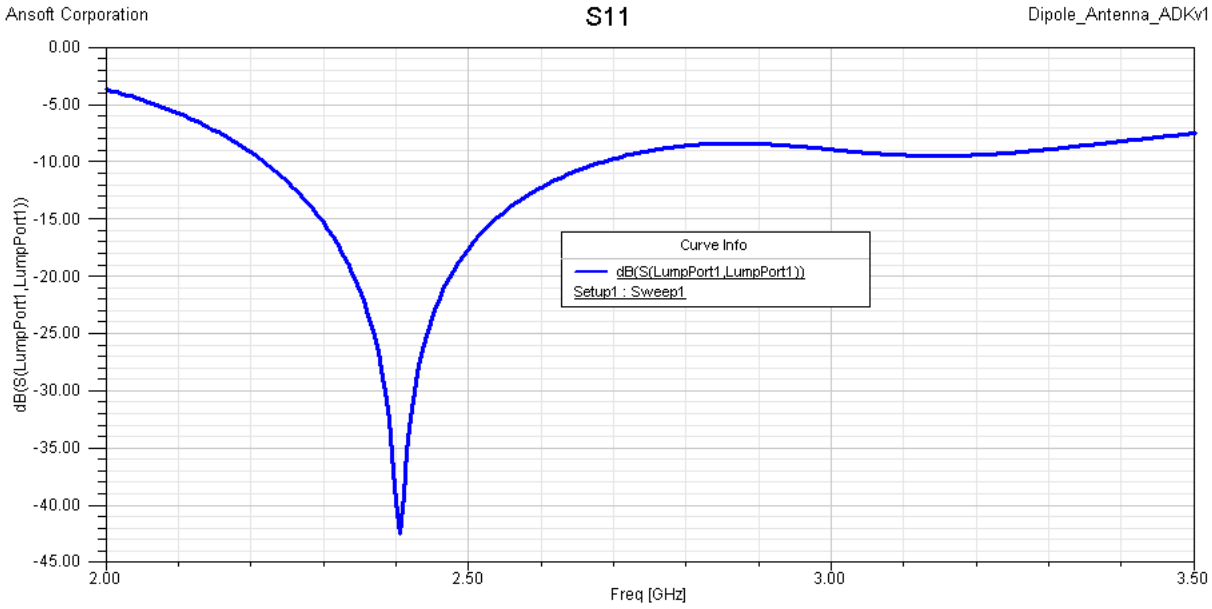

Figure 2.16: Return loss regarding the values from table 2.10.

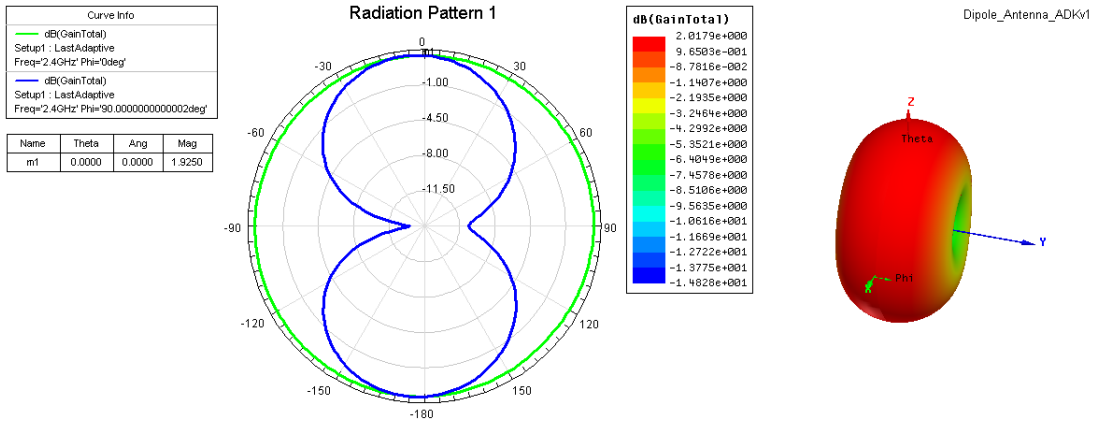

Figure 2.17: Radiation pattern regarding the values from table 2.10.

With the help of the simulator, it was possible to eliminate the effect of the addition of the SMA

connector by sweeping the width and length of the added conductors, as it is seen in figure 2.16. However, the radiation pattern could not be corrected and it is possible to conclude that it became pretty warped when compared to figure 2.6 (see figure 2.17). Probably, this happened due to the physical size of the antenna when compared to the size of the SMA connector.

2.3 Printed dipole - topology 2

The second topology that it is aimed to present is a printed dipole in which the arms lay in the opposite sides of the substrate layer, as it is shown in figure 2.18. In this situation the simulation without the pair of conductors was not performed because with that configuration is not possible to join the SMA connector, which is also valid for topology 1. The simulation from topology 1 without the conductors was done in order to analyse the effect on the return loss and radiation pattern traces of placing a two pair of conductors in the dipole's structure.

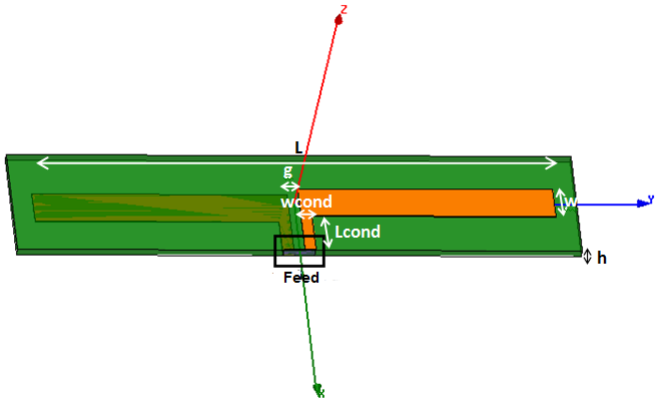

Figure 2.18: 3D-model used in simulations.

2.3.1 Topology 2 - Without the SMA connector

The 3D-model used to perform the next set of simulations is shown in figure 2.18. The plot provided below shows the return loss from the similar topology 1 (see section 2.2.2) and this topology, all regarding the dimensions presented in table 2.11.

Table 2.11: Printed dipole dimensions.

Parameter	Value (mm)
L	48
w	2.9
g	0.8
h	0.8
Conductor thickness	0.1
wcond	2.9
Lcond	5.075

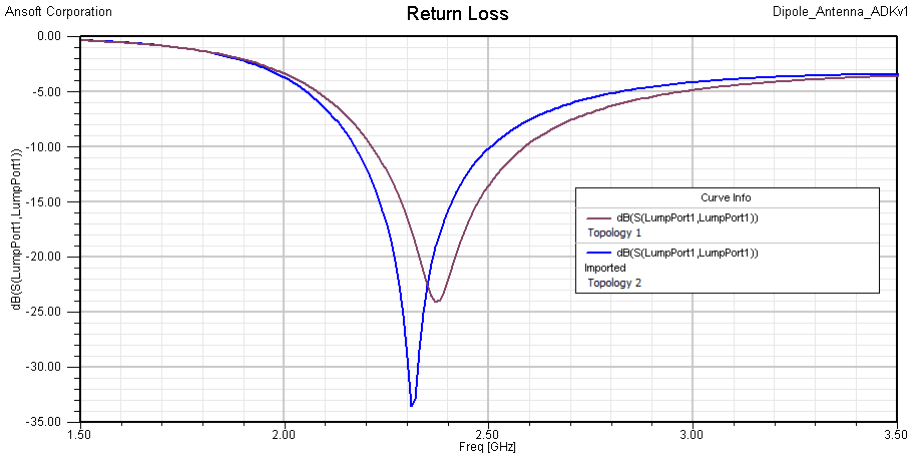

Figure 2.19: Return loss obtained from the two topologies.

In comparison with topology 1, there is a slight shift in frequency in the return loss trace when the arms are printed on opposite sides of the substrate layer. However, the return loss value is lower than the first case which represents a better antenna matching. When one looks at the radiation pattern, again compared with the one from topology 1, one could conclude that it remains unaltered in terms of gain and shape.

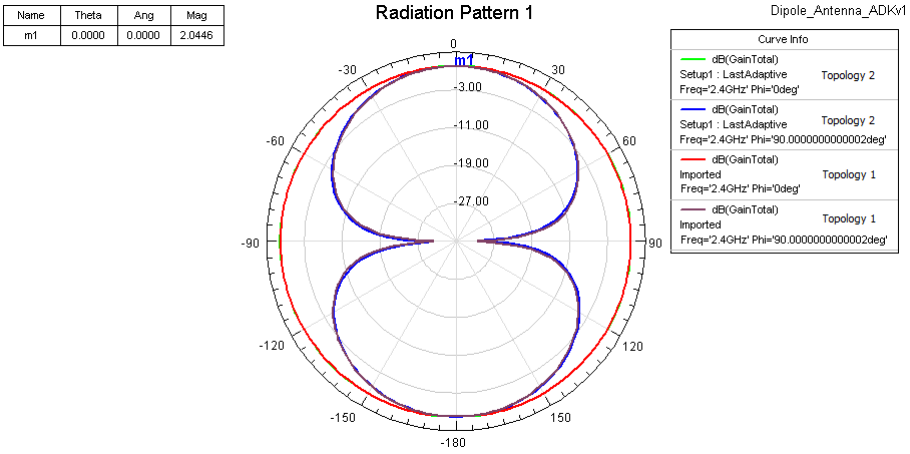

Figure 2.20: Return loss obtained from the two topologies.

Parametric study of the dipole dimensions *L, g, w, h, wcond* and *Lcond*

To avoid repetition it was decided to merge the different simulations of the various parameters into one section, for the reason that the only modification made to the antenna structure was printing the arms on opposite sides of the substrate layer. As result, the sweeps led to the same behaviours of topology 1, except for the L, w and h sweeps. Thus, these two simulations are referred with detail in this section.

Contrary to what was done in section 2.2 to determine the most adequate value for the length of the dipole when considering a resonance frequency of 2.4 GHz, i.e. beginning simulations using $L = \frac{\lambda}{2}$, this time the start point for L was 48 mm (see figure 2.20). The rest of the dimensions used in the simulations are provided in table 2.11.

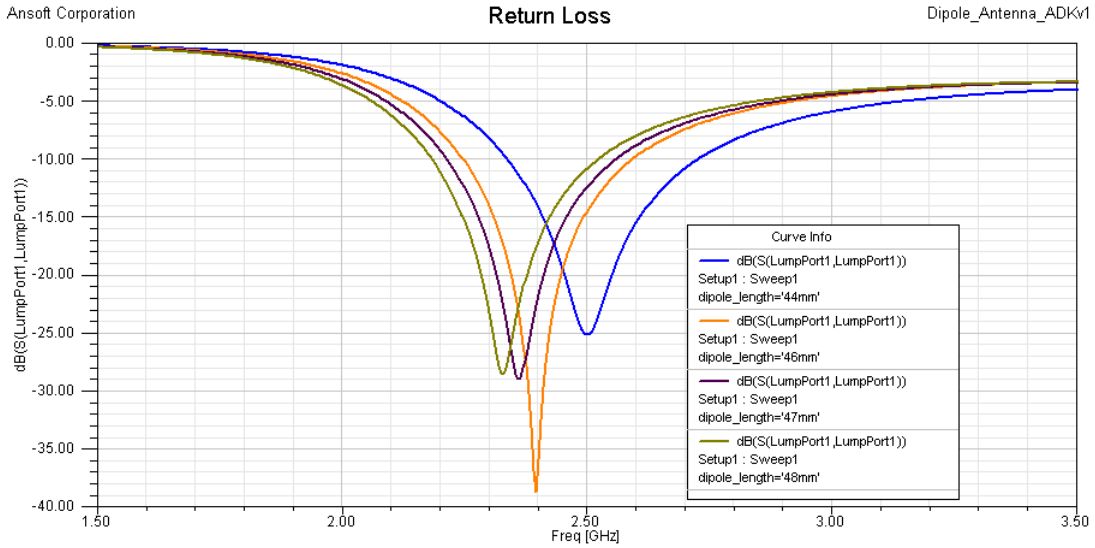

Figure 2.21: Return loss obtained from the L sweep.

In this case the most appropriate value for L is 46 mm in spite of 48 mm from topology 1. One possible reason that might explained this change in the total length of the printed dipole is the fact that the two arms are now separated by a dielectric with a specific thickness. The addition of the feed conductors would be discarded as an explanation, because they did not influence the length of the dipole in the topology 1. On the subject of radiation pattern, there are no changes from topology 1 to topology 2, in other words, its gain rounded the 2 dBi and its shape resembled a *doughnut*.

To perform the w sweep the values used are the same from table 2.11 except the fact that w is not a constant and the considered dipole length is 46 mm, which is not represented in that table.

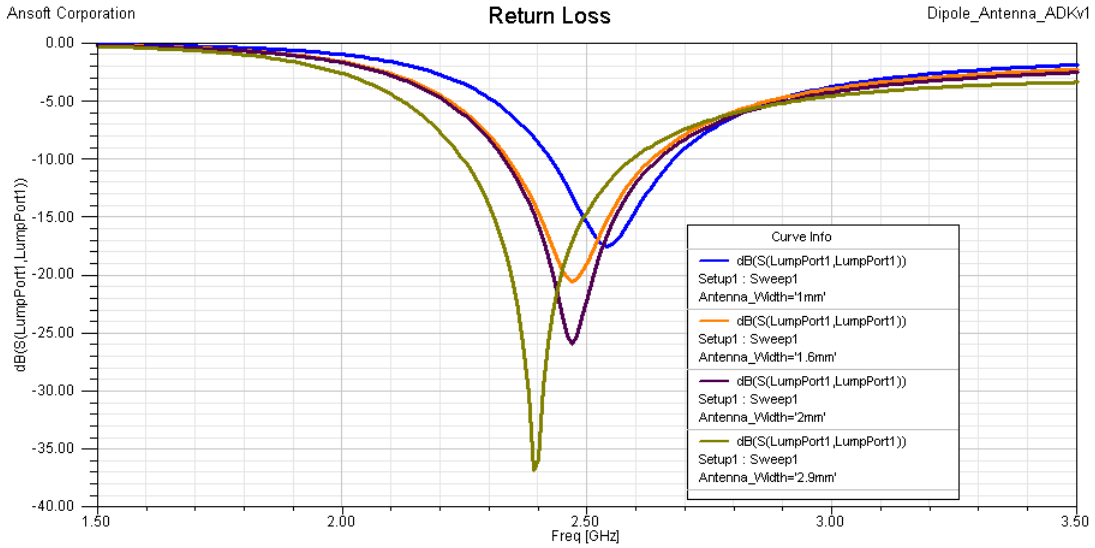

Figure 2.22: Return loss obtained from the w sweep.

The plot from figure 2.22 reveals a significant influence of the width of the arms in the antenna's behaviour, mainly in the matching to the desired resonance frequency. On one hand it introduces a slight shift in frequency, i.e., if one widen the arms the return loss trace shifts left. On the other hand, if one decreases the width of the arms, the return loss has a lower value and the antenna is better matched. It is important to refer that in the plot from figure 2.22 w is named *Antenna_Width* in the legend. Similar to what happened in topology 1, the variation of w did not induced a change in the radiation pattern plot.

The last simulation concerning topology 2 would be the sweep of the dielectric thickness. As

mentioned before only two values were to be used for h, 0.8 mm and 1.6 mm because they are the most common when using FR-4 substrate. The results presented were obtained using the dimensions granted in table 2.11, but considering L=46 mm.

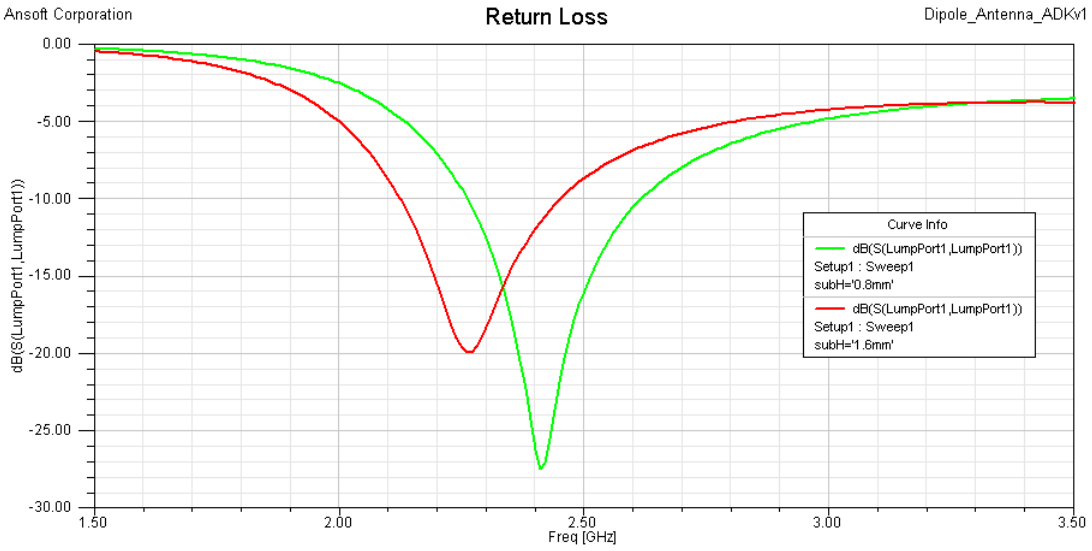

Figure 2.23: Return loss plot obtained from the h sweep.

Similar to the h sweep from section 2.2.1, when the dielectric thickness changed from 0.8 mm to 1.6 mm, there was a noticeable shift to the left in frequency. In contrast with the h sweep from topology 1, the thicker the dielectric is, the better matched the antenna becomes. This might be a result of the position of the arms in this dipole design. What is more, the radiation pattern is not influenced by the variation of the dielectric thickness in terms of gain or shape.

2.3.2 Topology 2 - Addition of the SMA connector

In this section the effects caused by introducing a SMA connector in the antenna's performance were analysed. The model used is provided below and it important to notice that the variables w, L, g, $wcond$and $Lcond$ refer to the same parameters shown in the figure 2.18, therefore they are not represented in this model.

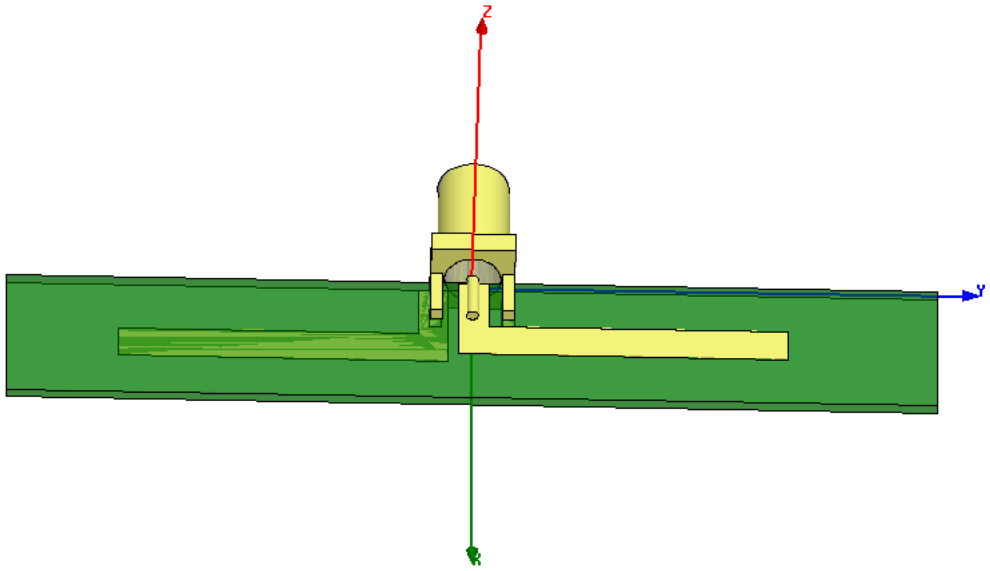

Figure 2.24: 3D-model used in simulations.

To analyse the effects produced by the SMA connector, the values from table 2.12) were assumed:

Table 2.12: Suitable values for printed dipole parameters at 2.4 GHz

Parameter	Value (mm)
L	46
w	2.9
g	0.8
h	0.8
Lcond	5.075
Conductor thickness	0.1
wcond	2.9

The dimensions provided for the parameters in the table 2.12 originated the radiation pattern and return loss plot shown in figure 2.25 and 2.26. In general, one can observe that the printed dipole has a radiation pattern similar to a *doughnut* with a maximum gain of 2.0293 dBi, despite the slight asymmetry noticed in figure 2.26. Furthermore, its return loss value for the 2.4GHz is about -37 dB, which is highly acceptable for the 2.4 GHz resonance frequency. In the figures below is also possible to see the effects produced by placing a SMA connector, which clearly influences the radiation pattern symmetry. These plot was also obtained using the values from table 2.12.

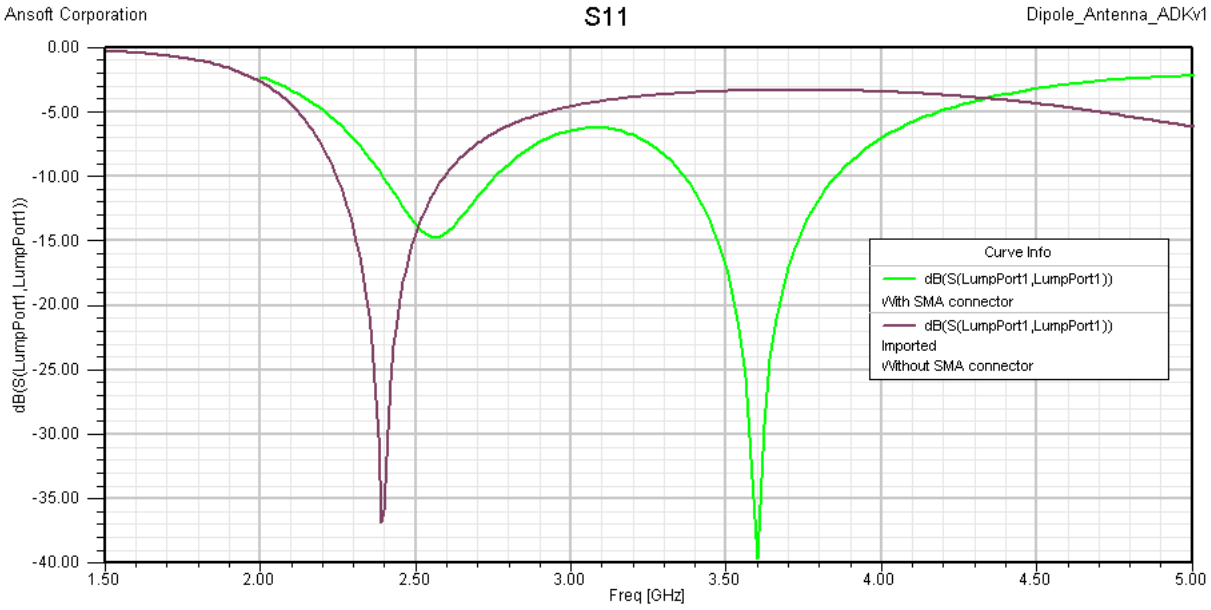

Figure 2.25: Return loss plot of the printed dipole before and after the addition of the SMA connector.

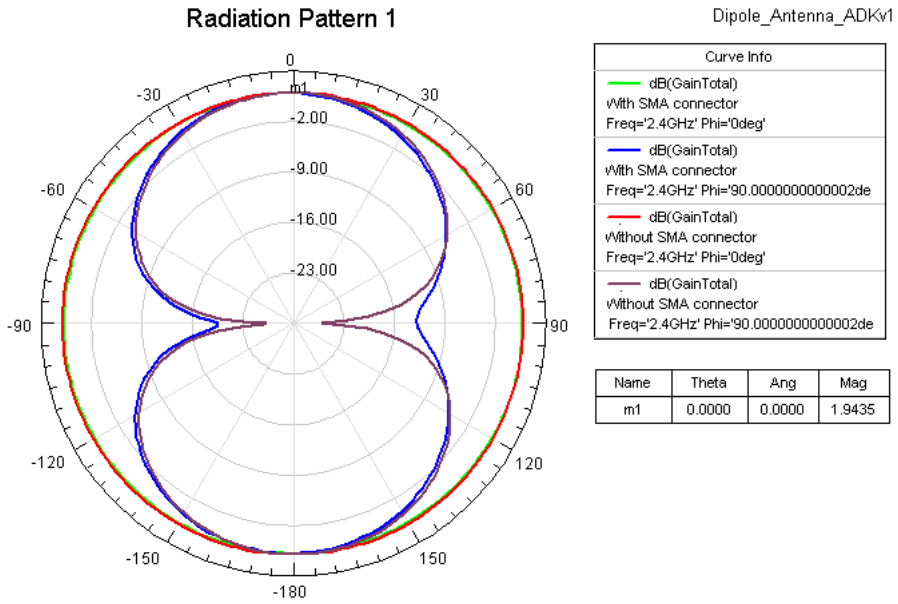

Figure 2.26: Radiation pattern of the printed dipole before and after the addition of the SMA connector.

Adjusting the dipole parameters to meet the resonance frequency

In this section, the return loss plots and radiation patterns obtained from the sweep of the main parameters that define the dipole geometry would not be provided, because they behave as shown in previous simulations. Using the HFSS simulator, all parameters were swept until an adequate behaviour for the printed dipole was obtained. The results achieved are provided in figures 2.27 and 2.28. These results were achieved with the values from table 2.12, but modifying the dipole length from 46 mm to 48 mm, the *Lcond* to 6 mm and the *w* and *wcond* to 1.5 mm.

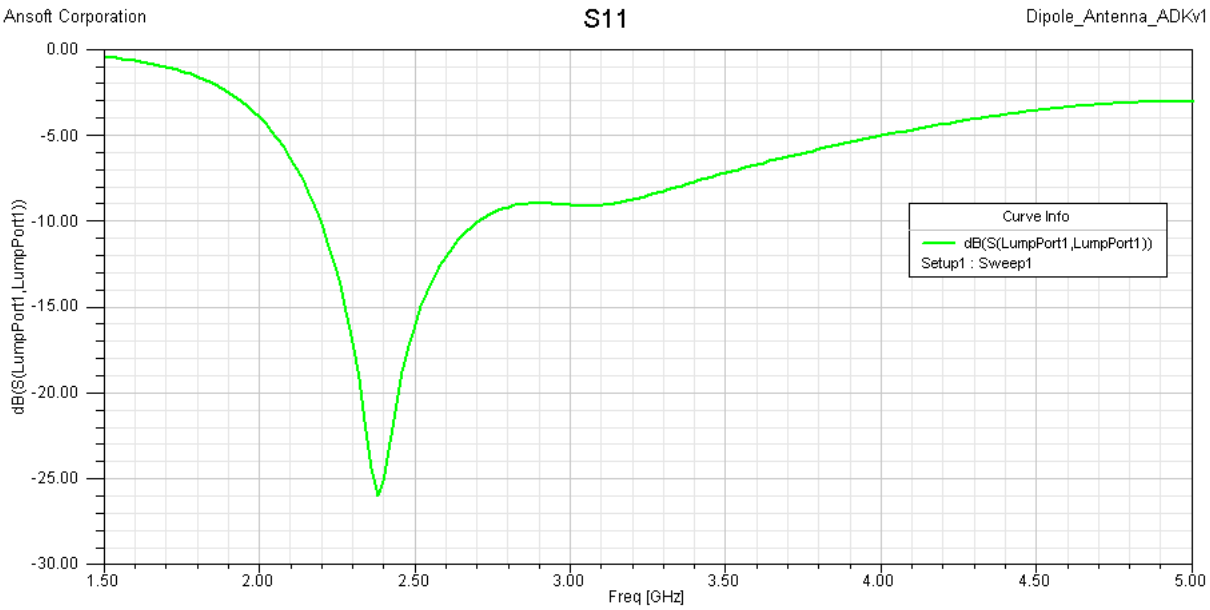

Figure 2.27: Return loss plot with the effected produced by the connector corrected.

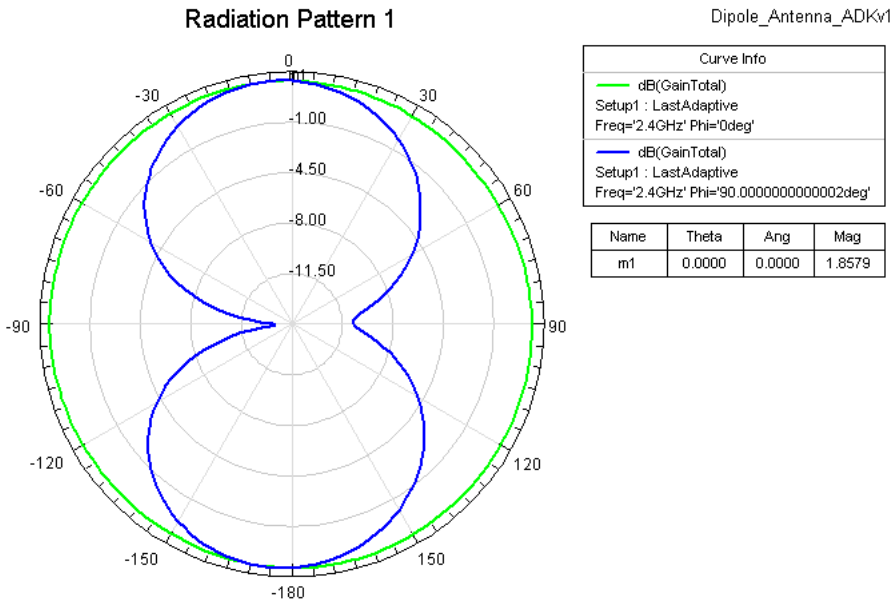

Figure 2.28: Radiation pattern plot with the effected produced by the connector corrected.

2.4 Measurement and analysis of printed dipoles

This section is dedicated to the measurement of two printed dipoles regarding topology 1. These experimental results only aim to confirm the simulation results previously produced by HFSS.

The printed dipole dimensions used to build the antennas are the ones from tables 2.9 and 2.10. In figure 2.29, one can see the differences between the simulator results and the ones measured for the two different substrates: FR-4 and fibreglass. To do the experimental measurements a VNA with a range of frequencies between the 1.5 GHz and the 3 GHz was used.

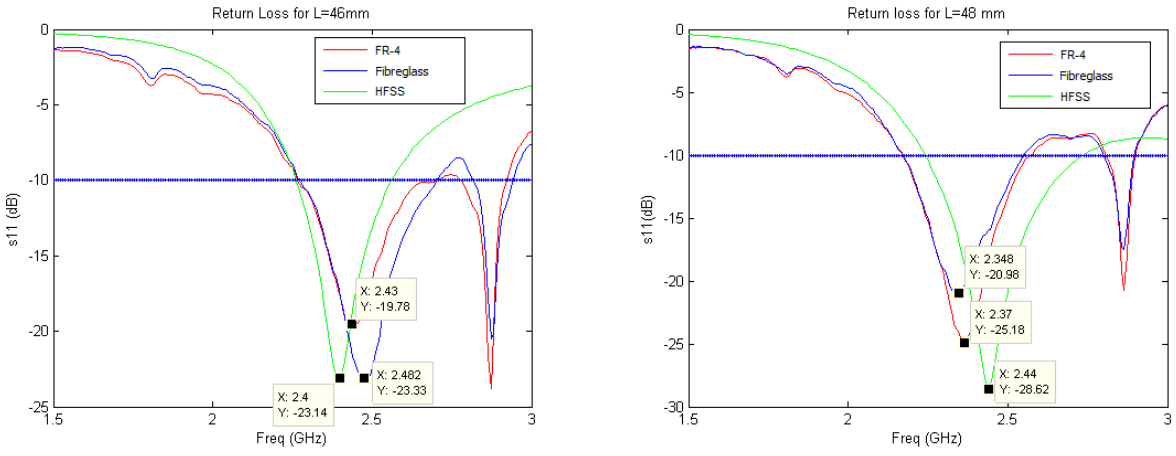

(a) (b)

Figure 2.29: Return loss plot comparing the simulations results using FR-4 substrate and the two printed antennas in FR-4 and fibreglass substrates for different values of dipole length (L).

There are two notorious differences between the simulation results and experimental ones. The first one concerns the shift in the return loss traces: when L=46 mm the return loss trace is shifted to the right whereas in the one with L=48 mm it shifted to the left. This fact might lead to the conclusion that the adequate dipole length should be between 46 mm and 48 mm. The other curious fact regarding the experimental results is the existence of a second resonance frequency, which was already verified in the simulator, but for a higher value of frequency. According to figure 2.15, the

second resonance frequency should be around the 3.2 GHz, whereas in plot from figure 2.29 it around the 2.9 GHz. As previously explained, it is believed that this second resonance frequency is provoked by the addition of the SMA connector. Based on the plot from figure 2.16, when L=46 mm that second match should not have appeared, but it did, as it is possible to see in figure 2.29(a). Despite these observations, both antennas are suitably matched for the resonance frequency of 2.4 GHz. The substrate that produces better results is the fibreglass considering the resonance frequency of 2.4 GHz, because the return loss value for this frequency is smaller than with FR-4 substrate.

2.5 Conclusions

In conclusion, after all the simulations that had been made, there are several aspects that should be highlighted. To begin with, no matter which topology one uses, the lengthening of L always introduces a shift to the left in terms of frequency. In addition, L has an influence in the radiation pattern too: if one chooses an L value too large, its radiation pattern narrows. When the sweep concerns the width of the arms (the SMA connector is not considered), there are differences between topologies. In topology 1 the return loss trace remains more or less unaltered, whereas in topology 2 one should be careful when choosing w, because it not only introduces significant changes in the return loss value, but also introduces a little frequency shift. The behaviour of these two topologies are the same when varying the value of the spacing between the arms of the dipole. In what concerns the height of the dielectric, an adjustment in the L value is required due to the frequency shift introduced by heighten the dielectric in both cases. If one looks at the sweeps of *wcond* and *Lcond* in the two topologies, the results obtained are very similar. However, it is important to realize that the return loss trace is very sensitive when varying these parameters. Moreover, one has to be careful when determining *wcond* and *Lcond* values and this task should be done with the help of the simulator in order to achieve the best results.

Another important aspect is the effect caused by the addition of the SMA connector, which was already described in previous sections of this work. Overall, there is a relation between the length and width of the conductors responsible for the connection to the SMA and the distance from the dipole arms to the SMA pins. The conductors should not be too large because of the mismatching of the dipole, and neither too short in order to avoid undesired behaviours. What is more, during simulations it was noticed that every time *wcond* equals w the results obtained were slightly better in terms of return loss.

Finally, the main difference noticed between both topologies is the slight variation of the L parameter to match the dipole to 2.4 GHz. In the first topology, the most suitable total length of the dipole is 48 mm, whereas in the second topology it is reduced to 46 mm. The lengths mentioned before do not refer to the topologies where the SMA connector is taken into account in simulations.

Chapter 3

Study of balanced feeding in printed dipoles

3.1 Printed dipole with balanced feeding

From the conclusions obtained from section 2, it was decided to use the topology where the arms of the dipole are printed in the same layer due to ease of design and construction. In fact, the differences found between the two topologies were not significant considering the main goal of this dissertation, so any of the two could have been used.

3.1.1 The balun and the balanced feeding

The usage of a balun

In order to avoid unexpected behaviours when interacting with the environment, antennas must be driven properly. In what concerns the dipole antennas, either linear wire or printed, the currents in the two arms have to be equal if the dipole is symmetric. However, when one intend to feed the dipole through a coaxial cable, which is by nature an unbalanced structure, the antenna would not be fed properly. In order to provide this balanced feeding, a balun would be added to the antenna, which is a three-port network responsible for the conversion from unbalanced to balanced.

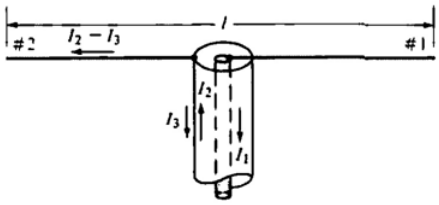

Figure 3.1: Unbalanced coaxial feeding of a dipole antenna [29].

The figure above shows a physical connection between the dipole and the coaxial cable (see figure3.1). As one can see, the current flows from the inside part of the cable to the right arm of the dipole, and it has a phase difference of 180° relative to the outer part of the cable. The problem with this connection arises from the outer conductor as it is also shown in figure 3.1. When one connects the left arm of the dipole to the outer conductor the current in this arm is I_2-I_3, when it was supposed to be just I_2, and in the right arm is I_1. This current leak leads to a unbalanced feeding, and therefore to an inadequate performance of the antenna. This inadequate performance specially manifests itself in the symmetry of the radiation pattern. To solve this problem it is necessary to nullify or block the undesired current I_3 in order to avoid unwanted radiation originated by the coaxial cable. This can be achieved by increasing the impedance of the outer conductor to infinite or by adding a balun.

The main goal is to obtain an equal distribution of the input signal, which can be accomplished by making the two input impedances seen from each arm equal. When considering a printed antenna, to perform the connections one needs to add a transmission line of $\frac{\lambda}{2}$ to each arm, because with this length the impedance does not change its value. This is confirmed by representing the impedance in the Smith Chart and then making a rotation of 180° ($\frac{\lambda}{2}$), ending up in the same point again. Afterwards, another transmission line of $\frac{\lambda}{2}$ is added to only one of the arms to produce the desired 180° phase shift. The illustration of this modification can be observed in figure 3.2.

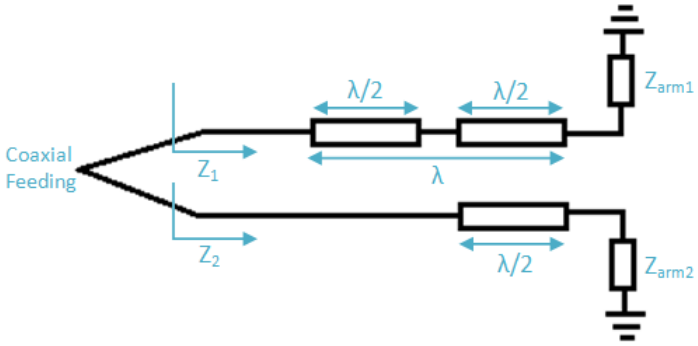

Figure 3.2: Balanced feeding of the dipole antenna.

To balance a printed dipole, a microstrip balun will be designed due to its suitability for higher frequencies, ease of fabrication and low cost. In addition to all of the advantages mentioned previously, it is easier to build because it is printed on the Printed Circuit Board (PCB) material, unlike the baluns made of coaxial cable, and also, it is more suitable when one intends to design an array of printed dipoles due to volume and weight constraints. On the other hand, the microstrip technology has two main disadvantages: high losses and low power handling capacity. It is also relevant to consider the coupling effects produced by the proximity of the microstrip transmission lines and the electromagnetic fields that can not be completely cancelled by the ground plane.

Brief introduction to microstrip technology

The structure associated with a microstrip line is provided in figure 3.3. A microstrip line consists of a ground plane, a dielectric substrate and finally, the metal strip.

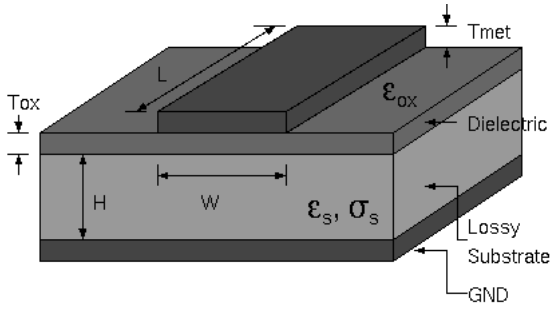

Figure 3.3: Microstrip topology [30].

In what concerns the behaviour of a microstrip line, it is known that the electric field flows from the conductor strip to the ground plane, going through the substrate with dielectric constant of ε_r, loss tangent of $\tan\delta$, and the air as well. Due to this fact, there is a need to determine an effective dielectric constant that represents the effects caused by those two different dielectrics, which can be calculated using equation 3.1.

$$\varepsilon_{reff} = \frac{\varepsilon+1}{2} + \frac{\varepsilon-1}{2} \times \frac{1}{\sqrt{1+\frac{12h}{w}}} \tag{3.1}$$

After the determination of the effective dielectric constant, the characteristic impedance of the transmission line can be calculated using equation 3.2:

$$Z_0 = \begin{cases} \frac{60}{\sqrt{\varepsilon_{reff}}} \ln(\frac{8h}{w} + \frac{w}{4h}), & \frac{w}{h} < 1 \\ \frac{120\pi}{\sqrt{\varepsilon_{reff}}\left[\frac{w}{h}+1.393+0.667\ln(\frac{w}{h}+1.444)\right]}, & \frac{w}{h} \geq 1 \end{cases} \tag{3.2}$$

Another relevant consideration is the dimension of the ground plane, which should have an infinite size, but this is not possible to implement physically. Usually, a good approximation is having a ground plane at least ten times larger than the width of the strip if the characteristic impedance is higher than 30 Ω, or five times larger if the characteristic impedance is below 30 Ω [31]. Finally, it is necessary to calculate $\frac{w}{h}$, in which w stands for the width of the conductor strip and h stands for the height of the substrate.

$$\frac{w}{h} = \begin{cases} \frac{8\times e^A}{e^{2A}-2}, & \frac{w}{h} < 2 \\ \frac{2}{\pi} \times [B - 1 - \ln(2B-1) + \frac{\varepsilon_r}{2\varepsilon_r} \times \{\ln(B-1) + 0.39 - \frac{0.61}{\varepsilon_r}\}], & \frac{w}{h} > 2 \end{cases} \tag{3.3}$$

with:

$$A = \frac{Z_0}{60} \times \sqrt{\frac{\varepsilon_r+1}{2}} + \frac{\varepsilon_1-1}{\varepsilon_r+1} \times \left(0.23 + \frac{0.11}{\varepsilon_r}\right)$$
$$B = \frac{377\pi}{2Z_0\sqrt{\varepsilon_r}}$$

Although the formulas that allows one to determine the microstrip parameters of the transmission line are presented above in equation 3.3, in this work the *LineCalc* tool of Advanced Design System (ADS) was used to perform the necessary calculations.

Design of a balun

To perform this task the substrate FR-4 was considered, whose parameters are presented in detail in table 3.1. A few reasons can be enumerated for this choice of material: low price, availability and the dielectric constant, which seems to be suitable for designing antennas.

Table 3.1: FR-4 characteristics.

Parameter	Value
ε_r	4.4
$\tan\sigma$	0.02
h	0.8 mm

The next step is to calculate the length of the microstrip line, which is influenced by the phase difference one aims to and by the dielectric constant too (see equation 3.4).

$$\varphi = \beta L = \sqrt{\varepsilon_{reff}} k_0 L \Leftrightarrow L = \frac{\varphi \times (\frac{\pi}{180^\circ})}{\sqrt{\varepsilon_{reff}} \times k_0} \quad with \quad k_0 = \frac{2\pi f}{c} \tag{3.4}$$

From section 3.1.1 it is known that the desired phase difference is 180° or half-wavelength, which leads to the following results considering $Z_0 = 50\Omega$:

Table 3.2: Microstrip line dimensions.

Parameter	Value(mm)
w	1.45
L	34.88

As previously stated, the balanced feeding is achieved by varying the length of the microstrip lines in order to have a 180° phase difference between the arms of the dipole (see figure 3.4):

$$\phi_4 - \phi_2 = \pi, \tag{3.5}$$

with:

$$\phi_4 = \beta \cdot L \; and \; \phi_2 = \beta \cdot (L + \Delta) \tag{3.6}$$

Then, replacing 3.6 in 3.5 we have:

$$\phi_4 - \phi_2 = \pi \leftrightarrow \beta \cdot L - \beta \cdot (L + \Delta) = \pi \leftrightarrow \beta \cdot L + \beta \cdot \Delta - \beta \cdot L = \pi \leftrightarrow$$

$$\beta \cdot \Delta = \pi \leftrightarrow \Delta = \frac{\pi}{\beta}, \quad with \; \beta = \frac{2\pi}{\lambda} \tag{3.7}$$

With 3.7 one came to the conclusion that $\Delta = \frac{\lambda}{2}$, and the balun would have a geometry like the one presented in figure 3.4.

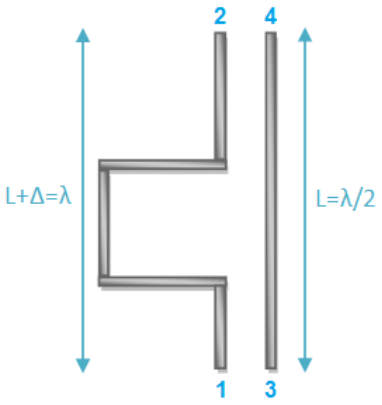

Figure 3.4: Microstrip balun geometry.

About the calculation of the wavelength, this obtained from the following expression, that takes into account the effective dielectric constant.

$$\lambda = \frac{c}{\sqrt{\varepsilon_{reff}} \times f} \tag{3.8}$$

After the determination of the wavelength, the two microstrip lines are joined between ports 1 and 3 by a microstrip line with the same width of the ones that compose the balun in order to add the quarter-wavelength transformer and measure the input impedance with the simulator. Finally, to complete this step, it is necessary to match the balun to the 50 Ω input port, and to achieve this a quarter-wavelength transformer is used. As its name indicates, the transformer is a microstrip line with a length of $\frac{\lambda}{4}$ with a characteristic impedance that makes the input impedance of the antenna equal to 50 Ω, like the input impedance of the SMA connector.

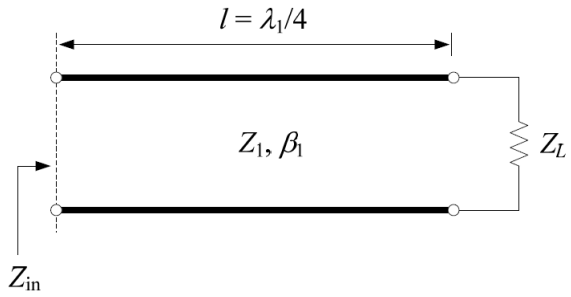

Figure 3.5: Quarter-wavelength transformer [32].

Considering figure 3.5, the input impedance is given by

$$Z_{in} = Z_1 \frac{R_L + jZ_1 \tan \beta_1 l}{Z_1 + jR_L \tan \beta_1 l} \tag{3.9}$$

Replacing the l in equation 3.9 by $\frac{\lambda}{4}$, then $\tan \beta_1 l = \frac{2\pi}{\lambda} \cdot \frac{\lambda}{4} = \frac{\pi}{2}\ rad.$ Consequently $\tan \frac{\pi}{2} \to \infty$, and the input impedance expression becomes

$$Z_{in} = \frac{Z_1^2}{R_L} \tag{3.10}$$

With the help of the simulator HFSS, the impedance at the point where ports 1 and 3 are joined together is measured, and then the characteristic impedance is determined by rearranging equation 3.10, which resulted in equation 3.11.

$$Z_0 = \sqrt{Z_{in} \times Z_L} \tag{3.11}$$

Balun's influence in the dipole's radiation pattern

The existence of the balun in the printed dipole is inevitable, because the antenna needs balanced feeding in order to operate adequately. However, with the balun, the radiation pattern of the dipole would be greatly damaged, in other words, the usual *doughnut* shape will result in the figure presented at figure 3.6.

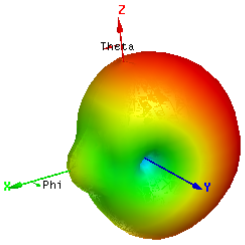

Figure 3.6: Example of a radiation pattern that is affected by the ground plane existence.

As matter of fact, this situation happens because of the ground plane, which prevents the dipole from radiating in the whole surface that is covered with copper from the ground plane. Despite this undesired effect, the balun and the quarter-wavelength provide a better match to the working frequency, higher gain and improves the antenna efficiency.

3.1.2 Design of a printed dipole with a microstrip balun

As mentioned previously, there is a need to convert unbalanced feeding to balanced feeding in order to improve the antenna's performance, therefore this is the aim of this section. First of all, a study of the effect of the ground plane in the dipole radiation pattern is provided. Afterwards, it is

presented a topology for the balun similar to the one showed in 3.4, and finally, the last task is to minimize the effect of the microstrip balun in the radiation pattern.

Study of the effects of the ground plane in the dipole's radiation pattern

In order to provide the printed dipole proper driving, it is necessary to use a balun in microstrip technology, but the ground plane existence highly deteriorates the shape of the radiation pattern. Before designing the microstrip balun, it is intended to discover if the ground plane effect is possible to eliminate or minimize by varying the distance between the dipole arms and the microstrip lines. The 3D-model used in the simulations is provided in figure 3.7, where one could see that the feeding is done by connecting directly the coaxial cable - *unbalanced feeding*.

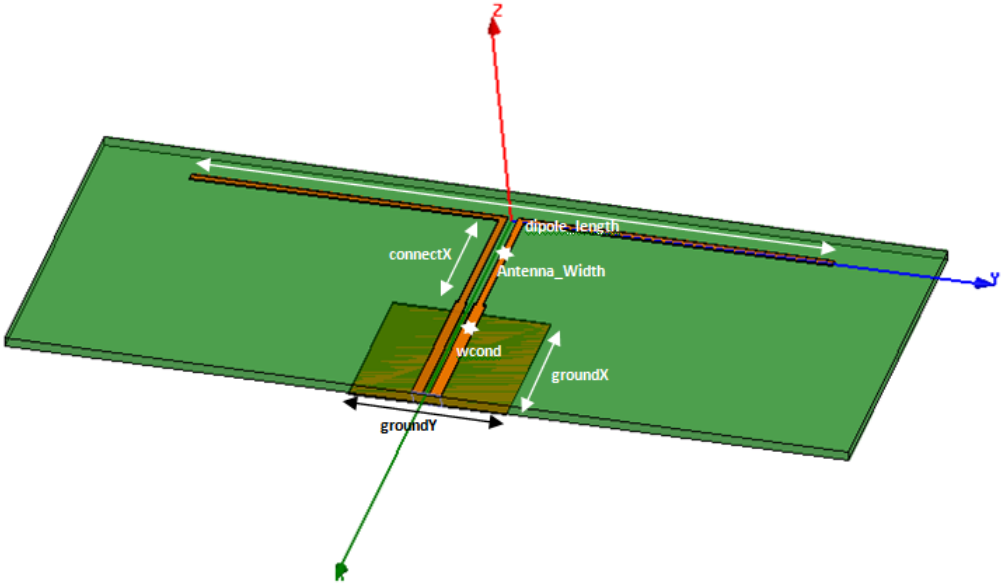

Figure 3.7: 3D-model used in simulations.

The model provided in figure 3.7 was modified during the simulations. The main modification applied to that model was the length of the ground plane, which varied between the total length of the substrate and the minimum length that it has to possess in order to consider the conductors microstrip lines i.e., ten times the width of the transmission line. Also, it was performed a sweep of the parameter *connectX* represented in figure 3.7, because that might help avoiding interference of the ground plane.

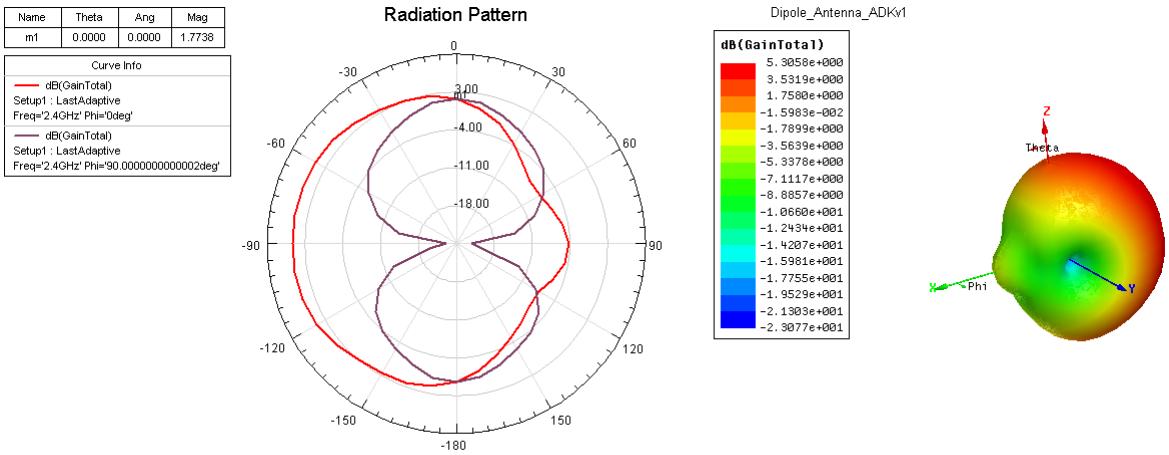

Figure 3.8: Radiation pattern from a printed dipole affected by the ground plane.

What was observed is that the radiation pattern is affected when the ground plane has a length

which is approximately the dipole length or larger, whereas the ground's length inferior to that, provides a shape similar to the traditional *doughnut*. The radiation pattern showed in figure 3.8 illustrates the influence of a ground plane with the length of the substrate. As one could see, the existence of the ground plane prevents the dipole from radiating backwards, similar to what happens in patch antennas. If one lengthens the ground plane nearly to the total length of the dipole, it becomes necessary to match the dipole to the desired frequency again. For example, when assuming a length of 40 mm for the ground plane, the following results were obtained for the return loss and the radiation pattern. The other dimensions respecting the dipole's geometry could be checked at table 3.3.

Table 3.3: Suitable dimensions for the dipole geometry.

Parameter	Value (mm)
Port gap width	0.8
Antenna width	1.5
groundY	40
dipole length	46.5
groundX	10
connectX	5
wcond	1.5

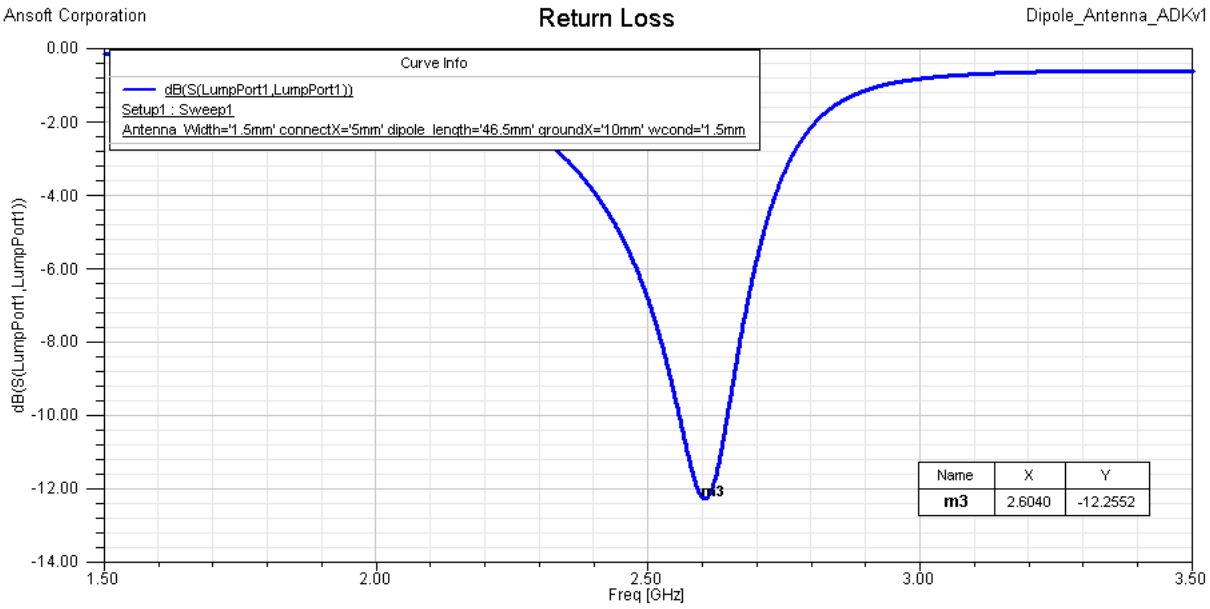

Figure 3.9: Return loss values considering a ground plane with 40 mm × 10 mm

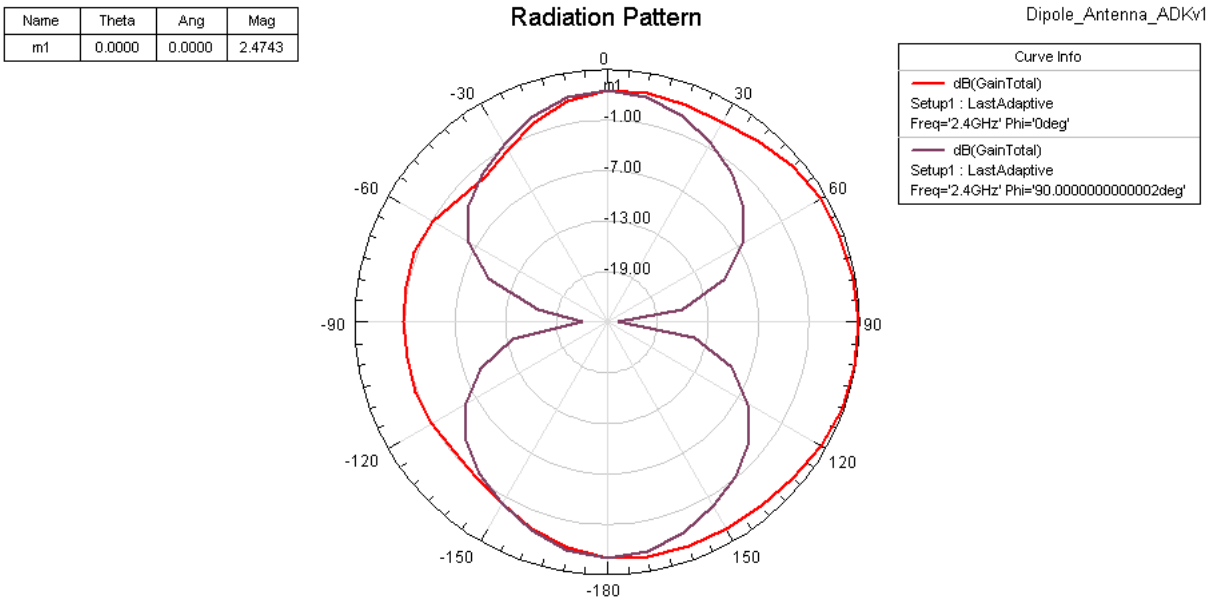

Figure 3.10: Radiation pattern considering a ground plane with 40 mm × 10 mm

From the figures presented above (figures 3.9, 3.10), it is noticeable that the dipole is now matched to the 2.6 GHz, but the radiation pattern starts to have an acceptable shape, even with the existence of the ground plane. To match the dipole to the 2.4 GHz, which is the resonance frequency assumed for the antenna, several possibilities were tried: decreasing the width of the arms, increasing the total length of the dipole and lengthening the distance between the ground plane and the dipole arms - see variable *connectX* provided in the figure 3.7. After trying to vary these parameters, it is possible to conclude that only lengthening the dipole arms would match the antenna to the 2.4 GHz. In addition, it is verified that there is a compromise when choosing the distance between the arms of the dipole and the ground plane, in other words, the increase of this distance leads progressively to the mismatching of the antenna.

What is more, when considering the dimensions used in section 2.2, it was realized that the addition of the ground plane slightly influences the dimension of the dipole arms as it is shown in figure 3.11. In this plot, the red line represents the printed dipole with the ground plane from the previous simulation, but with its arms length adjusted to meet a resonance frequency of 2.4 GHz, while the blue one is obtained considering the dimensions from section 2.2, where the ground plane was not considered.

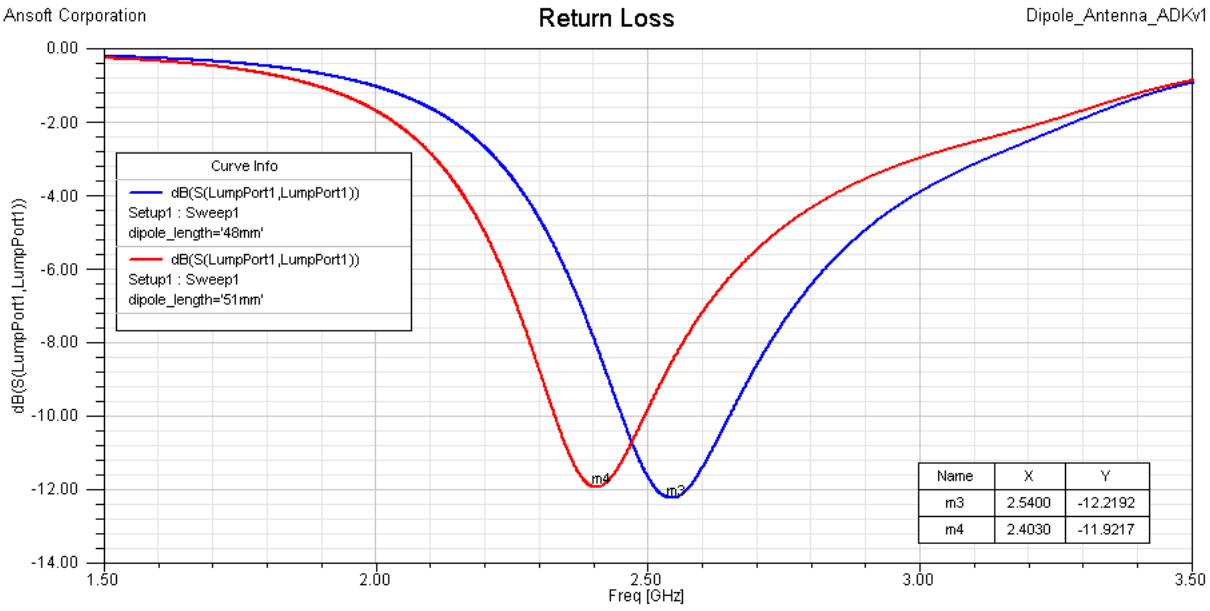

Figure 3.11: Return loss obtained in simulations.

when referring to the radiation pattern, one could conclude that there are no major differences comparing to the results obtained when there was no ground plane in the printed antenna (see figure 3.12).

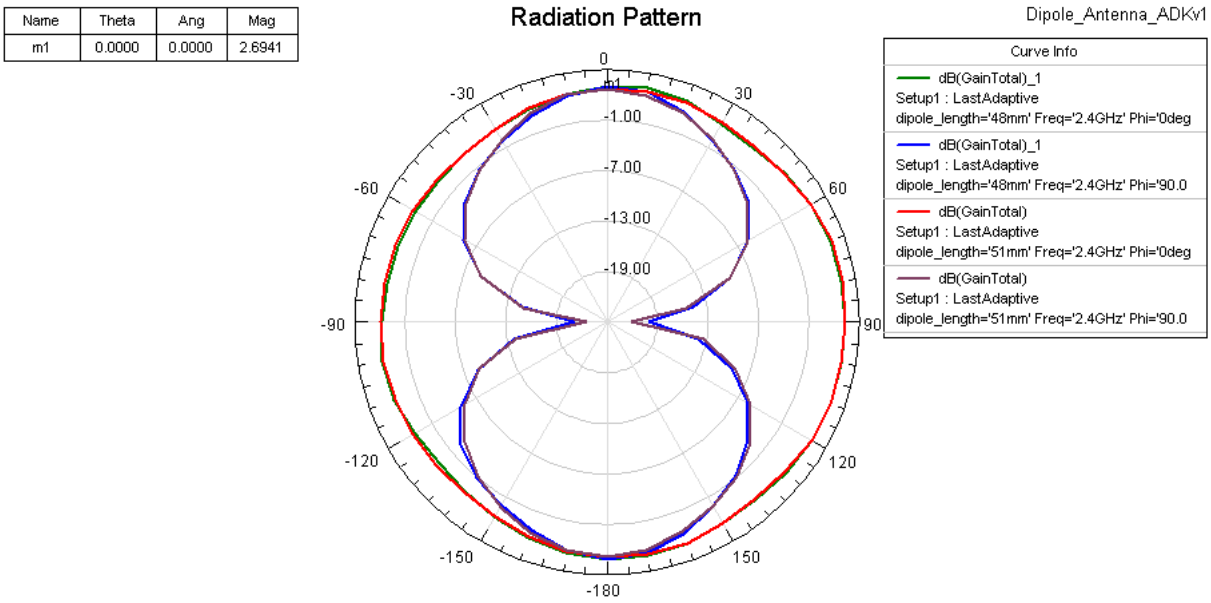

Figure 3.12: Radiation pattern considering a printed dipole matched to 2.4 GHz with and without ground plane

Now, with the dimensions for the printed dipole determined in section 2.2 the resonance frequency is approximately 2.5 GHz. To shift the return loss trace to the 2.4 GHz, the total length of the dipole had to be increased to 51 mm. Also, in this simulation the width of the arms equals to the width of the transmission line used, having a value of 1.5 mm. The reason for this modification is only related to the space occupied by the dipole structure.

After all these simulations, it was decided to use the ground plane with the minimum length possible i.e., ten times the width of the line, and the results provided in figure 3.13 and 3.14 were produced with the dimensions presented in table 3.4.

Table 3.4: Suitable parameters for the dipole geometry in presence of a ground plane.

Parameter	Value (mm)
Port gap width	0.8
Antenna width	0.5
h	0.8
dipole length	45.8
groundX	10
h	0.8
connectX	9
wcond	0.8
groundY	10wcond

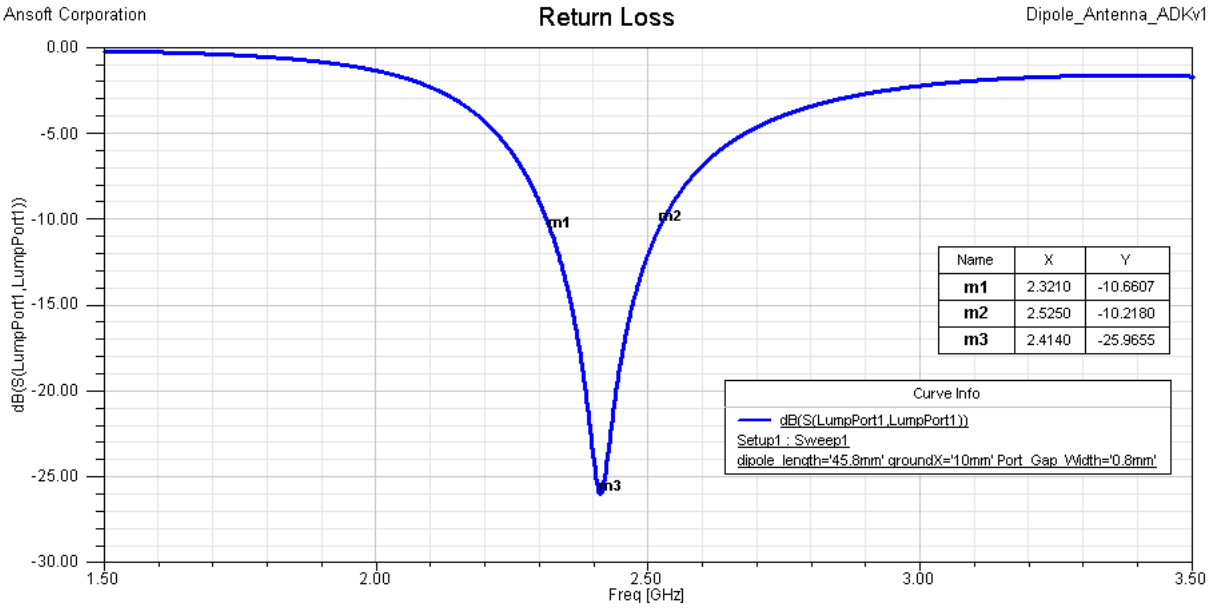

Figure 3.13: Return loss after adjusting the dipole dimensions to better match the antenna to 2.4 GHz.

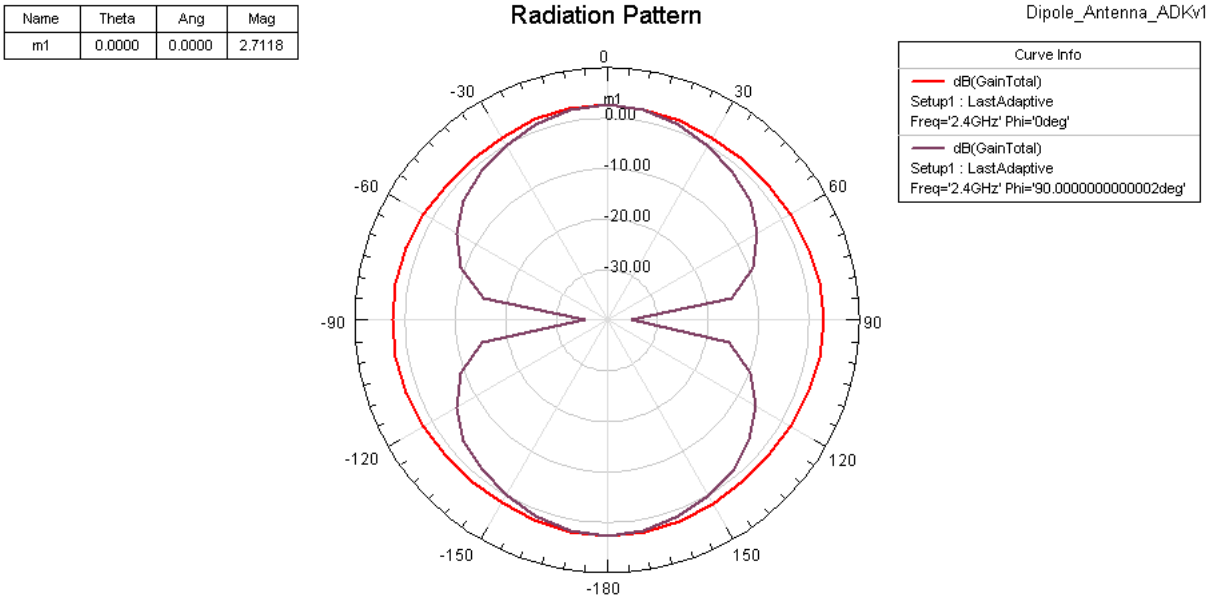

Figure 3.14: Return loss after adjusting the dipole dimensions to better match the antenna to the 2.4 GHz.

Addition of the balun to the printed dipole

After attenuating the effect caused by the ground plane in the radiation pattern, it was possible to proceed to the design of the balun. The geometry used is the one presented in figure 3.15, also including a quarter-wavelength transformer, which already includes a quarter wavelength transformer that is for matching the antenna to the 50Ω impedance of the SMA connector and the coaxial cable.

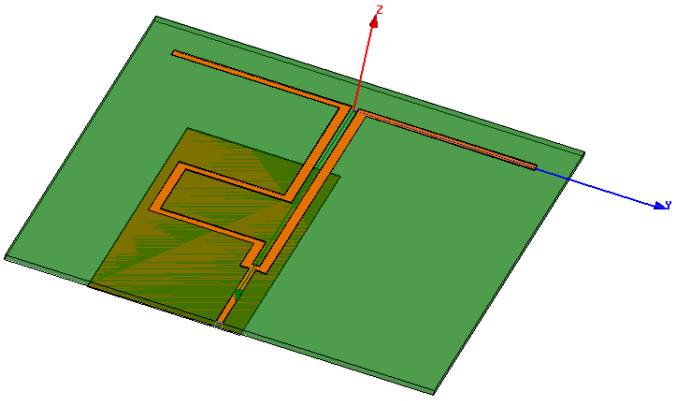

Figure 3.15: 3D-model used in simulations.

The conclusions reached in section 3.1.1 were used to design the balun i.e., it is necessary to have a transmission line $\frac{\lambda}{2}$ greater than the other in one of the arms. Then, a ground plane with the suitable size for the balun's geometry is placed, and finally, the two transmission lines are united. The balun consists of a pair of microstrip lines with characteristic impedance of 50 Ω, which corresponds to a width of 1.45 mm and physical length of $\frac{\lambda}{2} = 34.88mm$ - values obtained through the *ADS Line Calc* tool. After performing these tasks, the antenna was simulated even though it was not matched to the 50 Ω impedance of the input port. It had been decided to simulate the antenna this way because of the verification of the 180° delay between the arms at the desired frequency (2.4 GHz) and to measure the input impedance of the antenna through the use of the simulator. By measuring the input impedance with the help of the simulator, the aim was trying to have an impedance value with only real part, even though the imaginary part could not be eliminated completely. A more descriptive figure concerning the balun's geometry is provided below, where it is possible to see the lengths of the different lines that compose the balun (figure 3.16).

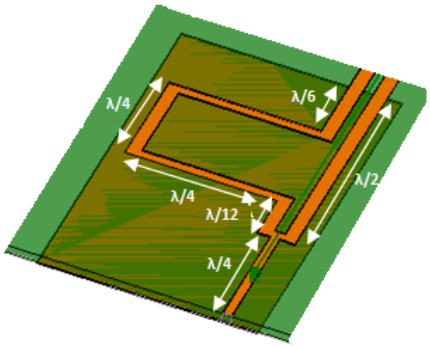

Figure 3.16: Description of the different lengths of the lines that composes the balun including the quarter-wavelength transformer.

Before performing the matching of the balanced dipole, the balun was simulated alone to confirm the phase difference between the different ports. According to the simulator results the phase difference between the two microstrip lines was 172.8484°, which implies an addition of a segment in the larger line to compensate:

$$\beta \cdot L = \frac{\phi^{\circ}\pi}{180} \Leftrightarrow \frac{2\pi}{\lambda} L = \frac{\phi^{\circ}\pi}{180} \Leftrightarrow L = \frac{7.1516\lambda}{360} \tag{3.12}$$

The results obtained from the first set of simulations, in which the quarter-wavelength transformer was not considered, are not provided in full. In fact, it was decided to show only the impedance plot, which is the one that is necessary to do the matching of the antenna. In short, the results provided by the simulator showed the return loss did not have any resonance frequency within the range of

frequency that was simulated - between 2 GHz and 3 GHz. This is confirmed by the impedance plot from figure 3.17, which shows a input impedance for the antenna of 14.8514+26.7838j Ω. The radiation pattern had a maximum gain very low (0.6446 dB) and was highly warped. In order to perform the antenna's matching, it is necessary to vary the parameters dimensions until a better value for the reactance is acquired. All of these results were produced considering the values provided in table 3.4.

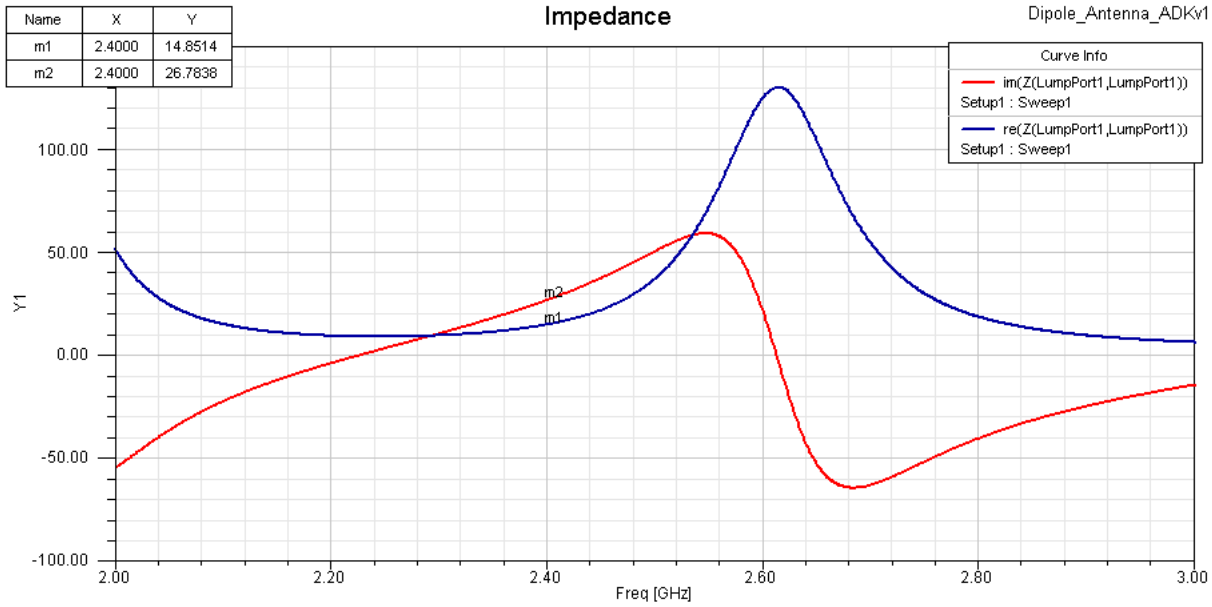

Figure 3.17: Impedance values obtained from the first set of simulations - without the quarter-wavelength transformer and before the phase difference correction.

In the following section, it is intended to minimize the effects of the addition of a microstrip balun, and also try to eliminate or reduce to near zero the reactance part of the input impedance in order to do the matching using only a quarter-wavelength transformer.

Minimization of the effects produced by the microstrip balun

This part of the work is a continuation of section 3.1.2, in other words, several modifications to the values of the dipole parameters are performed in order to meet the project specifications. The list below shows the various simulations and the reasons why there were done, still without the quarter-wavelength transformer:

1. *connectX* sweep - to eliminate the ground plane effect in the radiation pattern
2. *dipole_length* sweep - to match the dipole to the 2.4 GHz
3. *Port_Gap_Width* sweep - to verify the influence in the impedance values

The meaning of the variables mentioned in the list above can be found in figure 3.15. After these three simulations, several conclusions were drawn: first, it was observed that the parameter *connectX* had to be equal to $0.25\lambda_{FR-4}$ to produce an adequate shape for the radiation pattern; second the dipole had to be lengthened to shift the resonance frequency to 2.4 GHz; and finally the *Port_ Gap _ Width* did not influence significantly the simulation results. The design of the quarter-wavelength transformer was based on the following results, which were obtained with the dimensions provided in table 3.5.

Table 3.5: Suitable parameters for the dipole geometry in presence of the balun.

Parameter	Value (mm)
Port gap width	1.1
Antenna width	1.45
dipole length	51.5
groundX	$\frac{\lambda}{2}$
connectX	0.247λ
balunW	1.45

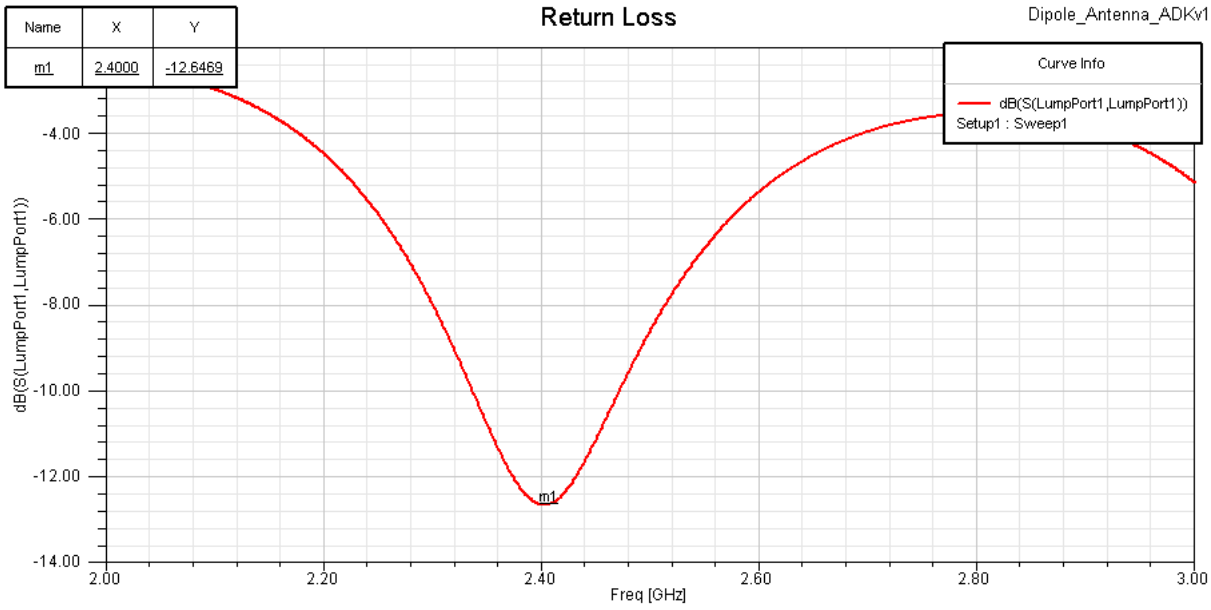

Figure 3.18: Return loss trace before the addition of the quarter-wavelength transformer.

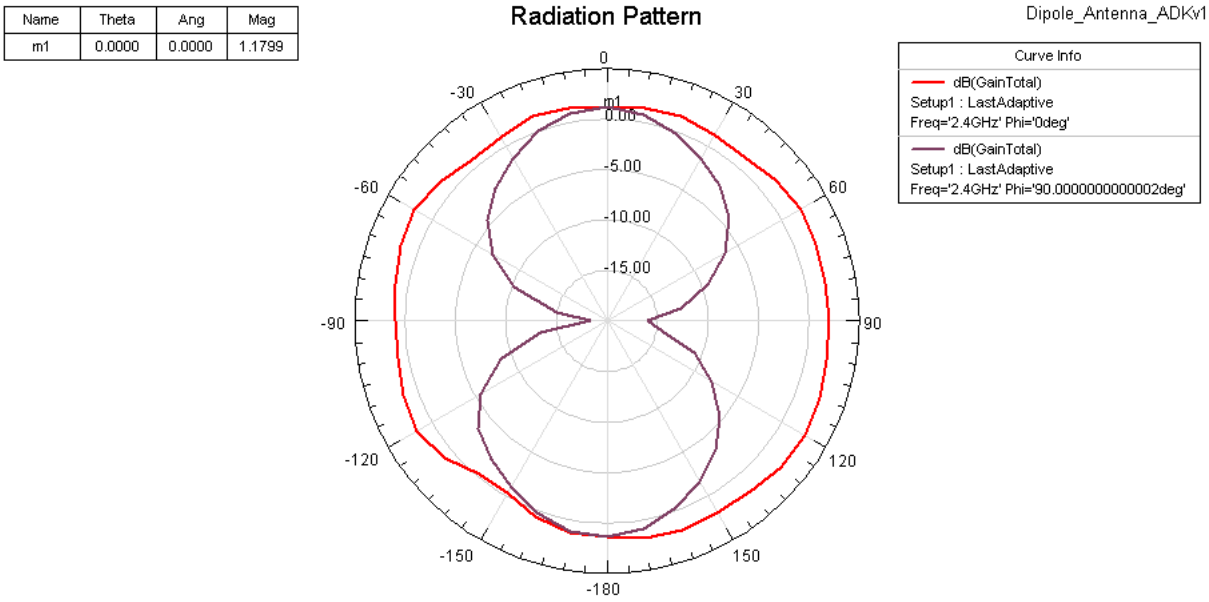

Figure 3.19: Radiation pattern before the addition of the quarter-wavelength transformer.

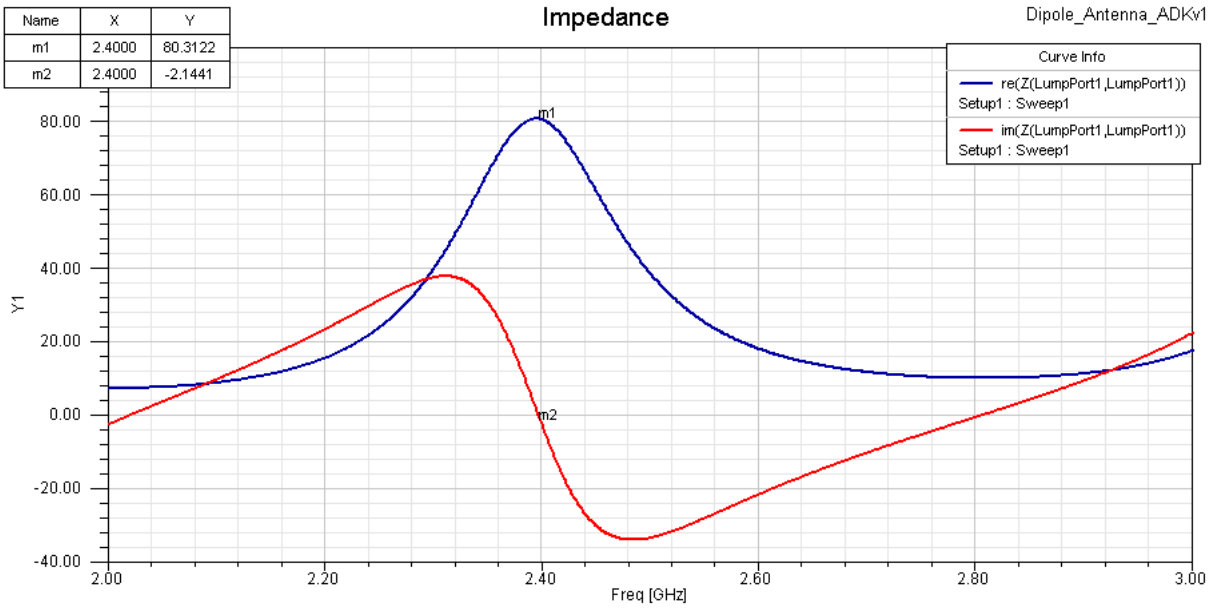

Figure 3.20: Impedance values before the addition of the quarter-wavelength transformer.

In accordance with the plots from figures 3.18 and 3.19, it is feasible to adjust the return loss to the 2.4 GHz and achieve a radiation pattern with an acceptable shape. With the further addition of the quarter-wavelength transformer, it is believed that the results will be improved.

From figure 3.20, one can see that the impedance equals 80.3122-2.1441j at 2.4 GHz. Using the equation 3.11: $Z_0 = \sqrt{Z_{in} \times Z_L} = \sqrt{50 \times 80.3122} = 63.3688\Omega$, where Z_L is the impedance value obtained from the plot of figure 3.20. To calculate the width and the length of the transformer, the *ADS - Line Calc* tool was used, whose results were 0.92 mm for the width and 17.8474 mm for the length. The results of the addition of the transformer are provided below in figures 3.21, 3.22 and 3.23.

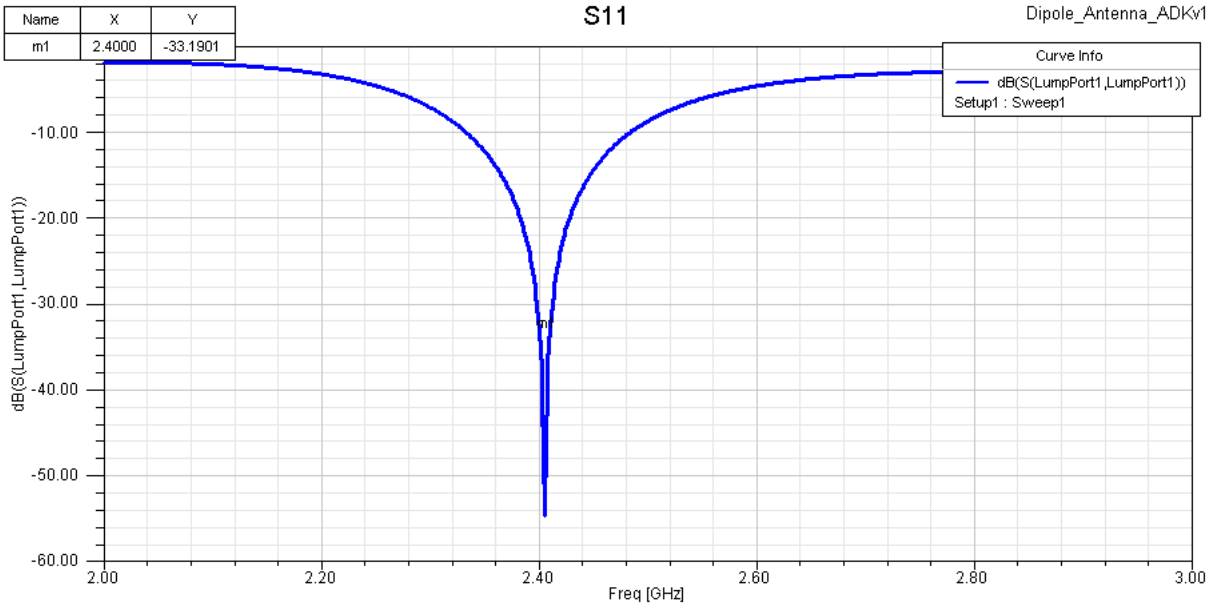

Figure 3.21: Return loss plot with the quarter-wavelength transformer.

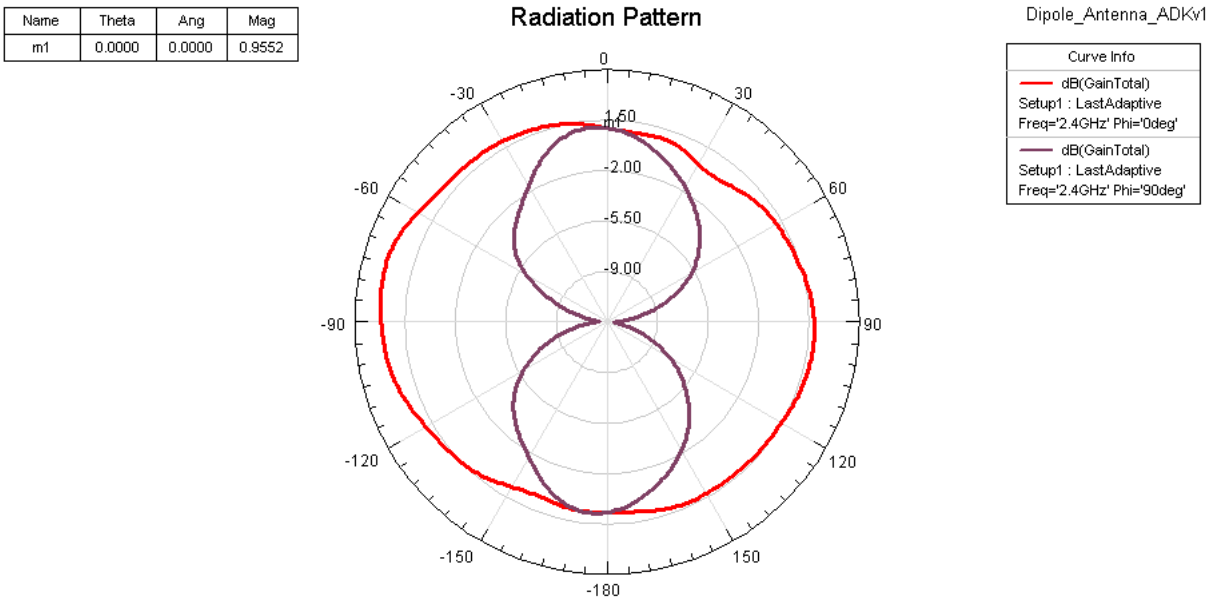

Figure 3.22: Return loss plot with the quarter-wavelength transformer.

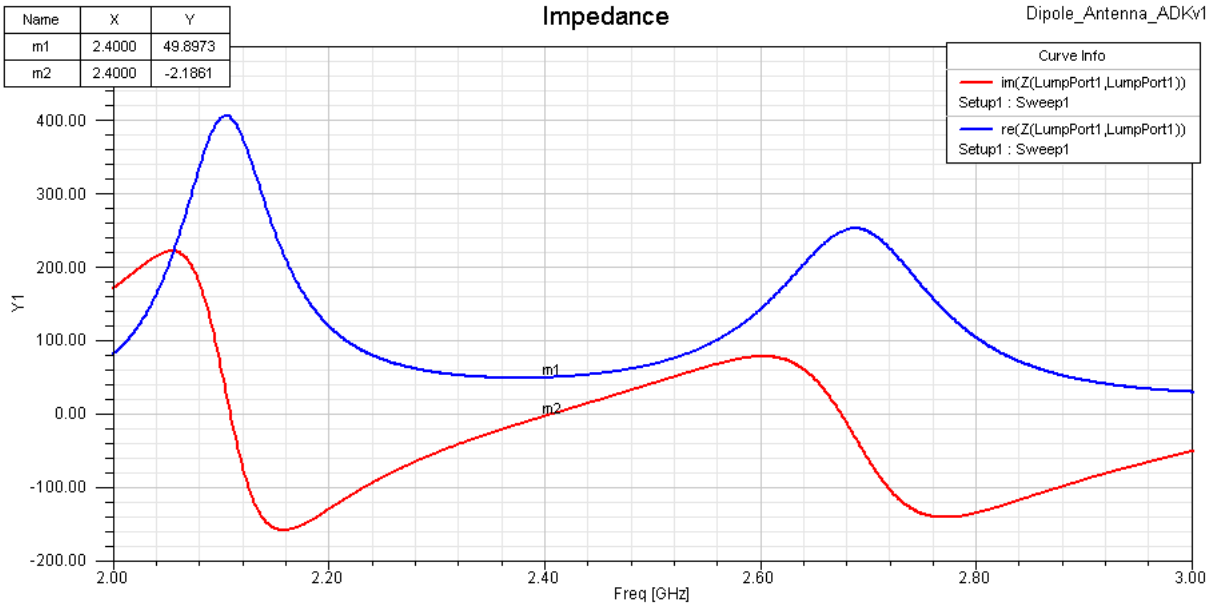

Figure 3.23: Impedance values with the quarter-wavelength transformer.

After the addition of the transformer responsible for the matching, the dipole length had to be reduced to 49.5 mm because the lowest value of the return loss plot was slightly shifted to the left. From the given pictures, it is noticeable that the printed antenna is highly matched to the 2.4 GHz with a return loss value of approximately -33 dB. The figure 3.22 shows that the dipole antenna has a radiation pattern similar to the *doughnut* shape, but quite warped by the existence of the ground plane, specially in the XZ-plane. Also, the maximum gain after the addition of the quarter-wavelength has decreased from 1.18 dB to 0.96 dB, which might be explained by the increase of the ground plane area. In what concerns the impedance, one could see that there is still an imaginary part, but the real part is nearly 50 Ω.

3.1.3 A different approach to microstrip balun's design

Due to the undesired effects produced by the balun's geometry of the previous section, it was decided to use a different model for the balun that would allow the minimization of its area. The main reason for doing this is to produce less damage to the radiation pattern, because the area that inhibits the dipole from radiating backwards is reduced. In general, if balanced feeding only requires a transmission line greater than the other $\frac{\lambda}{2}$, one could have any geometry as long as the transmission lines do not interfere with each other because of proximity - *coupling effect*. In the two following sections, it is provided two models slightly different from the one presented in section 3.1.2. To grant a better understanding of this work, it was decided to name the following topologies 2 and 3, whereas the conventional geometry from section 3.1.1 would be topology 1 from now on.

Topology 2

The second topology to be studied and its 3D-model used in the simulations are provided in the picture below (figure 3.24). The main change to the common topology of baluns is a compression in terms of the width of the balun. A closer view to the balun dimensions is provided in the same figure.

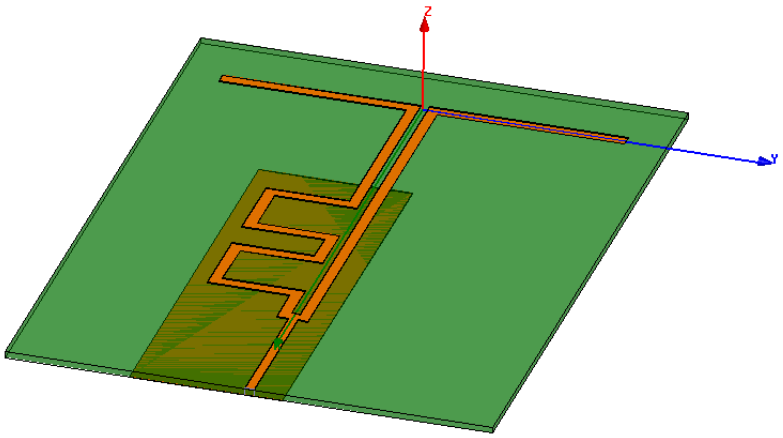

Figure 3.24: 3D-model used in simulations.

The approach to the design of the balun is the same applied in the previous simulations. First, the printed antenna is simulated with the balun and without the quarter-wavelength transformer in order to nullify the reactance part of the input impedance and to measure its value so that matching can be performed. In this set of simulations, it is important to refer that both of the microstrip lines are united at the feeding point. Also, this second topology for the balun is simulated alone to confirm that there is a 180° phase difference between the microstrip lines. Finally, when those goals are reached, the quarter-wavelength transformer is added.

About the balun simulation, the phase difference between the arms was 174.43°, so it was necessary to calculate the physical length of 5.57° in order to reach the 180° phase difference.

$$\beta \cdot L = \frac{\phi^{\circ}\pi}{180} \Leftrightarrow \frac{2\pi}{\lambda}L = \frac{\phi^{\circ}\pi}{180} \Leftrightarrow L = \frac{5.57\lambda}{360} \tag{3.13}$$

In summary, using the values from table 3.5, but considering the dipole length 49.5 mm, which were the adequate values acquired in topology, the results were:

Return loss - the value of return loss for the 2.4 GHz was approximately -17 dB, which means the antenna was already quite matched;

Radiation pattern - in terms of shape and gain it had improved when compared to topology 1 (see figure 3.22);

Impedance - for the 2.4 GHz the impedance value was 57.3803+14.8414j Ω, implying a new simulations to reduce the reactance.

After performing various sweeps, the values from table 3.6 produced the most satisfactory results. Actually, the main modification to the dipole geometry is the length of the arms, which had to be increased to 51.4 mm, compared to the 49.5 mm from the first set of the simulations. In what concerns the results, the radiation pattern truly resembled the desired shape of a *doughnut*, and the return loss plot showed a resonance frequency of 2.4 GHz with a return loss value of almost -22 dB. What is more, the imaginary part of the impedance was lowered to 1.2199j, which is a more acceptable value. As for the resistance part, it had a value of 58.6068 Ω.

Table 3.6: Suitable dimensions for the dipole geometry in presence of the balun.

Parameter	Value (mm)
Port gap width	1.1
Antenna width	1.45
dipole length	51.4
groundX	$\frac{\lambda}{2}$
balunW	1.45
connectX	0.25λ

To determine the quarter-wavelength dimensions, it was considered $Z_L = 58.6068$ according to the results previously obtained, ignoring the $im(Z_L) = 1.2199j$: $Z_0 = \sqrt{Z_{in} \times Z_L} = 54.133\Omega$.

After filling in the values in the *ADS Line Calc* tool, one was granted the values for the length and the width of the microstrip line of 17.57 mm and 1.26 mm, respectively. However, after the addition of the quarter-wavelength transformer, a shift to the left was noticed in the return loss plot, therefore the dipole's length had to be changed to 50.7 mm. The final results concerning the dimensions from table 3.6 - except for the dipole length - already with the transformer can be seen in figures 3.25, 3.26 and 3.27.

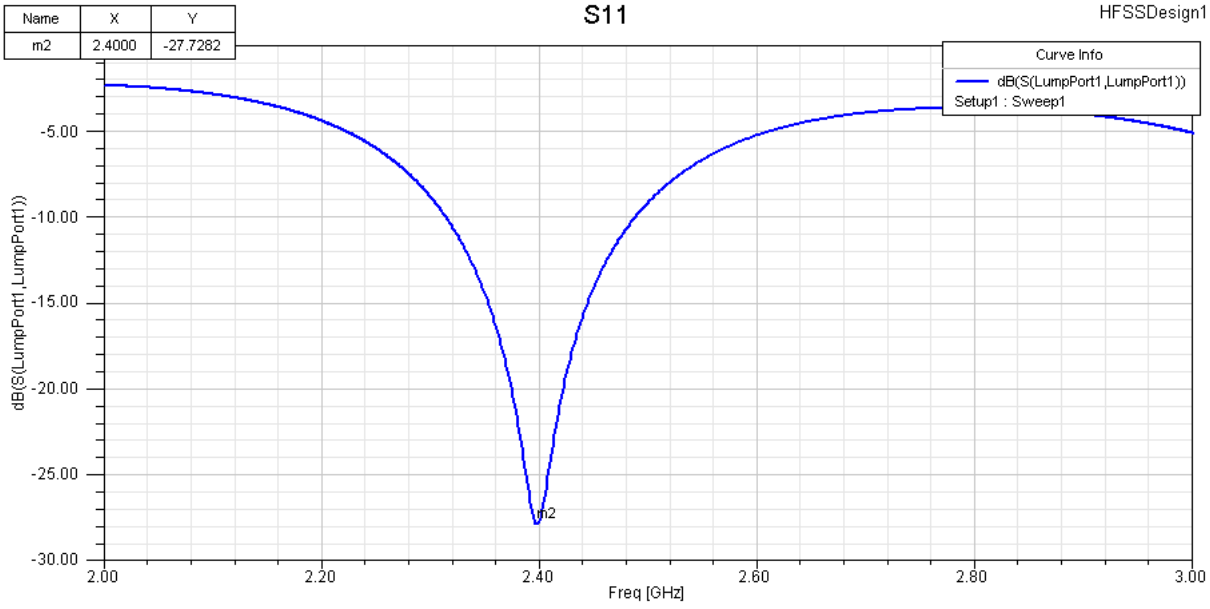

Figure 3.25: Return loss plot with the quarter-wavelength transformer.

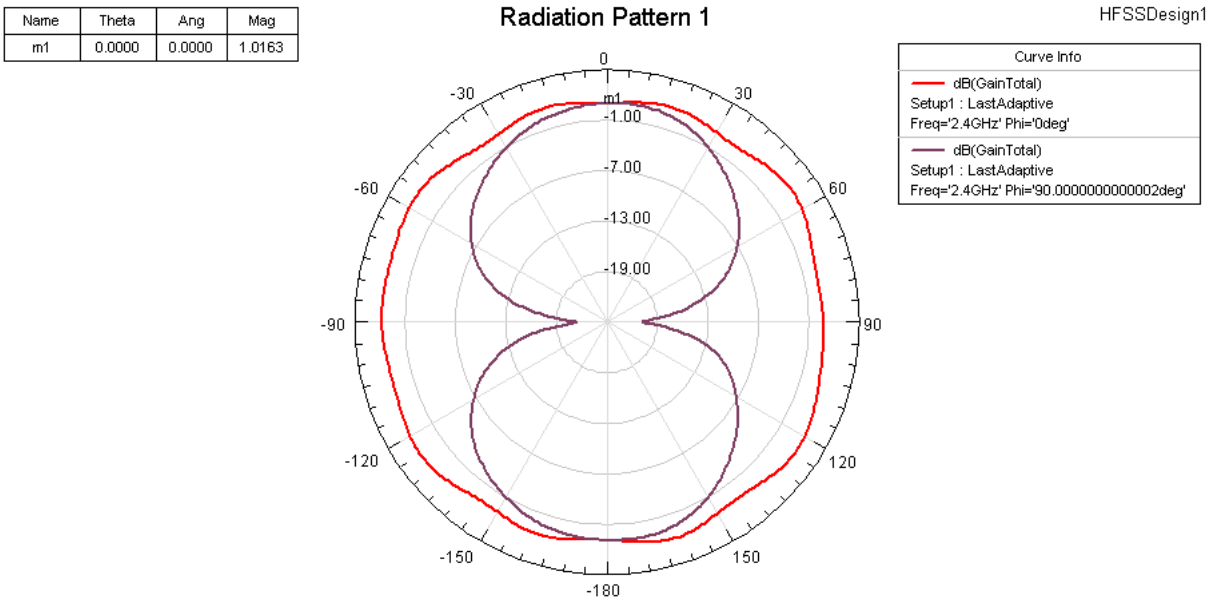

Figure 3.26: Radiation pattern obtained with the quarter-wavelength transformer.

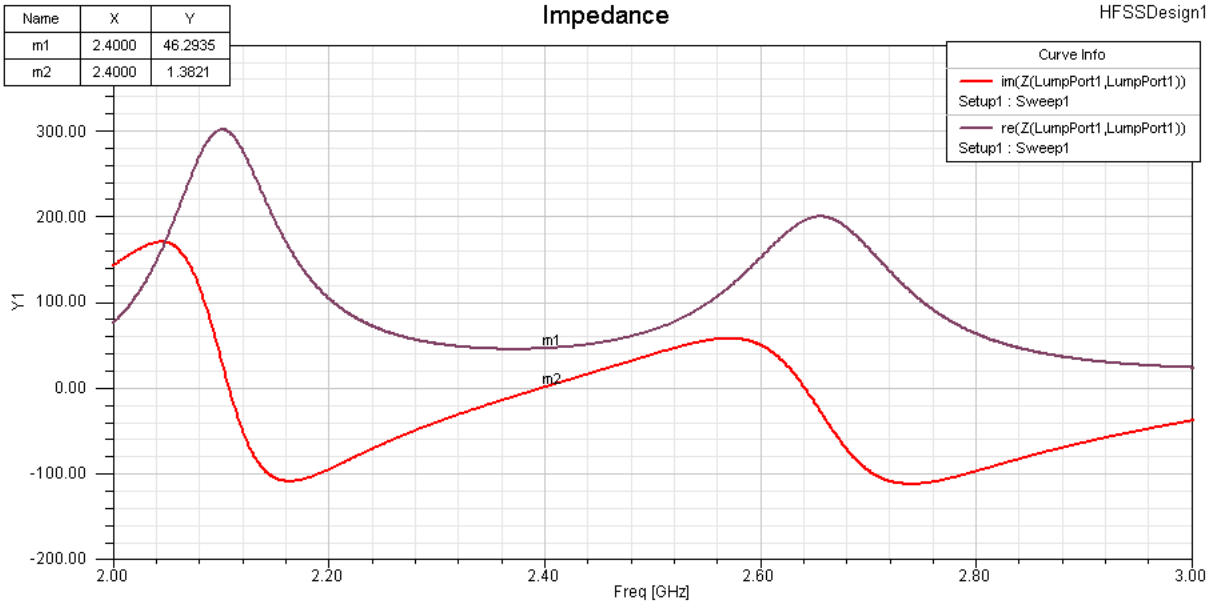

Figure 3.27: Impedance plot obtained with the quarter-wavelength transformer.

All in all, one could see that the printed antenna is well matched to the 2.4 GHz with a return loss value of approximately -28 dB (see figure 3.25). The radiation pattern is not so much affected by the ground plane as in topology 1. In fact, its shape has improved considerable with this new topology, it is more symmetrical than topology 1 and the maximum gain has increased to 1.73 dBi (see figure 3.26). As a matter of fact, this maximum gain of 1.73 dBi, which is inferior to the characteristic 2 dBi from the common dipole. As for the impedance plot from figure 3.27, it is possible to confirm that the matching was righteously performed, because the printed antenna has an input impedance of 46.2935+1.3821j Ω.

Topology 3

The next proposal for the balun is provided in figure 3.28. Once again, figure 3.28 has already the quarter-wavelength that will allow to match the printed antenna to the 2.4 GHz. The method

used to perform simulations in order to find adequate values for the antenna is the same described in previous sections. A closer view describing the lengths of the balun in detail is also provided.

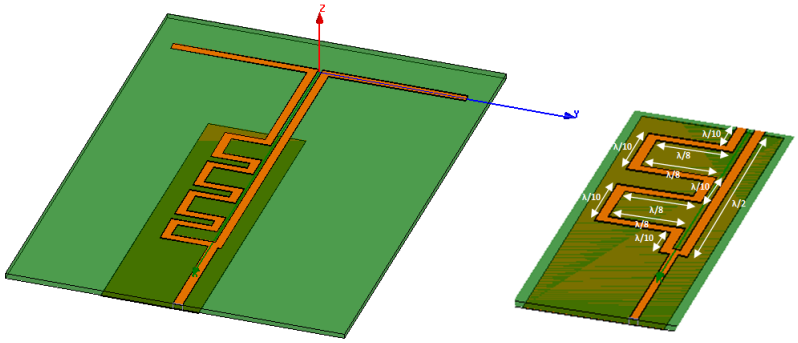

Figure 3.28: 3D - model used in the simulations.

As described before, first the balun is designed and simulated in order to measure the input impedance of the antenna. Then, a sweep of the length of the arms of the dipole, the port gap width and the distance between the arms and the ground plane is performed. The aim of these sweeps is to adjust the reactance part of the impedance as close as possible to zero. This time it was not necessary to adjust the balun's dimensions to meet the 180°, because according to the simulator results, it had already a phase difference of 182°, which is acceptable considering that the 2° that had to be eliminated, correspond to a very small physical length. The initial values for the dipole dimensions are provided in table 3.7, which are the adequate dimensions determined for topology 1.

Table 3.7: Dimensions used in the first set of simulations for topology 3.

Parameter	Value (mm)
Port gap width	1.1
Antenna width	1.45
dipole length	49.5
groundX	$\frac{\lambda}{2}$
connectX	0.247λ
balunW	1.45

In short, the results gathered with the dimensions from table 3.7 were:

Return loss - at the 2.4 GHz the return loss value rounded the -17 dB, which indicates that the antenna was acceptably matched;

Radiation pattern - it remained very similar to one from topology 2 before the impedance adjustment and the addition of the quarter-wavelength transformer. The ground plane still had influence in the shape of the radiation pattern, but not significantly;

Impedance - as already inferred from the return loss behaviour, the impedance value at the desired resonance frequency is near 50 Ω, but reactance value is very substantial. At the 2.4 GHz the impedance had a value of 54.8610-13.2972j Ω.

In accordance with the results obtained in the first set of simulations, an adjustment of the impedance at the 2.4 GHz was performed by sweeping the parameters. A range of sweeps was performed, including the port gap width, the length of the dipole arms and the distance between the arms and the ground plane. The best values that could be reached are described in detail in table 3.8.

Table 3.8: Suitable dimensions for topology 3.

Parameter	Value (mm)
Port gap width	0.65
Antenna width	1.45
dipole length	47.9
groundX	$\frac{\lambda}{2}$
connectX	0.25λ
balunW	1.45

In agreement with table 3.8, it is possible to see that the main modifications to the dipole structure were to decrease the length of the arms from 49.5 mm to 47.9 mm and the port gap width from 1.1 mm to 0.65 mm. Using these new dimensions, the return loss had the resonance frequency at 2.4 GHz, as desired. In what concerns the radiation pattern, there are no significant modifications either in the maximum gain or in its shape. As matter of fact, the most noticeable change is in the input impedance, which is near the 50 Ω: 45.7288+1.1338 j (Ω). Using the impedance value measured with the help of the simulator, the width and length of the transmission line that would turn 45.7288 Ω into 50 Ω was calculated. Ignoring the imaginary part of the impedance, the characteristic impedance of the quarter-wavelength transformer is: $Z_0 = \sqrt{Z_{in} \times Z_L} = \sqrt{50 \times 45.7288} = 47.8167\Omega$. To have a characteristic impedance of approximately 47.82 Ω on a FR-4 substrate, the transmission line would have to have a width of 1.57 mm and a length of 17.37 mm. The following pictures (figures 3.29, 3.30 and 3.31) show the performance of the printed dipole with the quarter-wavelength transformer maintaining the dimensions described in table 3.8.

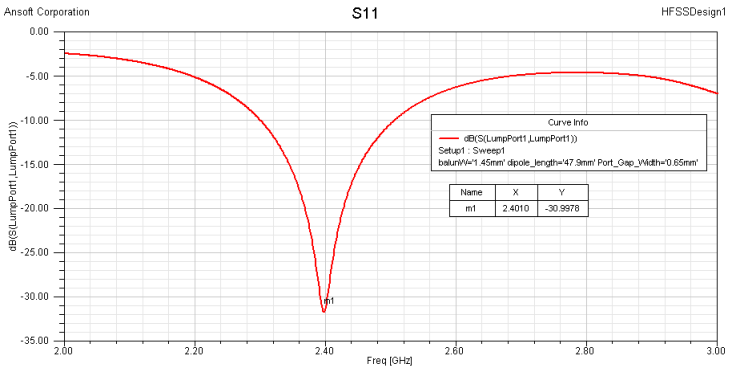

Figure 3.29: Return loss plot with the quarter-wavelength transformer.

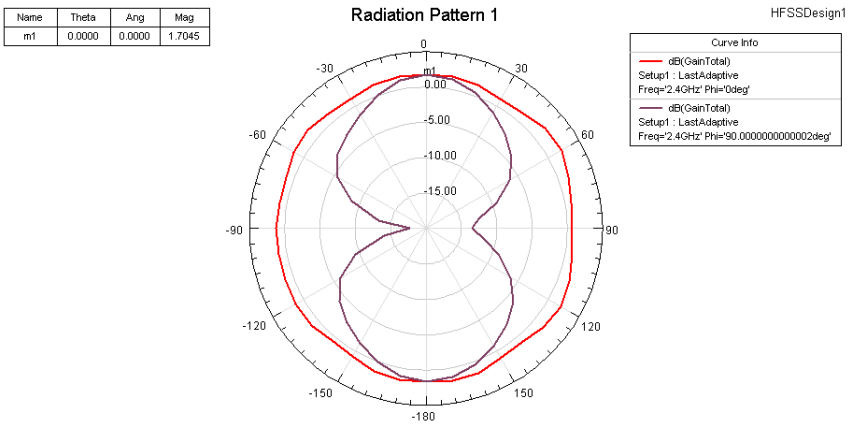

Figure 3.30: Radiation pattern obtained with the quarter-wavelength transformer.

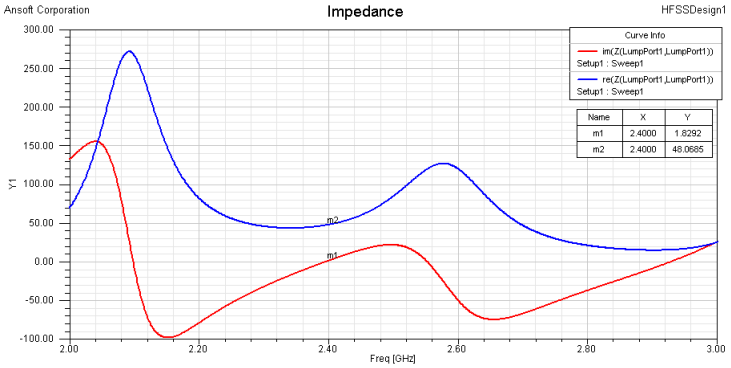

Figure 3.31: Impedance plot obtained with the quarter-wavelength transformer.

With the quarter-wavelength transformer the return loss at 2.4 GHz increased from -26 dB to -30 dB approximately, because the antenna is more adequately matched to the desired working frequency. In fact, this is confirmed by the impedance plot presented in figure 3.31, the real part of the impedance raised from 46 Ω to 48 Ω. As for the reactance value, it has increased from 1.1383j to 1.8292j. What is more, the radiation pattern shape became worse than without the transformer possibly due to the increase in the ground plane area.

3.1.4 Comparison between topologies

At this point, all simulations concerning printed dipoles had been done and its results analysed. Now, the aim of this section is to compare the results produced by the three topologies and conclude which one would suit best the project specifications. The table 3.9 shows the main differences there are between each printed antenna.

Table 3.9: Comparison of parameters between topologies.

Topology	Dipole length (mm)	Port gap width (mm)	Distance between the ground plane and the arms (mm)	Maximum gain (dBi)
1	49.5	1.1	0.247λ	0.95
2	50.7	1.1	0.25λ	1.02
3	47.9	0.65	0.25λ	1.70

As one could see, the main difference between topologies is the length of the dipole arms. As a matter of fact, this happens because the width of the ground plane was gradually decreased by compressing the balun. However, in topology 2 the length of the dipole has increased slightly compared to topology 1, which was not expected. When the effect of the ground plane was studied back in 3.1.2, it was concluded that widen the ground plane would also require the lengthening of the arms of the dipole to achieve the same resonance frequency. In the case of topology 2, the ground plane width diminished compared to the previous topology, but due to impedance matching, the best values were acquired for a length of 50.7 mm. The distance between the arms and the ground plane is always the same: 0.25λ, which is the adequate distance in order to avoid the degradation of the radiation pattern. In what concerns the port gap width, one would say that the differences of values between topologies are due to the impedance adjustment, in other words, elimination of the imaginary part.

The comparison between the return loss and radiation pattern between the three designs of the baluns are also provided. When looking at figure 3.32, it is proved that the different designs do not influence much the resonance frequency. In terms of the radiation pattern, one is tempted to conclude that there are no significant changes, but designs number 2 and 3 produced a more symmetrical shape and greater value for the maximum gain. In conclusion, one would state that any of the topologies would perfectly suit the project requirements. In fact, when it is important to consider the overall

dimensions of the antenna, one would say that topology 3 is more suitable due to its smaller size of the arms when compared to the other two topologies.

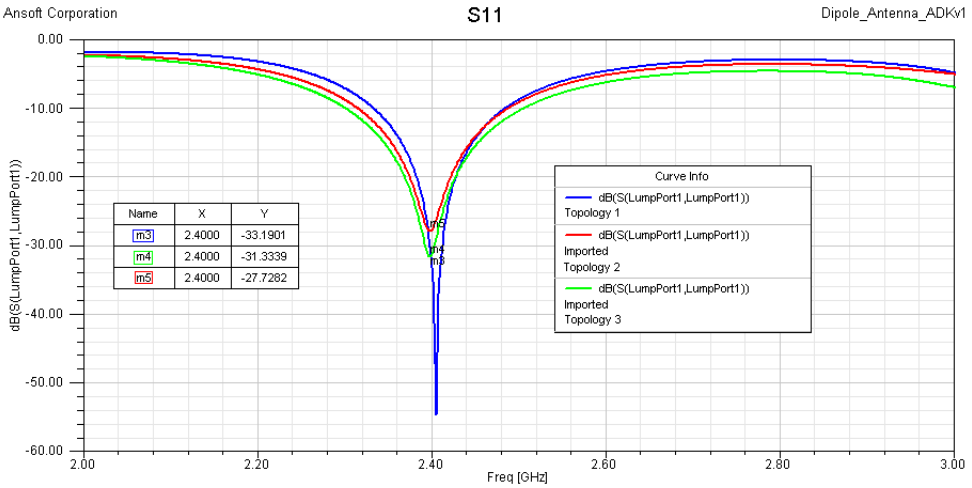

Figure 3.32: Return loss obtained from the three topologies.

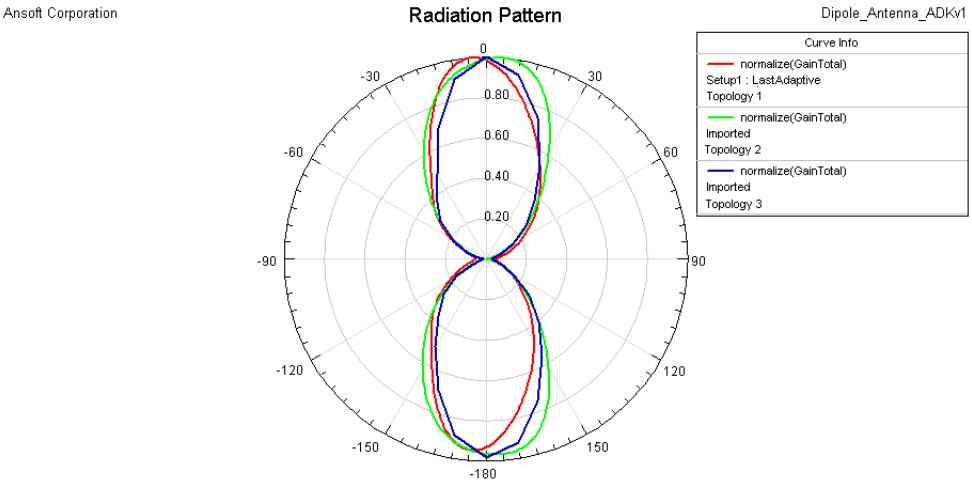

Figure 3.33: Radiation pattern obtained from the three topologies - XZ plane.

Chapter 4

Design and simulation of arrays of printed dipoles

4.1 The 2-element array of printed dipoles

As recommended in section 1.5, the single element that would be used in the array had been analysed, therefore permitting the design of the antenna arrays of printed dipoles. In this section, a study of arrays of two elements considering the many topologies provided in sections 3.1.2 and 3.1.3 will be presented. The main reason for doing this study is to try to tighten the radiation pattern of the dipole antenna gradually.

The method used for performing the next sets of simulations is the same used when designing the single element antennas. First, two single elements are placed in the same piece of substrate and then united. Thereafter, if necessary, the distance between elements would be adjusted until a value that produces the better results is found. Finally, the impedance at the input of the antenna is measured to verify if the reactance is near zero in order to design the quarter-wavelength transformer to match the dipole to the feeding port. It is important to clarify that if the imaginary part of the input impedance is too significant, the array parameters will have to adjusted until acceptable results are achieved - reactance near zero.

4.1.1 Topology 1

The first array of two elements simulated is the one given in figure 4.1, in which the phase difference is achieved through the use of the first balun topology presented previously.

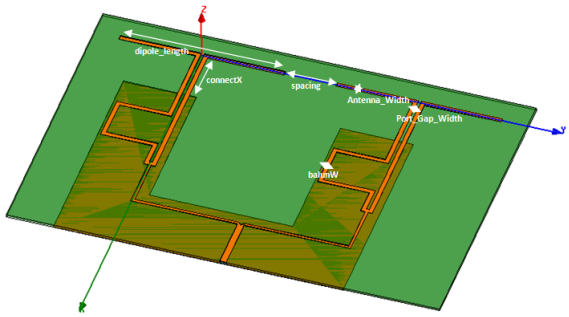

Figure 4.1: 3D - model of the 2-element array used in simulations.

It is important to notice that the figure provided above already possesses the quarter-wavelength transformer. In accordance with what was explained in chapter 1.5, to avoid the grating lobes the distance between the elements has to be inferior to the λ_{FR-4}. After testing several values for the *spacing* - distance between elements - it was decided to use 0.25λ. To avoid repetition it was decided only to present the results achieved with 0.25λ *spacing* and then with the addition of the quarter-

wavelength transformer. The dimensions for the printed array antenna used to accomplish the results without the quarter-wavelength transformer could be seen in table 4.1.

Table 4.1: Dimensions of the 2-element array using topology 1.

Parameter	Value
balunW	1.45 mm
Antenna_ Width	1.45 mm
connectX	0.247λ
dipole_ length	49.5 mm
Port_ Gap_ Width	1.1 mm
spacing	0.25λ

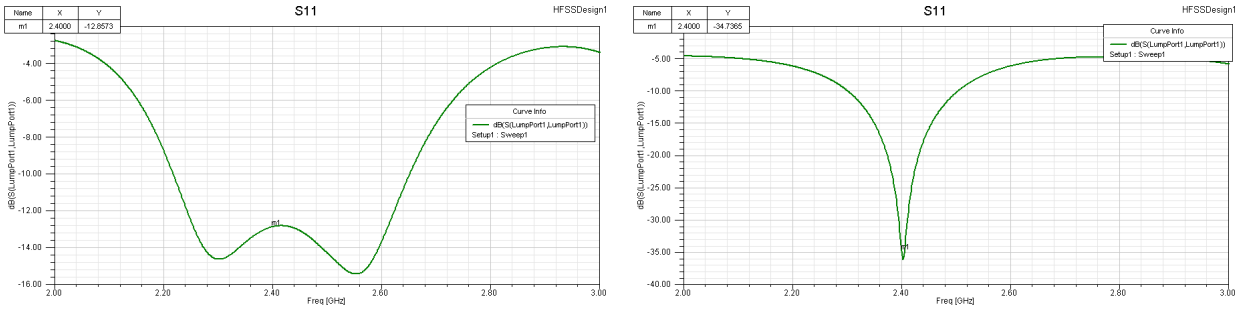

(a) Without the quarter-wavelength transformer (b) With the quarter-wavelength transformer

Figure 4.2: Return loss plot obtained with topology 1.

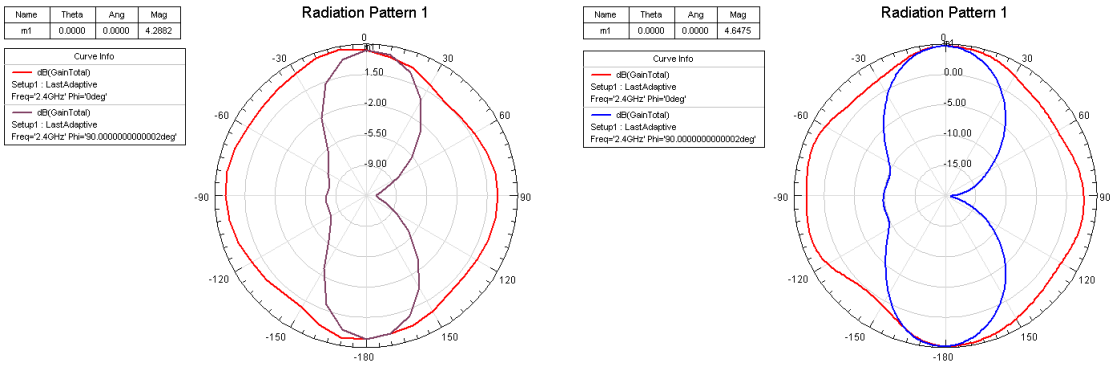

(a) Without the quarter-wavelength transformer (b) With the quarter-wavelength transformer

Figure 4.3: Radiation pattern obtained with topology 1.

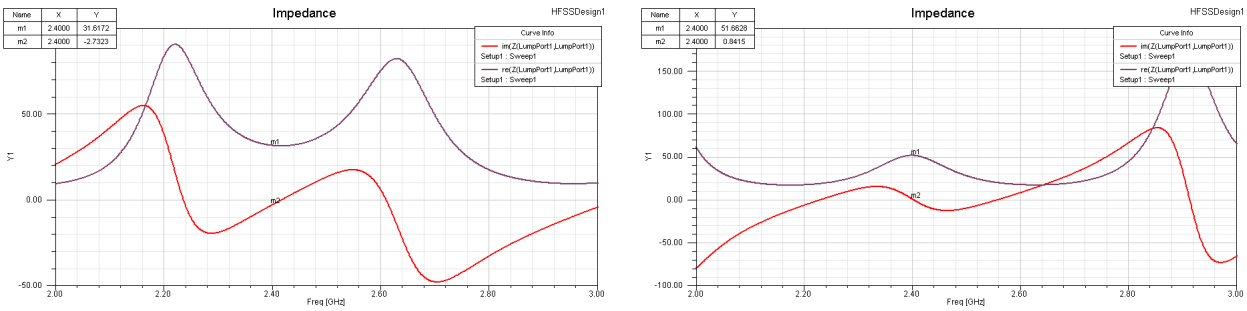

(a) Without the quarter-wavelength transformer (b) With the quarter-wavelength transformer

Figure 4.4: Impedance plot obtained with topology 1.

With the results provided by figure 4.4(a), one was now able to determine the characteristic impedance of the microstrip line of the quarter-wavelength transformer. According to the simulator the input impedance of the antenna at 2.4 GHz is $Z_L = 31.6172 - 2.7323j\Omega$, ignoring the imaginary part one has: $Z_0 = \sqrt{50 \times 31.6172} = 39.76\ \Omega$. Considering $Z_0 = 39.76\Omega$, the quarter-wavelength transformer must have a length of 17.09 mm and a width of 2.12 mm. If one takes a look at the plot from figure 4.4(b), one can conclude that after the addition of the transformer the input impedance of the antenna is closer to 50 Ω of the coaxial cable ($Z_L = 51.6628 + 0.8415j\ \Omega$) - see figure 4.4(b).

Before the addition of the quarter-wavelength transformer the antenna appeared to be matched to 2.4 GHz, but the return loss trace had a rather odd behaviour. Although the array was matched to 2.4 GHz after the addition of the quarter-wavelength transformer, it was decided to increase the dipole length to 51.3 mm in order to achieve a better performance for the printed antenna. In what concerns the radiation pattern, it becomes tighter compared to the ones produced by the single single and has a maximum gain of 4.6475 dB (see figure 4.3(b)). As a matter of fact, there is an increase of approximately 4 dB in the gain compared to the single element, which means that a 2-element array produces narrower radiation pattern than the printed dipole. No improvements in the shape or gain of the radiation pattern are registered after the addition of the transformer (see figure 4.3(a)). What is more, the secondary lobes, that are common when designing arrays, seems to be appearing [18].

It is important to refer that all the plots regarding the addition of the quarter-wavelength transformer had already the dipole's length modified to 51.3 mm.

4.1.2 Topology 2

The second topology to be analysed is shown in figure 4.5. Similarly to topology 1 of the 2-element array, the method used to adjust the antenna to the desired needs is the same.

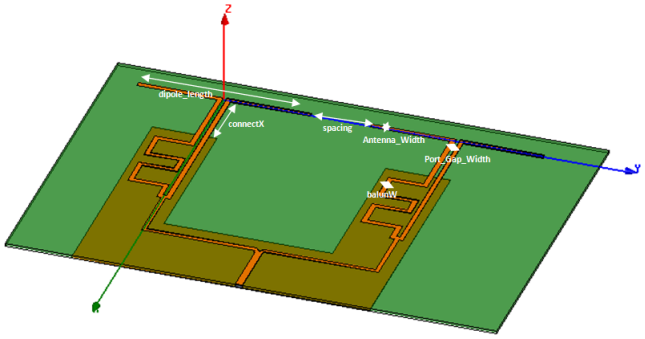

Figure 4.5: 3D - model used to perform simulations.

The values provided in table 4.2 are based on the dimensions obtained for the single element using the topology 2 of the balun, but it was necessary to adjust some of the dipole dimensions to obtain a better value in terms of impedance. As done in the previous topology, the *spacing* was swept until the desired behaviour was reached.

Table 4.2: Dimensions of the 2-element array considering topology 2.

Parameter	Value
balunW	1.45 mm
Antenna_ Width	1.45 mm
connectX	0.25λ
dipole_ length	50.6 mm
Port_ Gap_ Width	1 mm
spacing	0.25λ

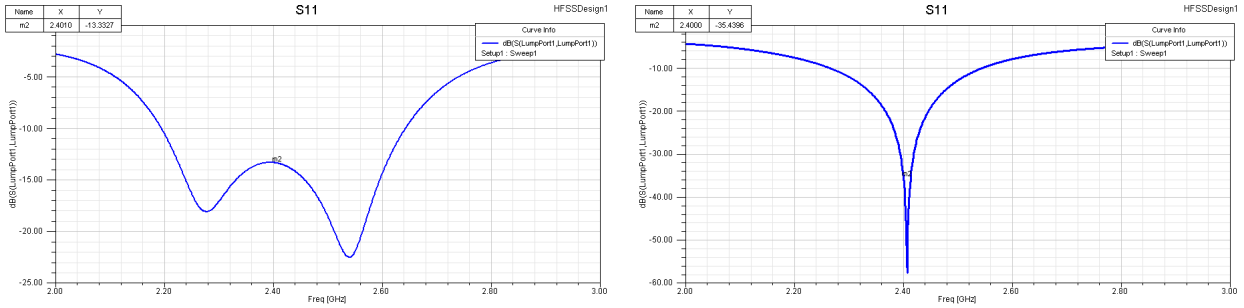

(a) Without the quarter-wavelength transformer (b) With the quarter-wavelength transformer

Figure 4.6: Return loss plot obtained with spacing equal to 0.25λ.

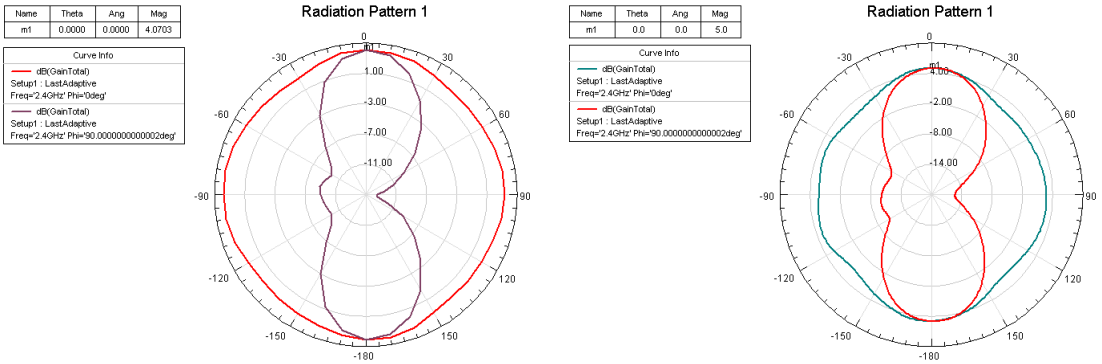

(a) Without the quarter-wavelength transformer (b) With the quarter-wavelength transformer

Figure 4.7: Radiation pattern plot obtained with spacing equal to 0.25λ.

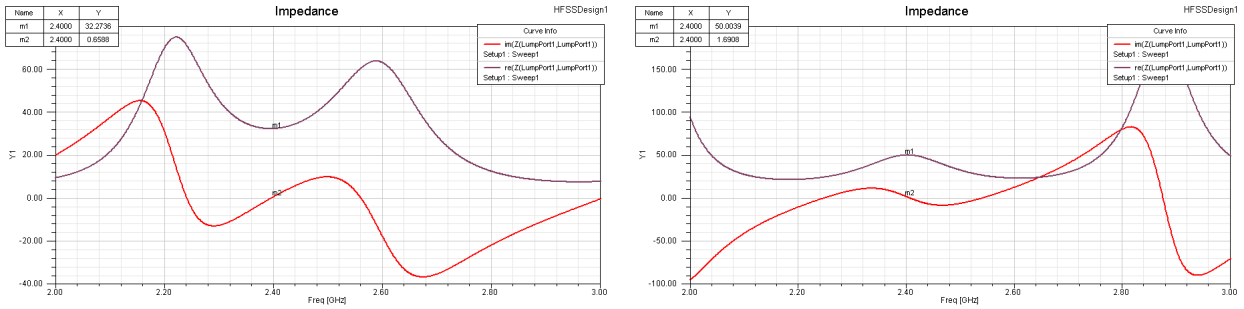

(a) Without the quarter-wavelength transformer (b) With the quarter-wavelength transformer

Figure 4.8: Impedance plot obtained with spacing equal to 0.25λ.

With the dimensions granted in table 4.2, the antenna was already matched to 2.4 GHz, having a return loss of approximately -13 dB (see figure 4.6(a)). The radiation pattern appeared to have a shape similar to the one from topology 1, but the secondary lobes seemed to be more enhanced (see figure 4.7(a)). However, the results obtained without the quarter-wavelength transformer are not much relevant, because the printed array was not matched.

According to the figure 4.8(a) $Z_L = 32.2736 + 0.6588\ j$, so: $Z_0 = \sqrt{50 \times 32.2736} = 40.17\Omega$, which implies a length of 17.10 mm and a width of 2.09 mm.

After performing the simulations with the transformer, it was noticed a minor shift in the return loss plot. In order to correct this the length of the arms of the dipole was changed from 50.7 mm to 50.8 mm. With this change, the minimum value for the return loss is precisely at 2.4 GHz as it observable in figure 4.6(b). It is important to underline that before this modification to the dipole length, the

antenna array was indeed matched to 2.4 GHz. The radiation pattern resembles the one from the previous topology, but appears to be more symmetrical. In this plot is also possible to conclude that the secondary lobes starts to appear. The maximum gain also increased to 5 dB, which represents an increase of 4 dB when compared to the single element gain (figure 4.7(b)). Finally, in agreement with figure 4.8(b), one could state that this antenna is perfectly matched, because its input impedance is $Z_L = 50.0039 + 1.6908j\ \Omega$. With these results, one can conclude that the antenna array is suitable for the desired working frequency.

4.1.3 Topology 3

The last antenna array simulated is presented below in which the third variation of the balun's geometry was used 4.9.

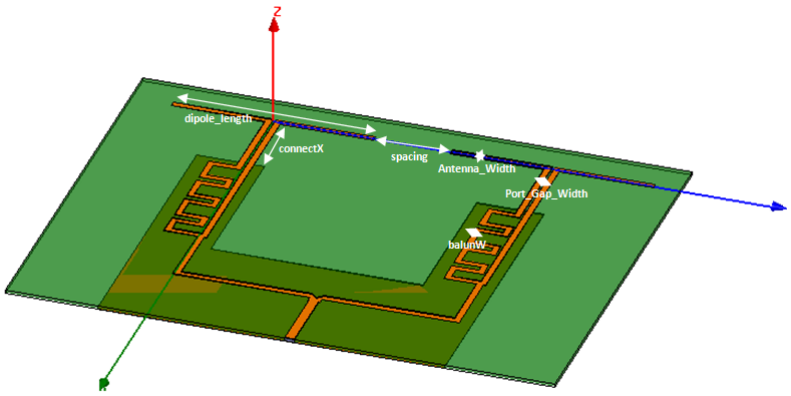

Figure 4.9: 3D - model used to perform simulations.

The first results achieved for the array of two elements could be observed in the next three figures. To produce these plots the dimensions used are described in table 4.3. The procedure for determining the dimensions provided in that table is same used in topology 1 and 2, therefore it already contains the best value achieved for the distance between elements.

Table 4.3: Dimensions of the 2-element array considering topology 3.

Parameter	Value
balunW	1.45 mm
Antenna_Width	1.45 mm
connectX	0.25λ
dipole_length	47.9 mm
Port_Gap_Width	0.65 mm
spacing	0.25λ

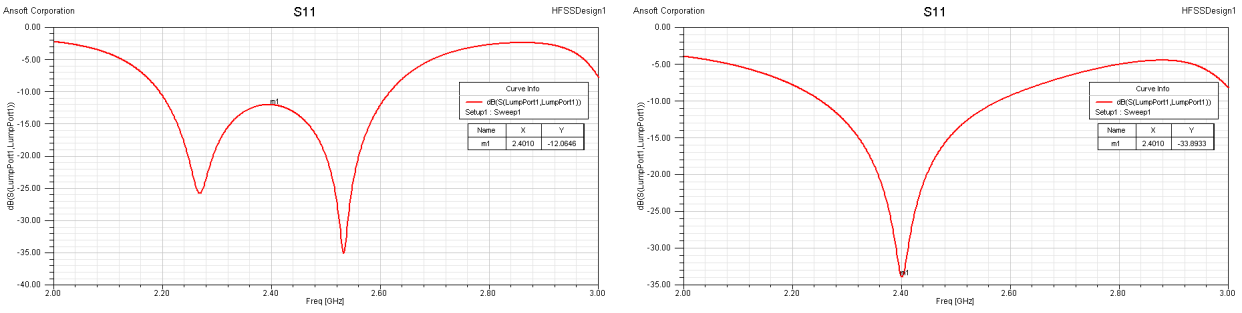

(a) Without the quarter-wavelength transformer

(b) With the quarter-wavelength transformer

Figure 4.10: Return loss obtained with a *spacing* of 0.25λ.

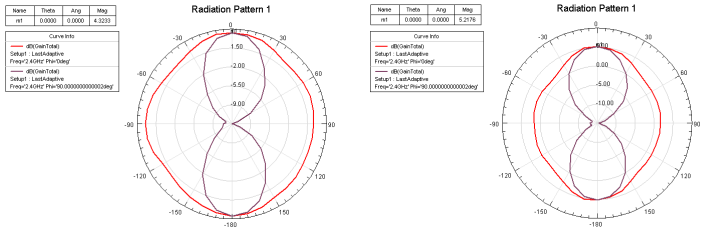

(a) Without the quarter-wavelength transformer

(b) With the quarter-wavelength transformer

Figure 4.11: Radiation pattern obtained with a *spacing* of 0.25λ.

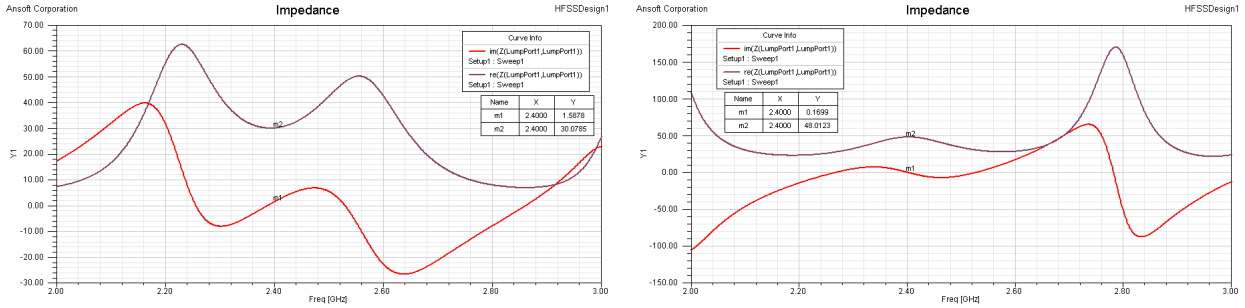

(a) Without the quarter-wavelength transformer

(b) With the quarter-wavelength transformer

Figure 4.12: Impedance plot obtained with a *spacing* of 0.25λ.

Considering the dimensions from table 4.3, the return loss behaved similarly to the ones from previous topologies. In addition, it seemed the antenna is more suitable for 2.52 GHz, but it still lacked the quarter-wavelength transformer that is responsible for providing a proper matching to 2.4 GHz (see figure 4.10(a)). When one looks at the radiation pattern, it is clear that it had tighten and its shape is very acceptable, almost a *doughnut* with no relevant secondary lobes (see figure 4.11(a)). Based on figure 4.12(a), with a *spacing* of 0.25λ the imaginary part has a value of 1.5878j, which could be ignored, and so the characteristic impedance is: $Z_0 = \sqrt{50 \times 30.0785} = 38.7805\Omega$. To achieve this value for the impedance of the microstrip line, the transformer would have to be 2.20 mm wide and 17.05 mm long. After the addition of the quarter-wavelength transformer, the results obtained from the simulator can be observed below.

As previously observed, the match to 50 Ω through a quarter-wavelength transformer improves significantly the results. The return loss has a value of approximately -34 dB at 2.4 GHz, contrary to the -12 dB of figure 4.10(a). Also, the maximum gain is higher (5.22 dB), but one would state that the YZ-plane starts to be affected by the ground plane due to the increase in its area. With this new topology the shape of the radiation pattern is more similar to the *doughnut*, but narrower than the radiation pattern from the single element. The secondary lobes are not significant when compared to the main lobe. Finally, and to confirm the results already provided by the return loss plot, the input impedance of the printed array is 48.0123+0.1699j at 2.4 GHz according to figure 4.12(b), which indicates that the antenna is very well matched to the desired resonance frequency.

4.1.4 Comparison between the three topologies

To finalize the study of three arrays of two dipoles with balanced feeding it is important to compare the results obtained with the three different topologies. The following plots represent the return loss and the radiation patterns of the XY and YZ planes. In what concerns the radiation patterns provided, one would like to state that the plots concerning the radiation pattern are normalized in order to make a proper comparison between the different arrays. To grant a better understanding of the behaviour between the different topologies, one decided to provide a table with some important values concerning dimensions, maximum gain and return loss at 2.4 GHz. In table 4.4 the dimensions $subX$ and $subY$ refer to the width and the length of the substrate, respectively.

Table 4.4: Dimensions of the different 2-element array.

Topology	subX (mm)	subY (mm)	Dipole length (mm)	Maximum gain[1] (dB)	$s11_{2.4GHz}$ (dB)
1	97.47	137.48	51.3	4.78	-34.74
2	97.45	167.44	50.8	5.04	-35.41
3	97.66	130	47.95	5.22	-33.89

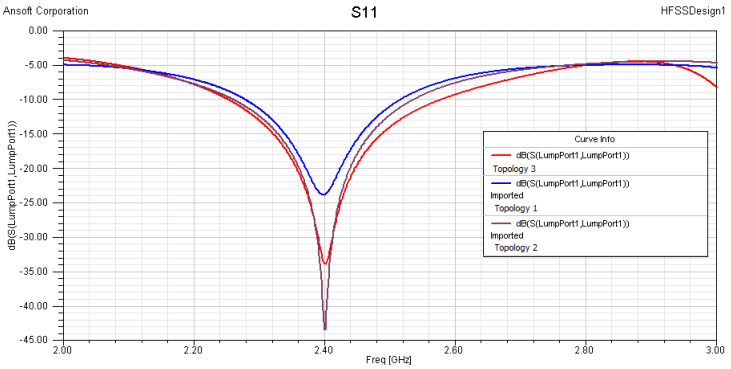

Figure 4.13: Return loss obtained from the different topologies of 2-element arrays.

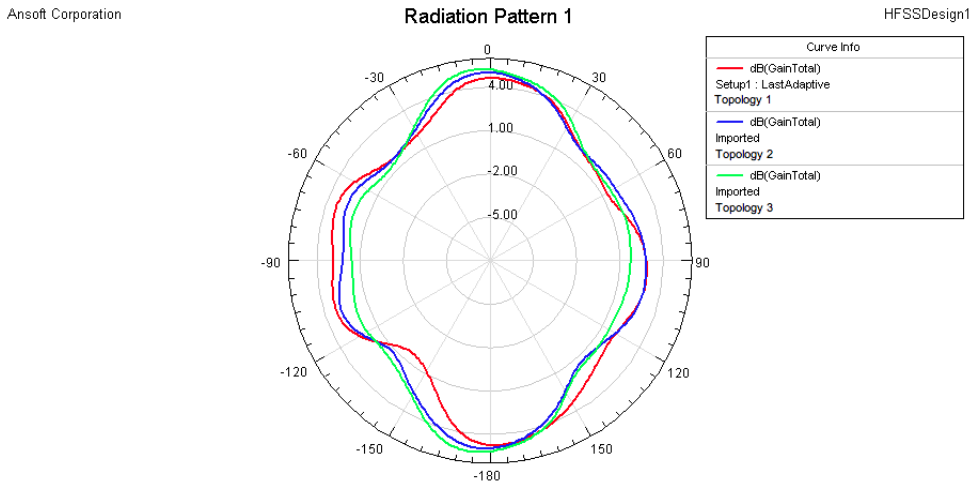

Figure 4.14: Radiation pattern of the XZ plane obtained from the different topologies of 2-element arrays.

[1]Values taken from the 3D-radiation pattern because the radiation pattern is slightly inclined - phase shift is not exactly 180°

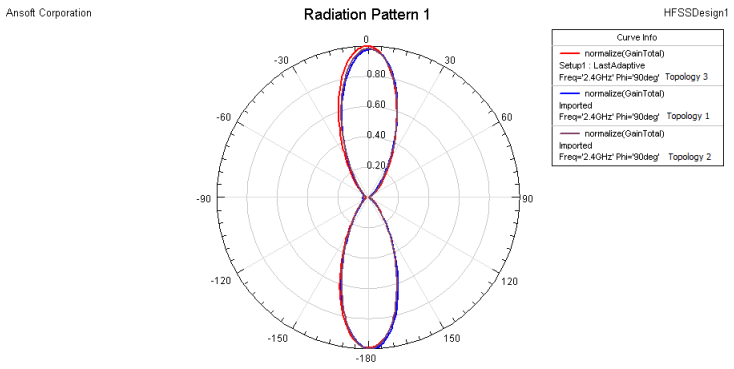

Figure 4.15: Radiation pattern of the XY plane obtained from the different topologies of 2-element arrays.

According to figure 4.34 one can see that topology 2 is the one that is best matched to 2.4 GHz, and the one that has the worst return loss value is topology 1. This is very important when choosing which topology of array one should use, because one is looking for an antenna well matched to the desired resonance frequency. When considering the radiation pattern, specially in the XZ-plane, any of the topologies would perfectly suit the project needs because the shape is quite uniform, i.e., the antenna radiates almost equally (see figure 4.14). Based on the results for the XY-plane (figure 4.15), it is observable that all the topologies have a very similar behaviour in terms of shape of the radiation pattern. There is another important conclusion to mention which is the influence of the balun in the size of the array i.e., the dipole length of topology 1 is a bit longer than the one from topology 3. In fact, this might happen due to the decrease in width of the ground plane. The importance of this arises when one aims to build an antenna as small as possible.

In conclusion, the maximum gain increases with the compression of balun's width, whereas the dipole's length decreases. Considering the results obtained until this point of the work, it is important to evidence that topology 3 has the best performance.

4.2 The 4-element array of printed dipoles

To tighten more the radiation pattern it was decided to build an antenna array of four elements. This time, to build the array the 2-element arrays previously presented were used i.e., the single element is now a couple of printed dipoles. This approach made the simulations easier to perform because the distance between the printed dipoles and the rest of the dimensions were already determined, therefore the two arrays of two elements of each topology has to be joined, and then the input impedance has to measured to match the array to 2.4 GHz with a quarter-wavelength transformer.

4.2.1 Topology 1

The first array of four elements to be analysed is the one provided in figure 4.16.

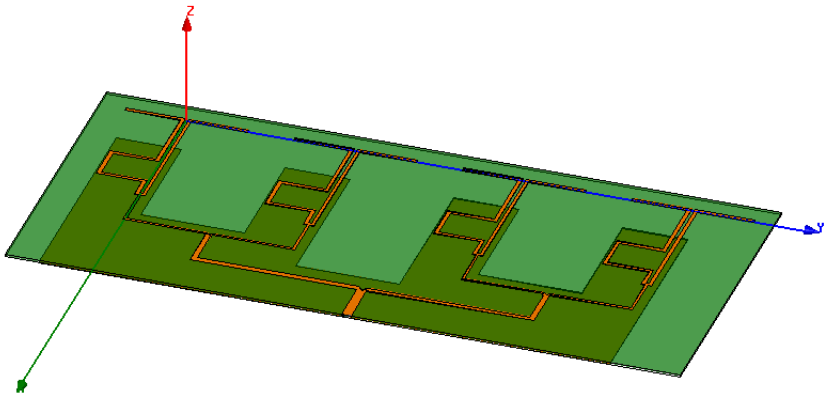

Figure 4.16: 3D-model used in simulations for the 4-element antenna array.

In agreement with what was said in the beginning of this chapter two arrays of two elements from topology 1 are joined together. Then, if the reactance was not near zero, the distance between the elements or any other of the parameters have to be swept in order to get better results. In fact, it was necessary to perform a sweep to lower the reactance part when the values of the 2-element array were used. To accomplish this the dipole length increased from 51.3 mm to 51.4 mm (see table 4.5).

Table 4.5: Dimensions of the 4-element array from topology 1.

Parameter	Value
balunW	1.45 mm
Antenna_ Width	1.45 mm
connectX	0.247λ
dipole_ length	51.4 mm
Port_ Gap_ Width	1.1 mm
spacing	0.25λ mm

Based on to the plots provided below (see figure 4.17), it is clear that the antenna is not matched to 2.4 GHz, but the imaginary part of the impedance is very low and can be ignored: -0.8622j. Although the radiation pattern produced by the array before the addition of the quarter-wavelength is not provided, it appeared to be gaining secondary lobes and was highly warped, but this can only be confirmed after the suitable matching was performed. It is known that the augment in the number of elements leads to the appearance of secondary lobes, which usually is a drawback when designing antenna arrays.

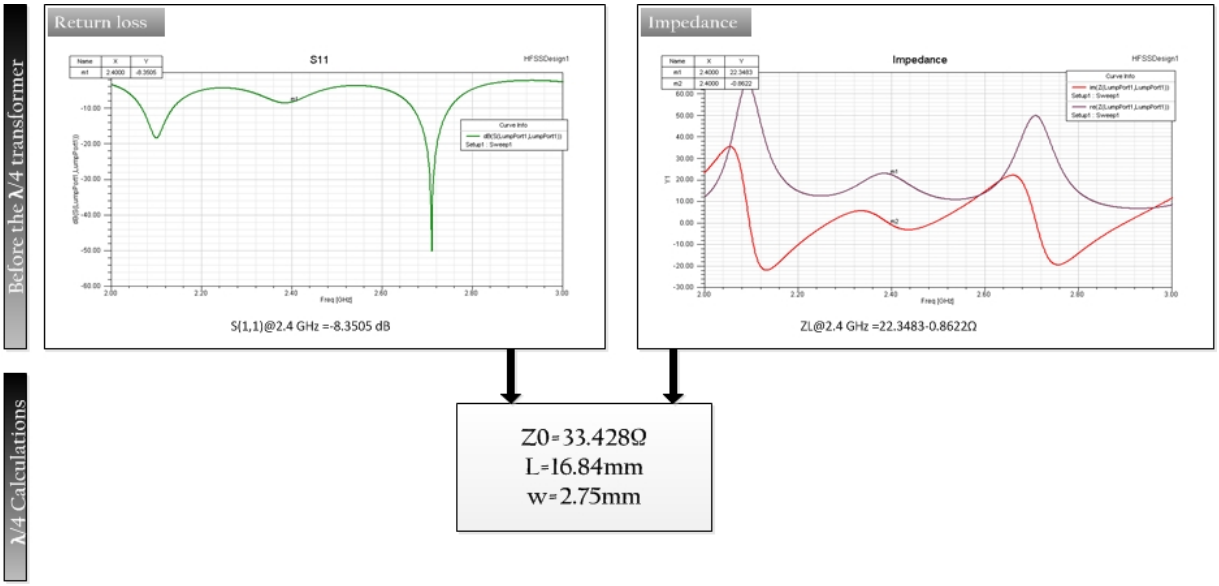

Figure 4.17: Plots obtained from the values of table 4.5 and the dimensions of the quarter-wavelength transformer.

The procedure to calculate the dimensions of the transformer is the same that was already done before: from figure 4.17 one can see that $Z_L = 22.3483 - 0.8622\Omega$, and then the characteristic impedance for the transmission line becomes $Z_0 = \sqrt{50 \times 22.3483} = 33.43mm$. To accomplish this value for the characteristic impedance the transmission line has to be 16.84 mm longer and 2.75 mm wider.

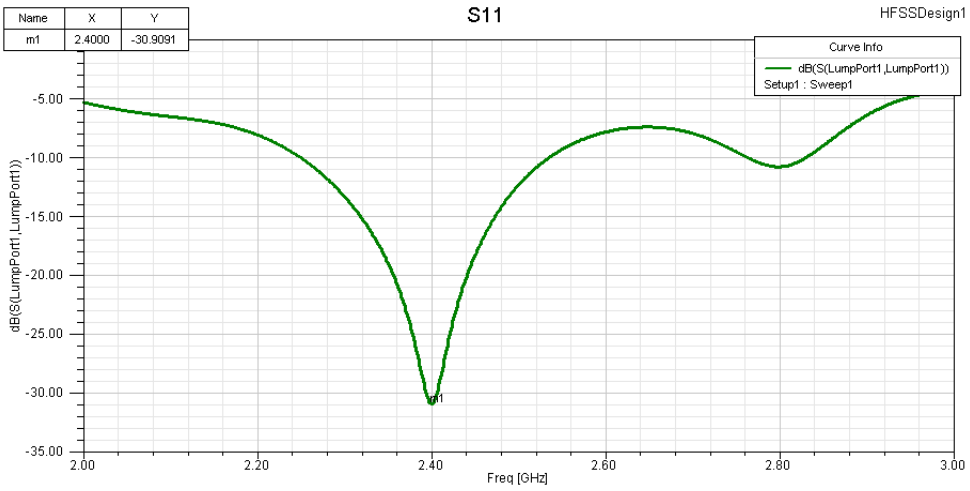

Figure 4.18: Return loss plot of the 4-element array using topology 1 for the balun design with the quarter-wavelength transformer.

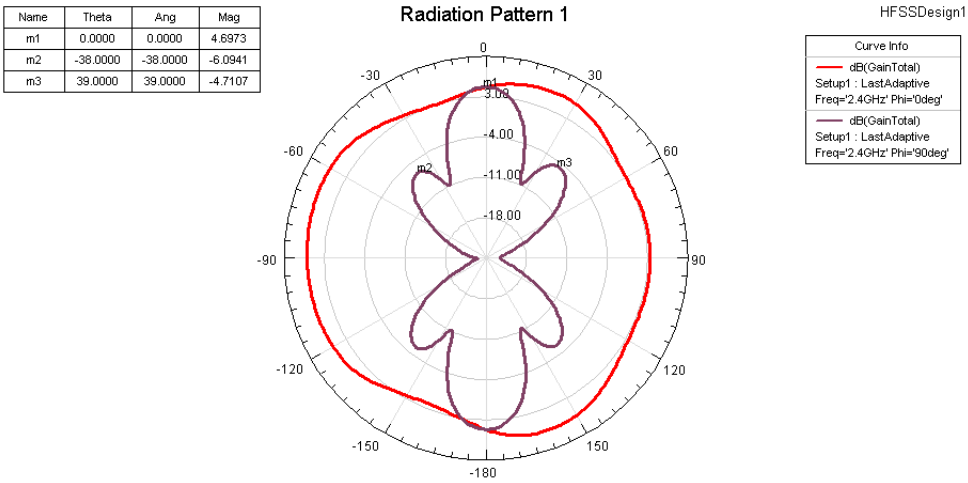

Figure 4.19: Radiation pattern of the 4-element array using topology 1 for the balun design with the quarter-wavelength transformer.

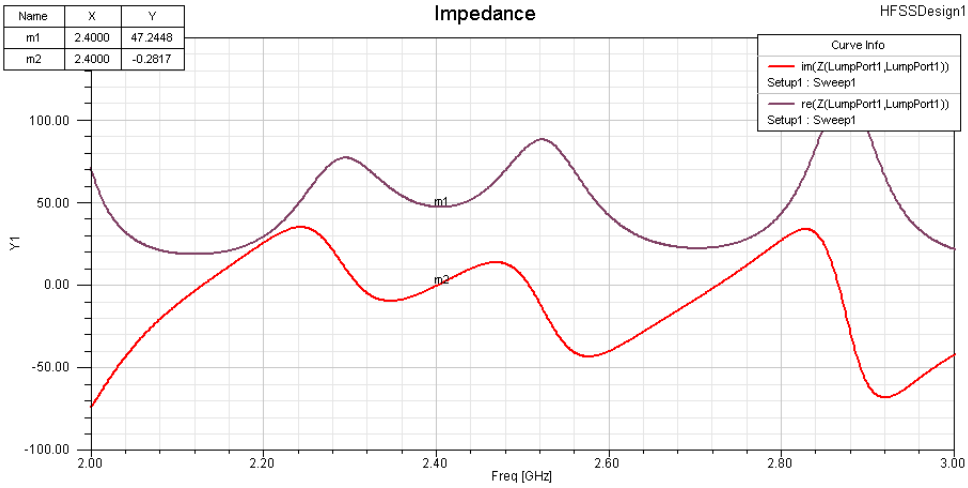

Figure 4.20: Impedance plot of the 4-element array using topology 1 for the balun design with the quarter-wavelength transformer.

After simulating the 4-element array with the quarter-wavelength transformer, it was noticed a slight shift to the left of the return loss plot, so the dipole length was adjusted to 50.45 mm to obtain the trace from figure 4.18. Still concerning the plot from figure 4.18, the antenna array is perfectly matched to 2.4 GHz with a return loss value of approximately -31 dB. As matter of fact, this is confirmed by the impedance plot as well, because the input impedance of the antenna at 2.4 GHz is $Z_L = 47.2448 - 0.2817j\Omega$(see figure 4.20). Contrary to what was observed before the addition of the quarter wavelength transformer, the radiation pattern has its secondary lobes less evidenced and its shape is symmetrical. It is also noticeable that these secondary lobes are not relevant because they are almost 9 dB above the main lobe, as one can conclude from the observation of figure 4.19

4.2.2 Topology 2

In this part of the work a four-element array of printed dipoles with baluns from topology 2 will be studied. The 3D-model used to perform simulations in HFSS is provided below in figure 4.21.

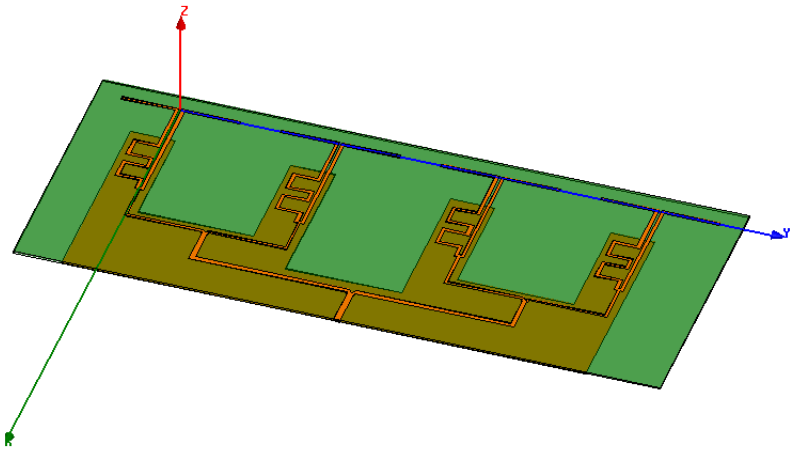

Figure 4.21: 3D-model of the 4-element array used in simulations.

As it was already explained for the first topology of the 4-element array, the simulations began by using the dimensions determined in section 4.1 , where the 2-element array of topology 2 was studied. Once more the suitable dimensions determined for the 2-element array did not lead to adequate results in terms of impedance, therefore the dipole length was reduced from 50.8 mm to 50 mm. Due to ease of reading the values are provided in table 4.6 and the results produced are following it.

Table 4.6: Dimensions of the 4-element array considering topology 2.

Parameter	Value
balunW	1.45 mm
Antenna_ Width	1.45 mm
connectX	0.25λ
dipole_ length	50 mm
Port_ Gap_ Width	1 mm
spacing	0.25λ mm

From figure 4.22 it is clear that at 2.4 GHz the antenna is totally mismatched, but instead it is quite matched at approximately 2.12 GHz and 2.70 GHz. In what concerns the input impedance plot shown in figure 4.22, the reactance is almost zero which is acceptable to do the matching of the antenna with a quarter wavelength transformer.

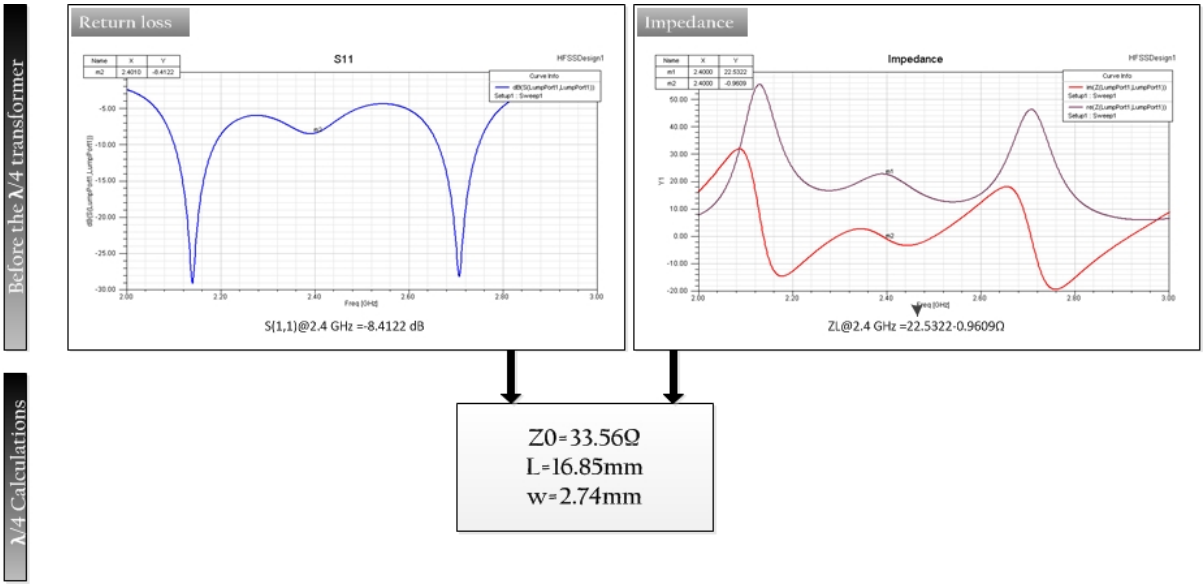

Figure 4.22: Plots obtained from the values of table 4.6 and the dimensions of the quarter-wavelength transformer.

After measuring the impedance at 2.4 GHz with the help of the simulator - $Z_L = 22.5322 - 0.9609\Omega$ - the characteristic impedance of the transmission line for the quarter-wavelength transformer is $Z_0 = \sqrt{22.5322 \times 50} = 33.565\Omega$, which corresponds to a width of 2.74 mm and a length of 16.85 mm. The simulation of the four element array with the quarter-wavelength transformer led again to minor shift in the return loss i.e., the minimum value for the return loss was not centred at 2.4 GHz. To achieve a better match at this frequency, the length of the dipole arms was swept and it was concluded that decreasing it to 48.45 mm grants better results (see figure 4.23).

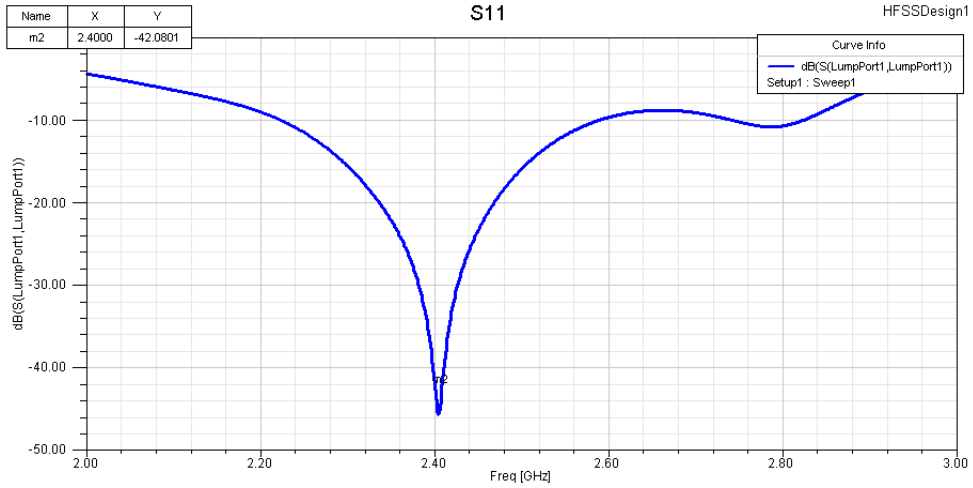

Figure 4.23: Return loss plot obtained with the addition of the quarter-wavelength transformer.

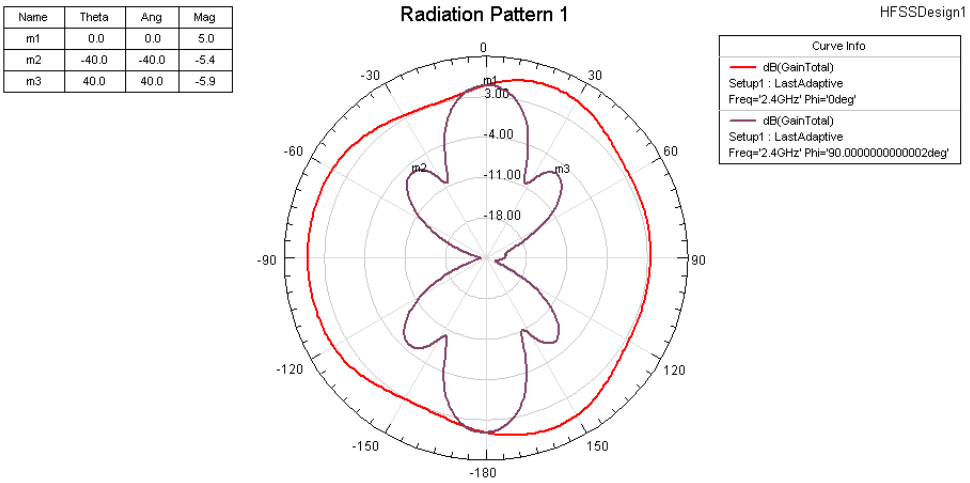

Figure 4.24: Radiation pattern obtained with the addition of the quarter-wavelength transformer.

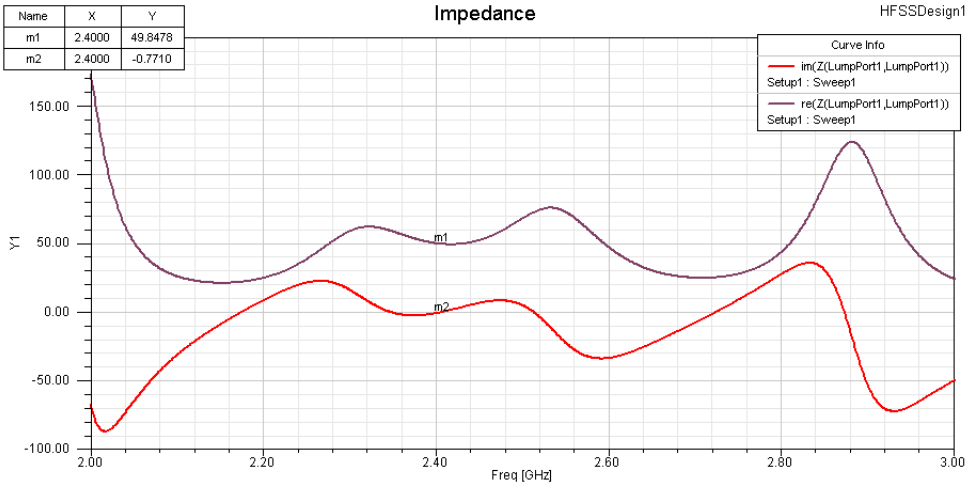

Figure 4.25: Impedance plot obtained with the addition of the quarter-wavelength transformer.

With the addition of the quarter-wavelength transformer and the sweep of the length of the dipole arms, it was possible to achieve a return loss value of -42.0801 dB. The change in the dipole length might be due to the ground plane area, which is increasing with the number of elements. In addition to this, the radiation pattern is affected, specially in the plane XZ. The maximum gain rounds the 5 dB and the secondary lobes are approximately 10 dB and 11 dB below the main lobe. In the XY-plane the radiation pattern shape obtained is more symmetrical and seems to be less affected by the ground plane. The impedance plots shows that at 2.4 GHz, the real part is almost 50 Ω and the imaginary part is insignificant.

4.2.3 Topology 3

This is the last array of printed dipoles that will be studied, and its 3D-model could be seen in figure 4.26. Once again, it is possible to observe that the 3D-model presented already includes the quarter-wavelength transformer that allows the matching between the the antenna and the feeding port for a resonance frequency of 2.4 GHz.

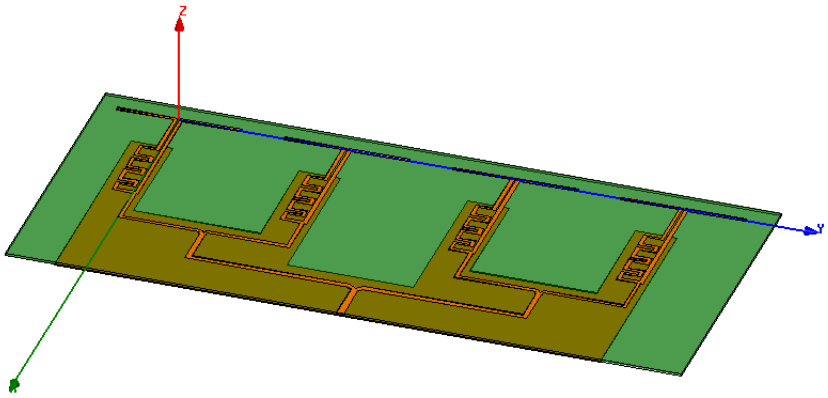

Figure 4.26: 3D-model used in simulations for the 4-element antenna array.

Using the dimensions from table 4.7, the results given by the simulator were not satisfactory, thus a sweep of the distance between elements and the dipole length was performed. The main reason that led to the sweep was to eliminate the imaginary part of the impedance at 2.4 GHz(see figure 4.27).

Table 4.7: Dimensions of the 4-element array considering topology 3.

Parameter	Value
balunW	1.45 mm
Antenna_ Width	1.45 mm
connectX	0.25λ
dipole_ length	47.9 mm
Port_ Gap_ Width	0.65 mm
spacing	0.25λ mm

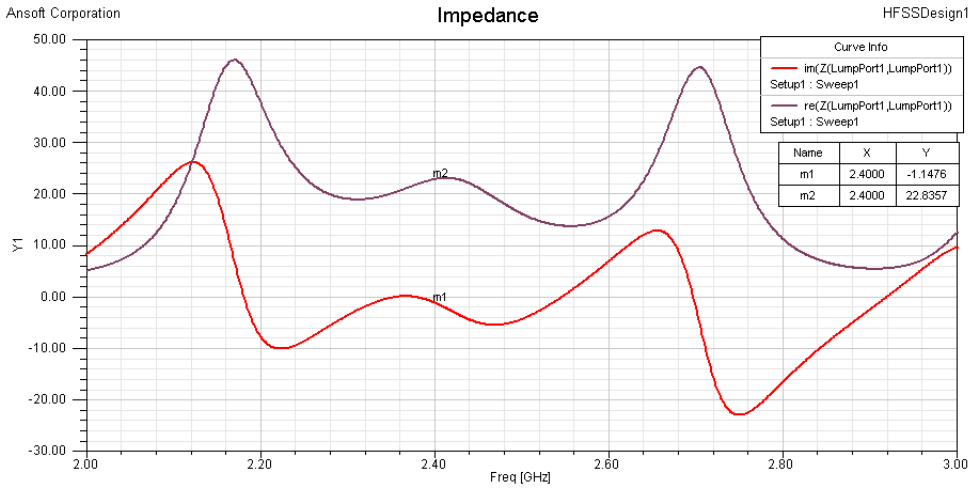

Figure 4.27: Impedance plot considering the dimensions provided in table 4.7.

After the sweep it was reached the conclusion that a *spacing* of 0.24λ and a dipole length of 47.95 mm would grant an impedance value of 23.7521-0.5219j, which is quite better than the one shown in figure 4.27. The following results were produced by the simulator before the addition of the quarter-wavelength transformer.

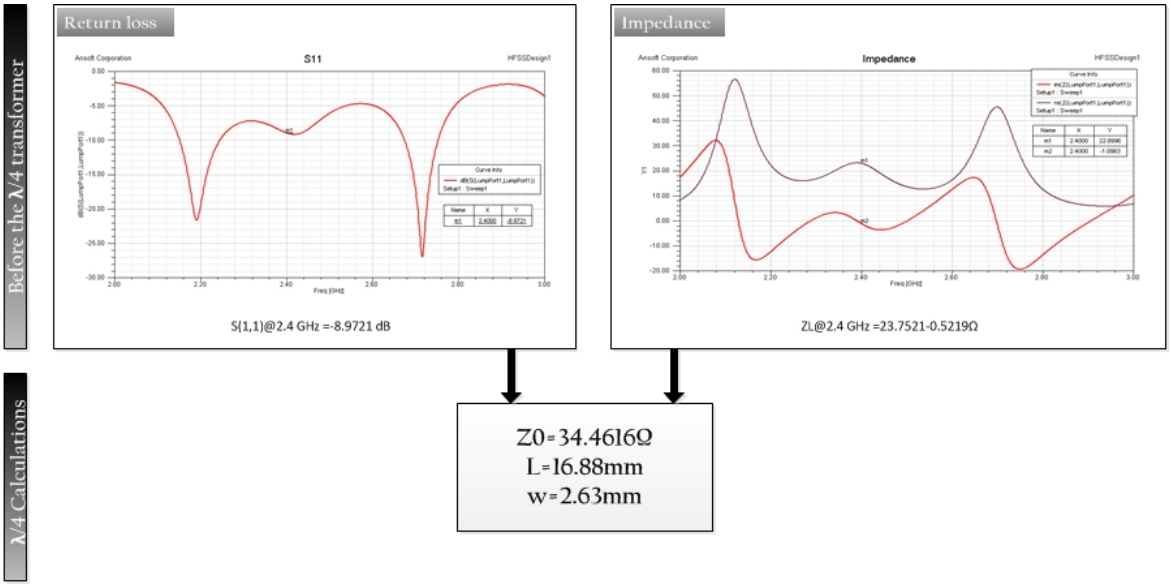

Figure 4.28: Plots obtained from the values of table 4.7, except for spacing which equals 0.24λ, and the dimensions of the quarter-wavelength transformer.

when considering figure 4.28 it is noticeable that the antenna is not yet matched to the desired resonance frequency. Moreover, the impedance value at 2.4 GHz given by the plot from figure 4.28, which is far from 50Ω - $Z_L = 23.7521 - 0.5219j\ \Omega$.

With a $Z_L = 23.7521 - 0.5219j\ \Omega$, ignoring the value of the imaginary part, one was ready to calculate the adequate characteristic impedance for the quarter-wavelength transformer: $Z_0 = \sqrt{23.7521 \times 50} = 34.4616\Omega$. To have a characteristic impedance of 34.4616 Ω in microstrip technology the transmission line has to be 2.63 mm wide and 16.88 mm long.

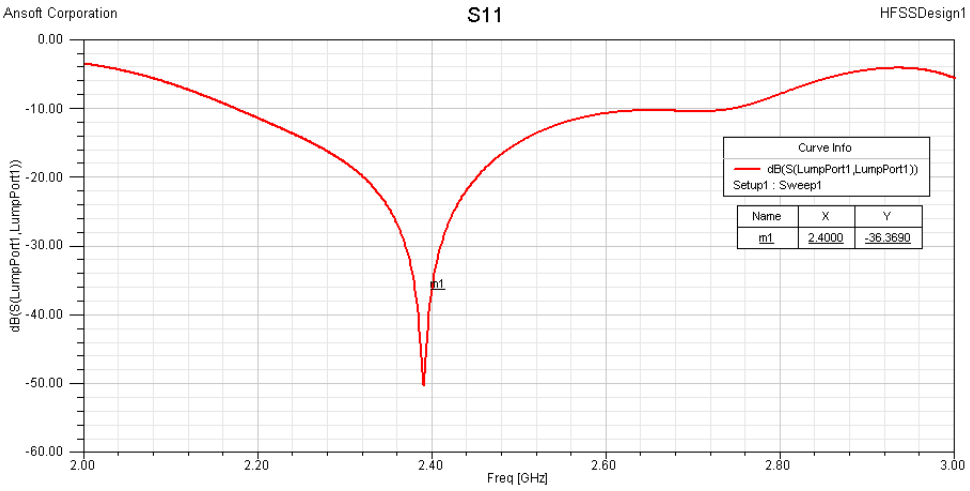

Figure 4.29: Return loss obtained after adding the quarter wavelength transformer to the 4-element array.

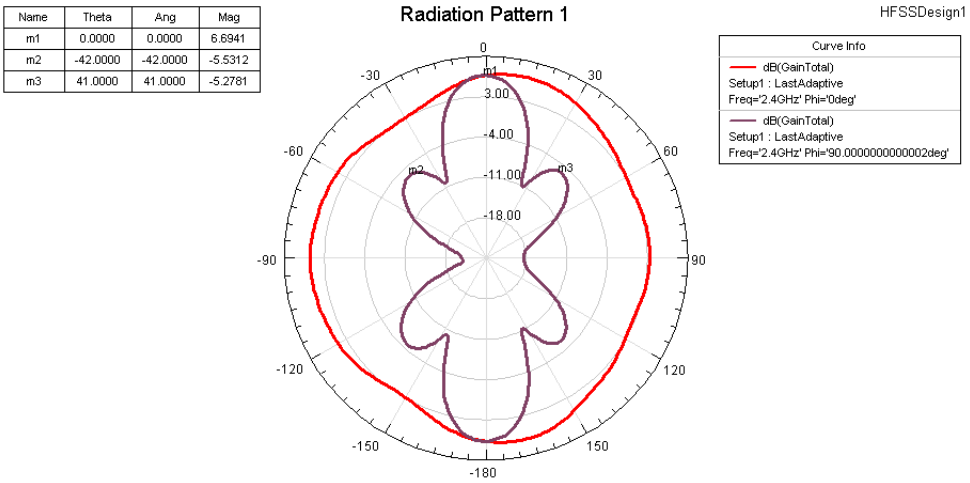

Figure 4.30: Radiation pattern obtained after adding the quarter wavelength transformer to the 4-element array.

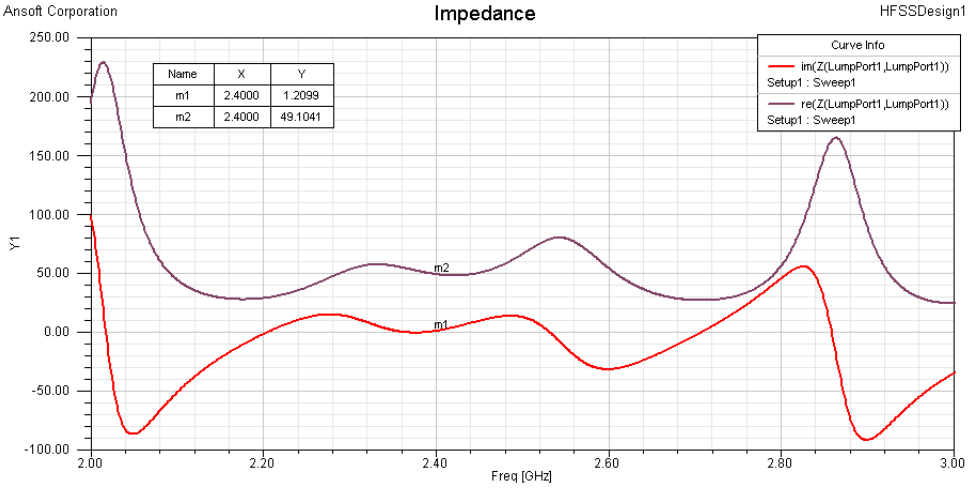

Figure 4.31: Impedance plot obtained after adding the quarter wavelength transformer to the 4-element array.

Although the minimum value of return loss obtained after joining the quarter-wavelength transformer and the array is not exactly at 2.4 GHz, the antenna has a return loss of -36 dB at that frequency. In fact, it was tried to shift the return loss trace to 2.4 GHz, but to achieve this the length of the dipole had to be modified to a value that is not possible build physically in the university department. The minimum precision that is available in the university is 0.1 mm and a length between 47.75 mm and 47.76 mm was needed. The plot from figure 4.29 was produced using a dipole length of 47.76 mm. It is believed that this change in the length of the arms of the dipole is due to the increase in the area of the ground plane. As it was proved before, the wider the ground plane the longer the dipole arms have to be in order to achieve a specific resonance frequency. In what concerns the match to 2.4 GHz, one would say that the input impedance has a reasonable value: 49.1041+1.2099 j. The radiation pattern is very similar to the ones already obtained with topologies 1 and 2. The maximum gain rounds 6.7 dB and its secondary lobes arise approximately 11 dB below, which is suitable for the project needs.

4.2.4 Comparison between the three topologies

The study of three proposed topologies for the arrays of four elements is now concluded, and to provide an overall view, the main differences registered during the simulations are resumed in table

Table 4.8: Dimensions of the different 4-element array.

Topology	subX (mm)	subY (mm)	Dipole length (mm)	Maximum gain [2] (dBi)	$S_{(1,1)_{2.4GHz}}$ (dB)
1	115.31	271.56	50.45	6.71	-30.90
2	115.30	275	48.45	6.82	-42.08
3	115.54	260	47.76	7.15	-36.37

In conclusion, the topology that has the best performance is topology three. When simulating these arrays of 4-elements, it was noticed that the length of the arms of the dipole had to be changed, therefore there is no major differences between them, contrary to what happened when studying the single dipole and the 2-element array. These modifications concern the return loss shifts observed after the addition of the quarter-wavelength transformer and also, the impedance adjustments. In those cases, if one shrank the width of the balun, the overall length of the arms decreased in order to reach the desired resonance frequency. However, no matter which geometry is chosen, any of the arrays would suit the project needs.

Another important consideration to take into account is the shape of the radiation pattern, which can be observed in figure 4.32. In the XY-plane the shape of the radiation pattern is very similar between topologies, but topology two is the one that produced more significant secondary lobes. Actually, topology 3 is the one that has its secondary lobes lower than the main lobe, which is an advantage when considering the system that is intended to develop. In what concerns figure 4.33, there are not significant differences between topologies but again, it is noticeable that the ground plane has a considerable effect in the radiation pattern of the various arrays. If it did not influence, the radiation pattern in the XZ-plane would be a "perfect" circle.

Although one have already referred the values of return loss for 2.4 GHz in table 4.8, it was decided to present a plot where it is possible to observe the three traces. One conclusion that can be taken from the same plot is that bandwidth increases significantly from topology 1 to topology 3. In addition, it seems that topology 2 and 3 are better matched to the desired resonance frequency than topology 1.

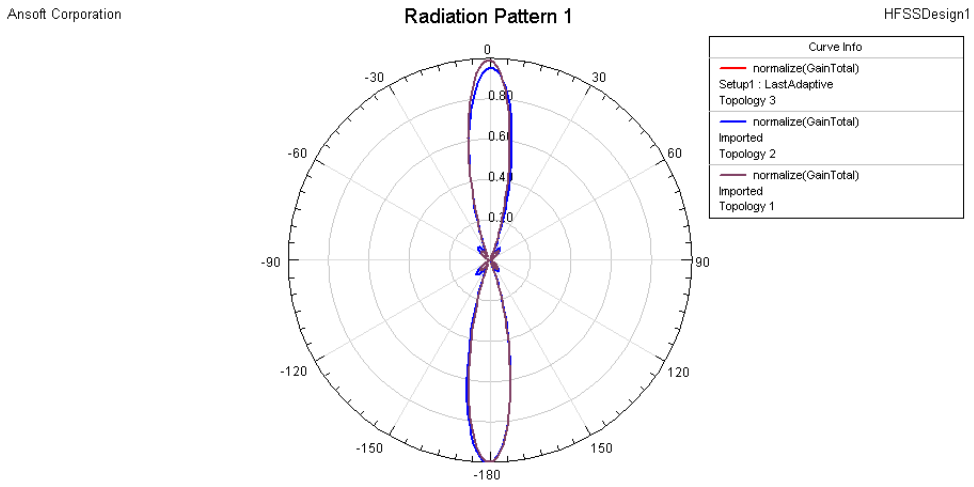

Figure 4.32: Radiation pattern of the three topologies in the XY-plane for 2.4 GHz.

[2]Values taken from the 3D-radiation pattern because the radiation pattern is slightly inclined - phase shift is not exactly 180°

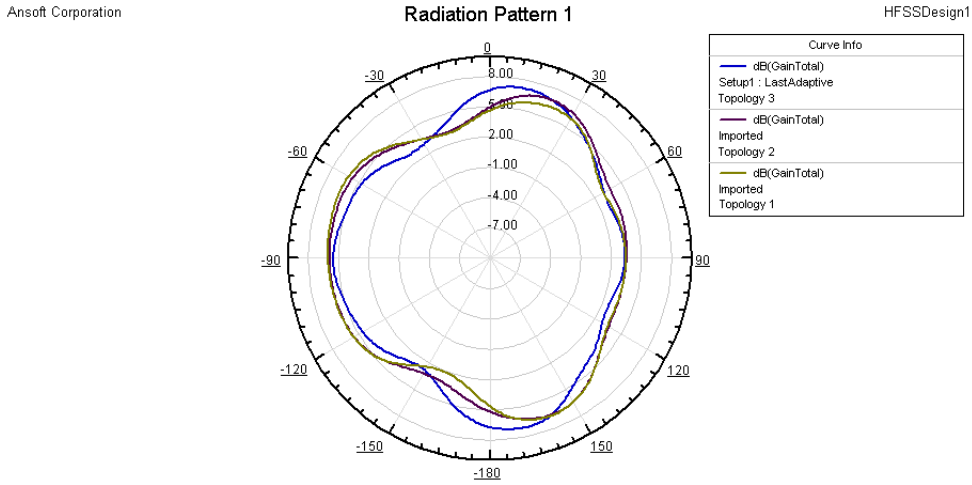

Figure 4.33: Radiation pattern of the three topologies in the XZ-plane for 2.4 GHz.

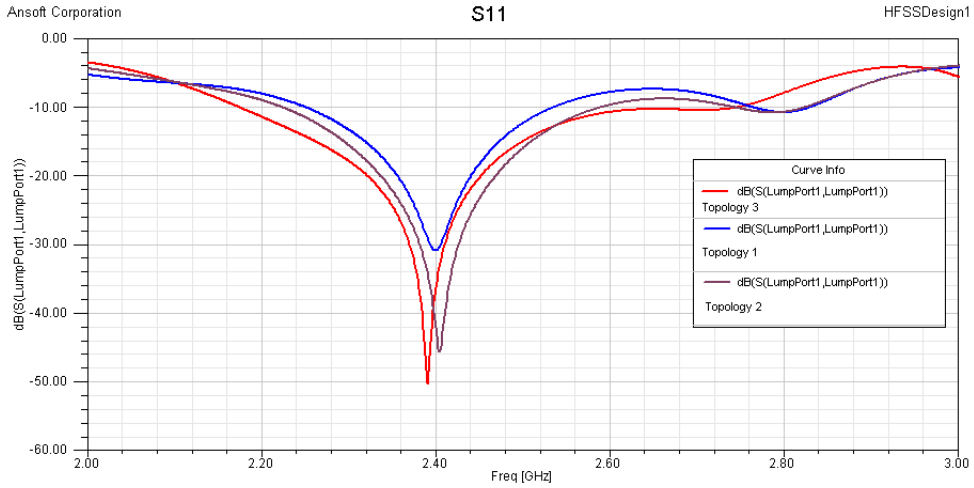

Figure 4.34: Return loss of the three topologies.

4.3 Comparison between single element, 2-element and 4-element printed dipole antennas

In this section it is aimed to prove that the augment of elements in an antenna leads to the increase in its directivity and consequently its maximum gain. Only the third topology will be analysed to avoid repetition, because all of them have similar behaviours. In line with the values from table 4.9, there is a significant increase in gain from a single dipole to an array of two or four elements. From the observation of figure 4.35, one could see that the radiation pattern has became tighter as desired, confirming that the array of printed dipoles designed became a broadside array.

Table 4.9: Maximum gain values for the different antennas using the balun from topology 3.

Antenna type	Maximum gain (dBi)
Single element	1.70
2-element	5.22
4-element	7.14

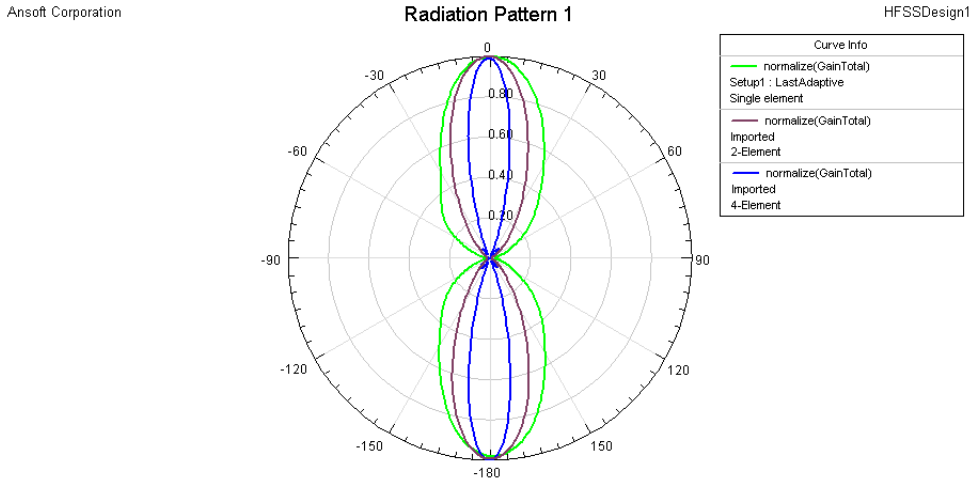

Figure 4.35: Radiation pattern produced by the different antennas studied of topology 3 -XY plane.

4.4 Measurement and analysis of printed arrays of dipoles

4.4.1 Experimental results produced by the VNA and the anechoic chamber

As previously explained in section 4.1.4, the antenna that had the best performance was topology 3. Nevertheless, any of the three would fit the project specifications, therefore it was decided to build topology 2 and analyse its performance. In figure 4.36 it is possible to see the antenna accompanied by a ruler so as to grant an idea of its physical size. Furthermore, it was decided to provide the back view of the antenna, where the ground plane lies.

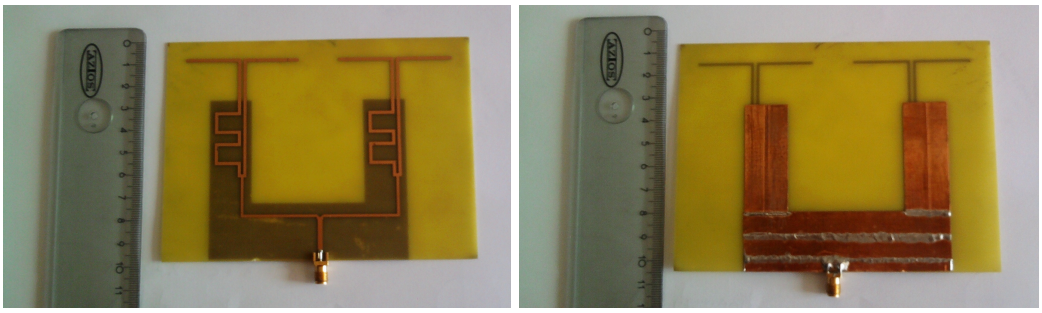

(a) Front view (b) Back view

Figure 4.36: 2-element array of printed dipoles from topology 2.

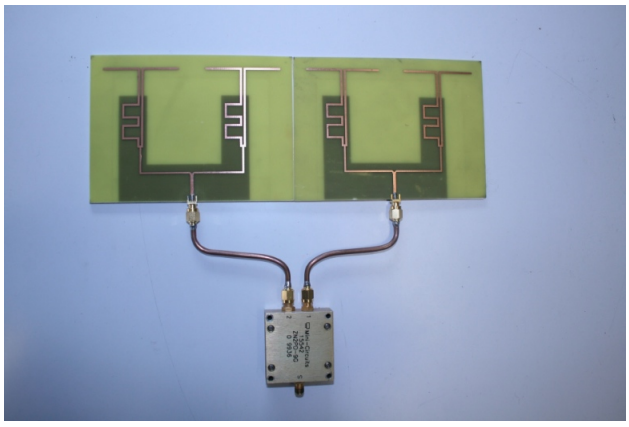

Figure 4.37: 4-element array of printed dipoles from topology 2.

The antenna array represented in figure 4.36 was the one chosen to do experiments and measurements. In addition, it was decided to build the 4-element array antenna using topology 2 with two 2-element array antennas from figure 4.36. To join the two antennas a power divider was used as it is shown in figure 4.37. As previously stated, the university facility does not allow the construction of such a large antenna, which led to this 'handmade' construction.

The experimental results obtained in the anechoic chamber and in the VNA are provided in figures 4.38, 4.39(a) and 4.39(b), concerning the 2-element and 4-element antenna arrays.

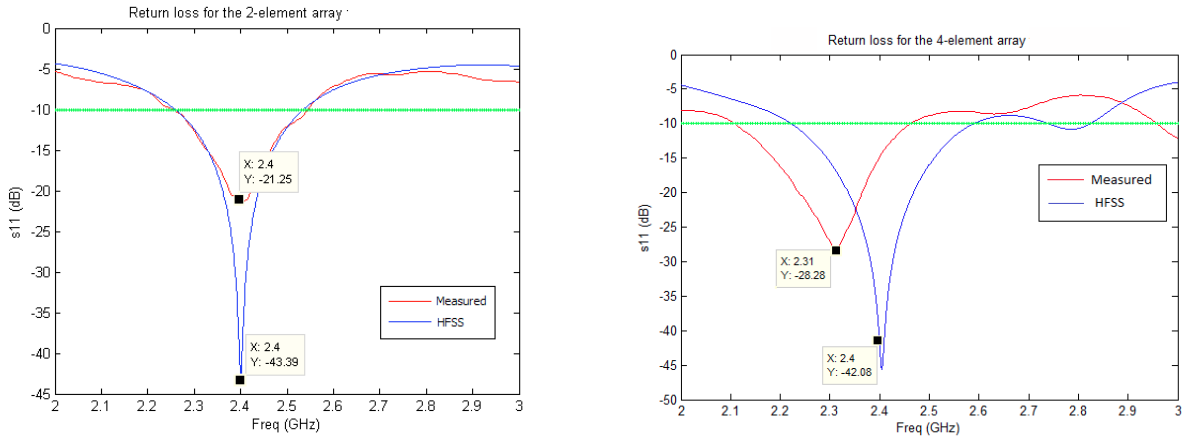

(a) 2-Element array.

(b) 4-Element array.

Figure 4.38: Return loss plot obtained in the simulator and in the VNA.

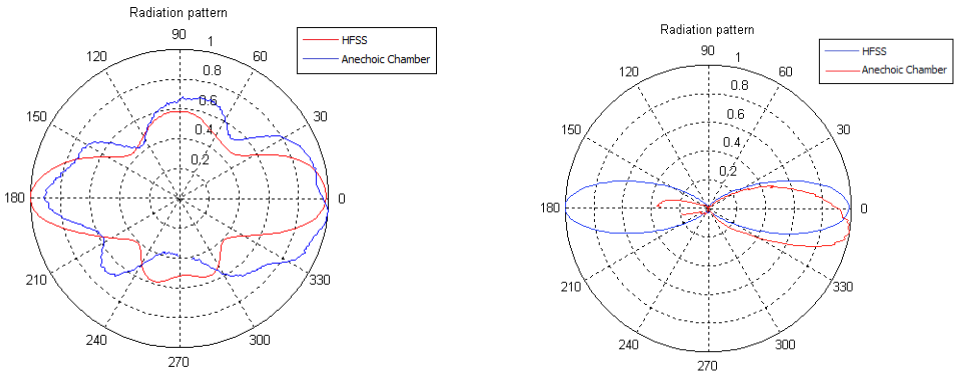

(a) XZ-plane

(b) XY-plane

Figure 4.39: Normalized radiation pattern plot obtained in the anechoic chamber and in the simulator for the 2-element array.

The results regarding figure 4.38(a) show that the measured resonance frequency is 2.4 GHz as designed in the simulator. Actually, the return loss plots granted by the simulator and the VNA are very similar, except that in the simulator the return loss value at 2.4 GHz is more significant: $S_{(1,1)_{2.4GHz(HFSS)}} = -43.39dB$ whereas the measured one is $S_{(1,1)_{2.4GHz(VNA)}} = -21.25dB$. In the same figure, it is also possible to see a green line at -10 dB with the aim of facilitating the determination of the array's bandwidth, which is from approximately 2.3 GHz to 2.55 GHz. From the plots of figure 4.39, it is possible to conclude that both radiation pattern planes do not differ much from the HFSS results. In fact, the main difference registered is in the XY-plane, in which seemed that the antenna was not radiating backwards. This might have happened because of the set-up that was holding the antenna, which might have caused some kind of interference, or even due to misalignment of the antennas.

About the antenna of four elements, the measurement of the return loss behaviour with the VNA was not as satisfactory as the 2-element array. In fact, this time the return loss trace is slightly shift to

the left i.e., the minimum value of return loss happens at 2.3 GHz instead of 2.4 GHz. This might be explained by the construction of the antenna, which has the coaxial cables, the power divider and new layer of material in which the antenna was glued. Actually, this material might alter the impedance of the antenna leading to the mismatch at 2.4 GHz. However, from the observation of figure 4.38(b), the antenna has a quite acceptable value of $S_{(1,1)_{2.4GHz(VNA)}} \simeq -12dB$, which is still below -10 dB.

4.4.2 Determination of the antenna's behaviour in a real situation

The measurements done in the previous section (4.4.1) do not portray correctly the indoor behaviour of the antenna. To verify the antenna's performance in providing the correct directions to identify the door, the set-up from figure 4.40 was used. In addition, figure 4.41 shows several marks on the ground, which represent the points where the power levels were measured. This set-up consisted of a signal generator in which the array of printed dipoles was attached , and a spectrum analyser with an antenna possessing a resonance frequency of approximately 2.4 GHz. In what concerns the receiver's antenna, it is known that it has linear polarization and its resonance frequency is 2.4 GHz as previously stated. There was no information about the gain or the radiation pattern (see figure 4.42(c)). Also, the receiver's antenna is stuck to a wood post, which is supposed to portray a person.

Figure 4.40: Set-up used to portray a real situation.

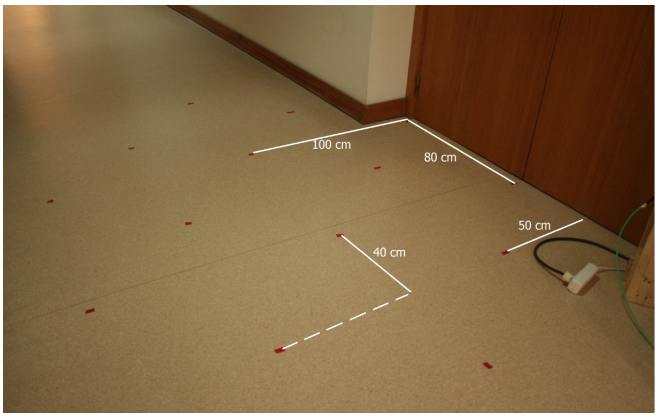

Figure 4.41: Closer view to the points on the ground where the power received was measured.

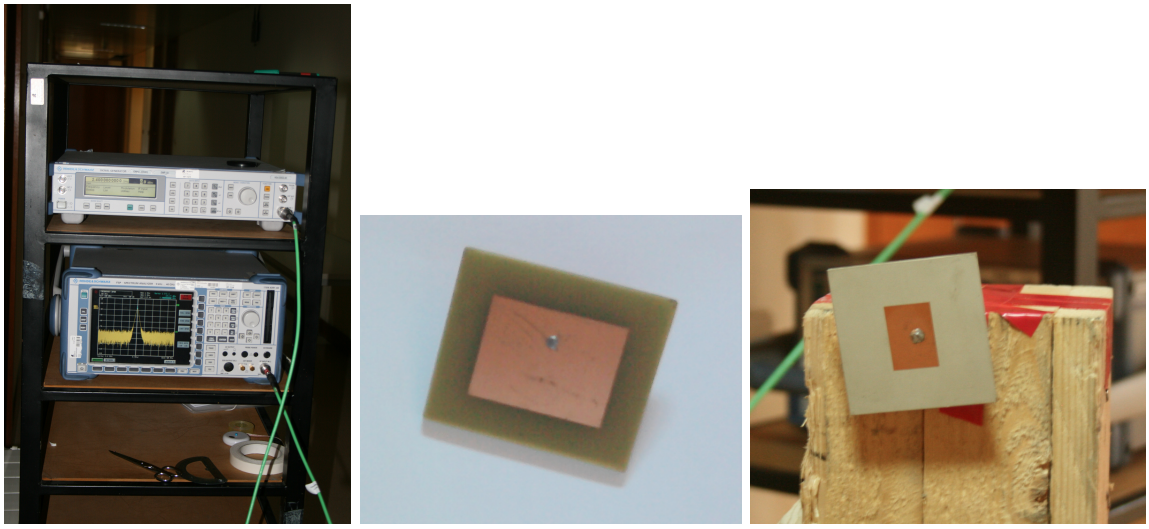

(a) Spectrum analyser and signal generator

(b) Antenna used in the receiver for the 2-element array.

(c) Antenna used in the receiver for the 4-element array

Figure 4.42: Closer view to the setup.

The overall idea that was aimed to reach with the proposed set-up, was to see if the power levels at the middle of the door entrance were higher than the ones from the surrounding area. If the antenna behaves that way, one could conclude that it is possible to help the blind or the visually impaired entering the room correctly. Before providing the experimental results, it is important to explain the reason why the antenna in figure 4.40 is only at 168 cm from the ground. The ceiling of the building where the testes were performed is all metallic, therefore if the antenna was placed very near the top, the radiation pattern would be highly damaged because it works as reflector, so instead of radiating equally in every direction of plane XZ, its superior part would be reflected downwards.

In the following plot (figure 4.43(a)) each point represents each mark shown previously in figure 4.41. It is only provided the 2-D plot because Z coordinate was a constant i.e., the experimental values were only taken at a height of 128 cm.

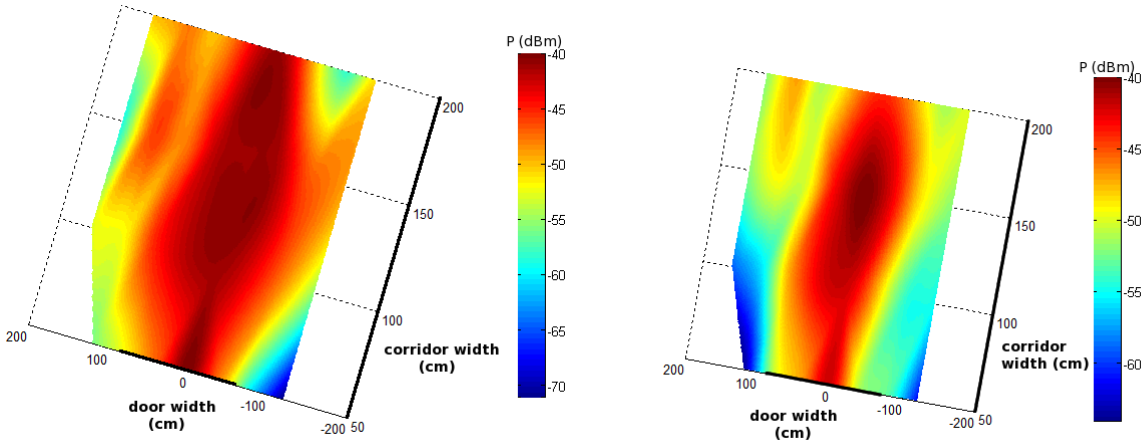

(a) Front view

(b) Back view

Figure 4.43: Experimental results obtained with the set-up from figure 4.40 for the 2-element array.

According to the results presented in figures 4.43(a) and 4.43(b), it appears that the printed antenna array is performing as desired. In fact, the higher values of received power are in the middle of the door entrance, as one could confirm by plots from figures 4.43(a) and 4.43(b). The front and back views mean that the antenna was measured inside and outside the room in order to verify if it was radiating backwards as desired. In those plots, the width of the door is represented by a widening the axis line (black line), as well as the corridor's width. The concentration of high power levels could be observed more clearly in the cubic interpolation plot (see figure 4.43(b)). Based on this plot and

knowing that the door width stays between [80;-80] cm, one would state that the higher power levels are obtained in the middle of the entrance, which is suitable for the system that is intended to be developed. It seems that for this door width the 2-element array would be suitable, but for narrower door entrances, a tighter radiation pattern is required. In agreement with the measurements it appears that the antenna is not radiating equally in the front and in the back.

The method used to see the behaviour of the antenna of 4-elements was exactly the same that was described for the 2-element array. The main differences between set-ups are: the frequency used is now 2.3 GHz due to the resonance frequency of the emitter antenna, and the array was placed at 136 cm from the ground because of the interference of the metallic ceiling. It is important to highlight that the receiver's antenna had a resonance frequency of 2.3 GHz as well. The results obtained are provided in figure 4.44, which are already the interpolation using the discrete measured according to the matrix from figure 4.41.

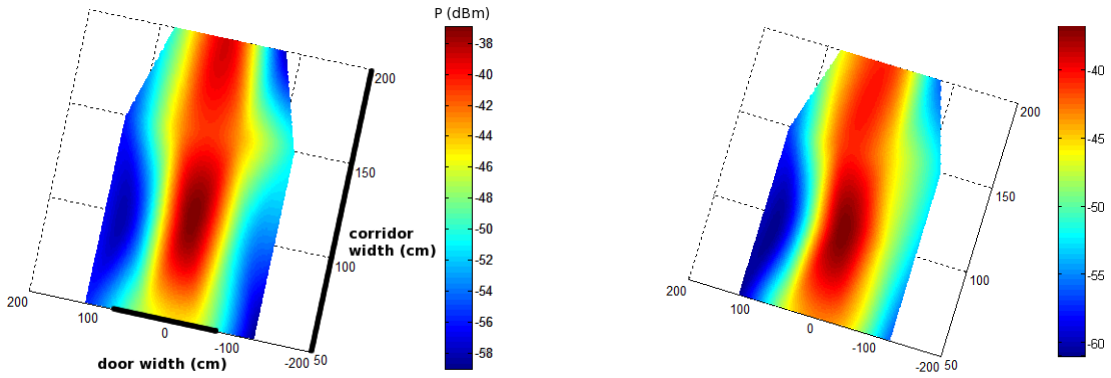

(a) Front view

(b) Back view

Figure 4.44: Cubic interpolation plot using the experimental results obtained with the set-up from figure 4.40 for the 4-element array.

Based on the results from figure 4.44, it is clear that with a four element antenna the radiation pattern is tighter than the one from figure 4.43(b) as it was expected. As a matter of fact, this new antenna leads to a better performance of the system in terms of precision because the area where the maximum values were registered is narrower. In addition, it was confirmed that the antenna is radiating backwards according to the back view from figure 4.44 as desired. This will allow the person to find the way out of the room as well. When comparing to the results obtained for the 2-element array, it seems that a four element array produces better and more symmetrical results.

Chapter 5

Conclusions and further work

Based on the results from the previous section, the printed array suitably fits the project needs. Although the 2-element array seemed to be enough to provide proper guidance to the blind or the visually impaired, the 4-element array works better, because its radiation pattern is narrower leading to a higher level of precision. The major importance of having a tighter radiation pattern is when one wants to apply this system to less wider door entrances. Unfortunately, the 4-element antenna is not possible to build in our university facility due to its large size, thus its construction had to be 'handmade'. A possible solution to this problem would be designing the same antenna for a higher resonance frequency, which was not done in this work. Reducing the antenna dimension is also advisable because of indoor esthetic i.e., the antenna is supposed to be unnoticed.

What is more, the system that was proposed in chapter 1 is not completed yet, as the focus of this dissertation was on the emitter's antenna. It is still necessary to develop the antenna for the receiver and the receiver itself. In addition, it is important to build the emitter were designed antenna would be attached.

In what concerns the drawbacks of the proposed solution for guiding the blind or the visually impaired inside building, there are several things that are necessary to refer. First, the radiation pattern of the antenna is largely influenced by the building materials i.e., the ceiling, the floor, the furniture, etc. For instance, the metallic ceiling that exists at the building where the experimental values were measured, required an increase in the distance between the ceiling and the antenna itself. Also, everything that surrounds the antenna influences the signal reception due to phenomena like multipath (see section 1.5.4). The second disadvantage is related to the first one, which says that the proposed system does not work with metallic doors due to signal reflections. Another problem that needs to be fixed is the small inclination of the higher power levels showed in figure 4.43(b), which signifies that the phase difference between the arms of the dipoles was not precisely obtained. Finally, it is important to determine a way of distinguishing the various doors of a building. In fact, the emitter signal should be modulated in order to provide accurate door identification.

As already mentioned in previous sections, the most difficult task to achieve in this project was to drive properly the printed dipole antenna. Actually, the problem was to implement a balun that would not damage the characteristic radiation pattern of a linear wire dipole. Due to the option of using a printed antenna, it was necessary to design a microstrip balun, which would highly alter the radiation pattern because of the ground plane existence. Thus, the balun dimensions and geometry had to be carefully designed, and the ground plane should have the minimum area that microstrip technology requires.

In conclusion, the results obtained were quite satisfactory, but the system still needs several improvements and there are many things to finish up. Another important conclusion concerns the geometry of the antenna, in which one was able to driven the dipoles properly without damaging significantly the radiation pattern. This is a major achievement because of the type of radiation pattern that this system demands i.e., very narrow and with a *cookie* shape. This is shape is necessary because the very same antenna is supposed to perform similarly when the person is trying to get out of a room. Although the goals proposed in the beginning of this work were considerably accomplished, there are still many improvements that could be done.

In summary, to have this system completed it is still necessary to discover a way of distinguish-

ing between various doors, which would probably be possible with a use of modulation techniques. Additionally, it would be necessary to increase the resonance frequency to diminish the antenna's size and to avoid interference with other signals. However, it is necessary to take into account the RF propagation indoor. Another matter of interest is the development of the emitter and the receiver. A study of the effects caused by people who pass near by the antenna is also welcome. The last task is to find a solution to avoid the deterioration of the system behaviour when there are metallic surfaces around it.

Bibliography

[1] http://en.wikipedia.org/wiki/Instrument_landing_system. Accessed on the 4th May 2011.

[2] http://darrenfower.mycouncillor.org.uk/2011/04/29/open-door-policy-to-continue/.

[3] http://blind.wikia.com/wiki/Loadstone-GPS. Accessed on the 1st June 2011.

[4] http://www.ibridgenetwork.org/usu/wayfinder. Accessed on the 1st June 2011.

[5] Gps for the blind or visually impaired. http://www.navigadget.com/index.php/2007/06/26/gps-for-the-blind-or-visually-impaired.

[6] Humanware. http://www.humanware.com/en-usa/products/blindness/braillenotes/_details/id_55/braillenote_gps.html.

[7] Bettina Pressl and Manfred Wieser. A computer-based navigation system tailored to the needs of blind people. Technical report, Institute of Navigation and Satellite Geodesy, Graz University of Technology.

[8] NFB's Access Technology Staff. Gps technology for the blind, a product evaluation. http://nfb.org/legacy/bm/bm06/bm0602/bm060206.htm.

[9] Zenon Chaczki Bruce Moulton, Gauri Pradhan. Voice operated guidance systems for vision impaired people: Investigating a user-centered open source model. *International Journal of Digital Content Technology and its Applications*, 3(4), December 2009.

[10] http://www.esri.com/what-is-gis/index.html.

[11] Phongsak Keeratiwintakorn Sakmongkon Chumkamon, Peranitti Tuvaphanthaphiphhat. A blind navigation system using RFID for indoor environments. In *5th International Conference on Electrical Engineering/ Electronics, Computer, Telecommunications and Information Technology*, Krabi, Thailand, May 2008. ECTI-CON.

[12] Suguru Kobayashi Xiaohan Liu, Hideo Makino and Yoshinobu Maeda. Design of an indoor self-positioning system for the visually impaired - simulations with rfid and bluetooth in a visible light communication system. In *29th Annual International Conference of the IEEE Engineering in Medicine and Biology Society*, Lyon, France, August 2007. IEEE EMBS.

[13] Suguru Kobayashi Xiaohan Liu, Hideo Makino and Yoshinobu Maeda. An indoor guidance system for the blind using fluorescent lights. In *28th Annual International Conference of the IEEE Engineering in Medicine and Biology Society*, New York City, USA, August 2006. IEEE-EMBS.

[14] George Agollah Eric Worley Brey Danels, Oluakode Ogunmakin. Blind audio guidance system.

[15] Abbas M. Ali and Md Jan Nordin. Indoor navigation to support the blind person using weighted topological map. In *International Conference on Electrical Engineering and Informatics*, Selangor, Malaysia, August 2009.

[16] Thomas Ertl Andread Hub, Joachim Diepstraten. Augmented indoor modeling for navigation support for the blind. Technical report, University of Stuttgart.

[17] Xiaodong Yang and Yingli Tian. Robust door detection in unfamiliar environments by combining edge and corner features. In *IEEE Computer Society Conference on Computer Vision and Pattern Recognition Workshops*, New York, USA, June 2010.

[18] Constantine A. Balanis. *Antenna theory: analisys and design.* John Wiley and Sons, Inc., 1997.

[19] Y.-C. Kan T.-C. Huang L.-C. Kuo, H.-R. Chuang and C.-H. Ko. Study of planar printed dipole antennas for wireless communication applications. *J. of Electromagn. Waves and Appl.*, 21(5):637–652, 2007.

[20] Panos Kostarakis Constatinos I. Votis and Antonis A. Alexandridis. Design, analysis, and measurement of an antenna structure for 2.4 GHz wireless applications. *International Journal of Antennas and Propagation*, 2010.

[21] T. Wu-K. Lim J. Laskar R. L. Li, B. Pan and M. M. Tentzeris. A broadband printed dipole and a printed array for base station applications. *Antennas and Propagation Society International Symposium*, July, 2008.

[22] Chen Yu and Wei Hong. A new printed dipole array omnidirectional antenna with bandwidth enhancement. *International Symposium on Signals Systems and Electronics (ISSSE)*, 2, September 2010.

[23] E. V. Chubar A. P. Gorbachev, V. M. Egorov. Dipole printed array antennas for mobile radio systems. *Journal of Communications Technology and Electronics*, 53(2):203–207, 2008.

[24] K. Özsoy M. Dogan and I. Tekin. Printed dipole array fed with parallel stripline for ku-band applications. In *PIERS Proceedings*, Moscow, Russia, August 2009.

[25] Mao-Hsiu Hsu Jhin-Fang Huang and Fu-Jui Wu. Design of a double-sided and printed wideband dipole array antenna on 5.2 GHz band. In *6th International Conference on ITS Telecommunications Proceedings*, Chegdu, China, June 2006.

[26] Jia-Wei Lian Jhin-Fang Huang and Sen-Te Chang. Broadband printed dipole array antenna for WLAN access point. In *First International Conference on Communications and Electronics*, Hanoi, Vietnam, October 2006.

[27] Steve Rackley. *Wireless Networking Technology - From Principles to Successful Implementation.* Elsevier, 2007.

[28] `http://people.seas.harvard.edu/~jones/es151/prop_models/propagation.html`.

[29] Dario Vojvodič. Coupled line baluns in microwave circuits. Technical report.

[30] `http://wcalc.sourceforge.net/ic_microstrip.html`.

[31] R. S. Khandpur. *Printed circuit boards: design, fabrication, assembly and testing*, chapter 4, page 178. McGraw-Hill, 2005.

[32] Keith W. Whites. Lecture 9: Quarter-wave transformer matching. Technical report, South Dakota School of Mines and Technology, 2008.

[33] Jeng-Wen Lai Kin-Lu Wong and Fu-Ren Hsiao. Omnidirectional planar dipole-array antenna for 2.4/ 5.2 ghz WLAN access points. *Microwave and Optical Technology Letters*, 39(1), October 2003.

[34] Tiago Varum. Antena para comunicacões DSRC. Master's thesis, Universidade de Aveiro, 2010.

[35] M. Z. A. Abd. Aziz A. Asrokin M. H. Jamaluddin, M. K. A. Rahim. Microstrip dipole antenna for WLAN application. In *1st International Conference on Computers, Communications, and Signal Processing with Special Track on Biomedical Engineering*, Kuala Lumpur, Malaysia, November, 2005.

[36] Myron Kayton and Walter R. Fried. *Avionics navigation system.* John Wiley and Sons, Inc., 1997.